https://doi.org/10.35662/unine-thesis-3062

PhD Thesis

Quantum Cascade Lasers for Frequency Comb-based Mid-Infrared Applications

Presented by

Kenichi N. Komagata

A dissertation submitted to:

University of Neuchâtel
Faculty of science

PhD jury:

Prof. Thomas Südmeyer	Director
Dr. Valentin Wittwer	Examiner
Prof. Jérôme Faist	Examiner
Prof. Anne Amy-Klein	Examiner
Prof. Piotr Masłowski	Examiner

Neuchâtel, June 2023

Université de Neuchâtel
Faculté des sciences

Rue Emile-Argand 11
CH-2000 Neuchâtel
doctorat.sciences@unine.ch

IMPRIMATUR POUR THESE DE DOCTORAT

La Faculté des sciences de l'Université de Neuchâtel autorise l'impression de la présente thèse soutenue par

Monsieur Kenichi Nicolas KOMAGATA

Titre :

"Quantum Cascade Lasers for Frequency Comb-based Mid-Infrared Applications"

sur le rapport des membres du jury composé comme suit :

- Prof. Thomas Südmeyer, directeur de thèse, Université de Neuchâtel, Suisse
- Dr Valentin Wittwer, Université de Neuchâtel, Suisse
- Prof. Jérôme Faist, ETH Zürich, Suisse
- Prof. Anne Amy-Klein, Université Sorbonne Paris Nord
- Prof. Piotr Masłowski, Nicolaus Copernicus University, Torun, Pologne

Neuchâtel, le 24 juillet 2023

Le Doyen, Prof. R. Bshary

Acknowledgments

I would like to acknowledge and thank all the people who were involved in my thesis or supported me during this time. You have, directly or indirectly, also contributed to these results and I value that.

First and foremost, I am grateful to my wife, Emi, for her kind support and encouragement. I thank my parents, siblings, and in-laws, as well as my friends for their presence and the fun we shared along: Anaïs, Helena, Jorge, Katia, and Nicolas among others. I also thank Rafael, David, Diana and Mihai, for the transformational work they facilitated, and Sandrina, who has always been very understanding and competent.

Turning to my mentors in the scientific circle, I thank: Thomas, for the scientific guidance, the broad perspectives, his trust, and his enthusiasm; Stéphane, for the supervision at the beginning of my thesis, especially in technical regards; Pierre, who introduced me to the experimental platform at the beginning, phase lock loops for example, and for his inspiring entrepreneurship; Alexey, who encouraged and supervised me in taking the results from my Master's thesis to publication; Valentin, for the supervision and his careful attention to the details both in manuscripts and experiments; Michele, for the great measurement campaign we had together, for supervising me in writing the results, and for introducing me to spectroscopic concepts; Benoît, who shared his know-how on frequency stabilization during his visit to our lab; and Jérôme, who provided sincere and valuable feedback when I needed them. I also want to acknowledge Lukas, Andreas, Mathieu, and Johannes for their various support.

Furthermore, I would like to thank all my colleagues for making it more fun to do a PhD: Norbert, Nayara, Marin, Julian, Atif, Micheal, François, Renaud, Etienne. In addition to the fun, special thanks goes to: Jakub, who helped me many times with electronics and do it yourself solutions; Maëlys, for her commitment during her internship; and Alexandre, for our close, and successful collaboration.

Lastly, I also want to mention some of the many people whom I have met at conferences and from whom I have personally learned something: Aleksandra, Annina, Esther, Gerard, Gregorz, Ibrahim, Johann, Lukasz, Philipp, Piotr, Raphael, Roderik, Ruichen, Takuma, and many, many others.

Keywords - Mots clés

Keywords

Optical frequency combs, mid-infrared spectroscopy, quantum cascade lasers, frequency metrology, laser stabilization.

Mots clés

Peignes de fréquence optique, spectroscopie dans le moyen-infrarouge, lasers à cascades quantiques, métrologie de fréquence, stabilisation de lasers.

Abstract

The mid-infrared (MIR) part of the electromagnetic spectrum is characterized by strong molecular interactions with light and low scattering losses. Thus, it is a strategic wavelength range for sensing, free-space telecommunications and high-precision spectroscopy. Optical frequency combs (OFCs or FCs) excel in these applications, making their generation in the MIR highly relevant. Quantum cascade lasers (QCLs) are a possible source of MIR OFCs, and present the unique merits of high emission power, simple operation, and compatibility with mass-production. However, QCL OFCs have not yet been employed in a wide range of MIR applications despite their potential. In fact, there is a lack of established methods for their coherent control such as frequency stabilization: techniques from other OFC technologies could not be adapted in a straightforward manner. So far, they have been used almost exclusively for dual comb spectroscopy (DCS), where active stabilization was not imperative. In the absence of other simple OFC sources in this spectral range, they have been producing excellent results in this configuration. But enabling QCL FCs to drive the manifold of comb applications will require advanced stabilization techniques that ideally do not undermine simplicity and compactness.

In this thesis, I investigated frequency stabilization, calibration, and the application of QCLs with the goal of demonstrating their fitness as versatile MIR FC sources. In a first approach, I tackled the issue of low duty-cycle impaired by the computational correction necessary for free running DCS. I developed a scheme to mutually lock two QCL FCs and to allow real-time processing of the multiheterodyne beat. One challenge for QCL comb stabilization schemes is the moderate frequency response of the usual control method based on electrical feedback. In a second approach, I characterized the influence of near-infrared light on a QCL FC and developed a locking scheme employing a standard telecommunication laser, improving the tight-locking ability to a satisfactory level for most applications. Moreover, I demonstrate high spectral purity across the bandwidth of the comb and reveal the comb coherence at new time-scales. In a third experiment, I performed the full frequency stabilization of a MIR QCL FC. I then implemented comb-calibrated spectroscopy and retrieved the center frequency of several molecular transitions. The accurate agreement between the retrieved and literature values proves that QCL FCs are suited for frequency metrology applications. In a final experiment, I tackled the issue of frequency calibration in fast and high-resolution DCS. I designed and tested a scheme that allowed the critical combination of high frequency accuracy, acquisition speed, resolution, and sensitivity. It was found that the particularly high repetition rate of QCLs is actually an advantage for direct comb spectroscopy.

All these results can already be transferred to applications. For example, the tight-locking capability will allow the use of enhancement cavities for increased sensitivity. Moreover, frequency calibration in fast and high resolution DCS allows QCLs to be employed for high precision studies of the physics of molecules. However, the reported results represent only the tip of the iceberg in the potential of QCL OFCs to harness the prospects of the MIR. While they merely scratches the surface, they establish concretely that QCLs are fit in terms of frequency stabilization and calibration as versatile MIR FC sources. Further development towards photonic integration, pulse emission, and low power consumption promise to make QCLs ubiquitous in the society of the future.

Résumé

La région de l'infrarouge moyen (IRM) du spectre électromagnétique est caractérisée par de fortes interactions moléculaires avec la lumière et de faibles pertes par diffusion. Il s'agit donc d'une gamme de longueurs d'onde stratégique pour la détection, les télécommunications en espace libre et la spectroscopie de haute précision. Les peignes de fréquence optiques (PFO ou PF) excellent dans ces applications, ce qui rend leur génération dans l'IRM très pertinente. Les lasers à cascade quantique (LCQ) sont une source possible de PFO dans l'IRM et présentent les avantages uniques d'une puissance d'émission élevée, d'un fonctionnement simple et d'une compatibilité avec la production de masse. Cependant, malgré leur potentiel, les PF LCQ n'ont pas encore été utilisés dans une large gamme d'applications dans l'IRM. En fait, il y a un manque de méthodes établies pour leur contrôle cohérent, comme la stabilisation de la fréquence : les techniques d'autres technologies de PFO n'ont pas pu être adaptées de manière directe. Jusqu'à présent, les PF LCQ ont été utilisés presque exclusivement pour la spectroscopie à double peigne (SDP), où la stabilisation active n'était pas impérative. En l'absence d'autres sources de PFO simples dans cette gamme spectrale, elles ont donné d'excellents résultats dans cette configuration. Mais pour que les PF LCQ puissent accéder aux nombreuses applications de peigne, il faudra des techniques de stabilisation avancées qui, dans l'idéal, ne nuisent pas à la simplicité et à la compacité des LCQ.

Dans cette thèse, j'ai étudié la stabilisation de la fréquence, l'étalonnage et l'application des LCQ dans le but de démontrer leur aptitude en tant que sources polyvalentes de PF dans l'IRM. Dans une première approche, j'ai abordé le problème du faible rapport cyclique causé par la correction computationnelle nécessaire à la SDP en fonctionnement libre. J'ai développé un schéma pour verrouiller mutuellement deux PF LCQ et pour permettre le traitement en temps réel du battement multihétérodyne. Un défi pour les schémas de stabilisation des peignes LCQ est la réponse en fréquence modérée de la méthode de contrôle habituelle basée sur la rétroaction électrique. Dans une deuxième approche, j'ai caractérisé l'influence de la lumière de l'infrarouge proche sur un PF LCQ et j'ai développé un schéma d'asservissement utilisant un laser de télécommunication standard, améliorant la capacité de verrouillage fin à un niveau satisfaisant pour la plupart des applications. En outre, j'ai démontré une grande pureté spectrale sur toute la largeur de bande du peigne et révélé la cohérence du peigne à de nouvelles échelles de temps. Dans une troisième expérience, j'ai réalisé la stabilisation complète de la fréquence d'un PF LCQ dans l'IRM. J'ai ensuite mis en œuvre une spectroscopie calibrée par peigne et récupéré la fréquence centrale de plusieurs transitions moléculaires. L'accord précis entre les valeurs

extraites et celles de la littérature prouve que les PF LCQ conviennent aux applications de métrologie des fréquences. Dans une dernière expérience, j'ai abordé la question de l'étalonnage de la fréquence dans le cadre de la SDP rapide et à haute résolution. J'ai conçu et testé un schéma qui a permis la combinaison critique de précision de fréquence, de vitesse d'acquisition, de résolution et de sensibilité élevées. Il s'est avéré que le taux de répétition particulièrement élevé des LCQ est en fait un avantage pour la spectroscopie à peigne direct.

Tous ces résultats peuvent déjà être transférés vers des applications. Par exemple, la capacité de verrouillage fin permettra d'utiliser des cavités d'amélioration pour augmenter la sensibilité. En outre, l'étalonnage de la fréquence en SDP rapide et à haute résolution permet d'utiliser les LCQ pour des études de haute précision sur la physique des molécules. Cependant, les résultats rapportés ne représentent que la partie émergée de l'iceberg en ce qui concerne le potentiel des PF LCQ pour exploiter les possibilités de l'IRM. Bien qu'ils ne fassent qu'effleurer la surface, ils établissent concrètement que les LCQ sont adaptés en termes de stabilisation de fréquence et d'étalonnage en tant que sources de PF polyvalentes dans l'IRM. Des développements supplémentaires en matière d'intégration photonique, d'émission d'impulsions et de faible consommation d'énergie promettent de rendre les LCQ incontournables dans la société de l'avenir.

Contents

List of acronyms

CMNS	Common mode noise subtraction
DCS	Dual comb spectroscopy
DFB	Distributed feedback
DFG	Difference frequency generation
FC	Frequency comb
ICL	Interband cascade laser
IBN	Intermode beat note
LWIR	Long-wave infrared
MIR	Mid-infrared
NIR	Near-infrared
NEA	Noise-equivalent absorbance
OFC	Optical frequency comb
OPO	Optical parametric oscillator
PIC	Photonic integrated chips
PLL	Phase lock loop
PSD	Power spectral density
QCL	Quantum cascade laser
RF	Radio-frequency
SI	International System of Units
SNR	signal-to-noise ratio
WMS	Wavelength modulation spectroscopy

Publication list

Journal papers

[1] K. N. Komagata, V. J. Wittwer, T. Südmeyer, L. Emmenegger, and M. Gianella, "Absolute Frequency Referencing for Swept Dual-Comb Spectroscopy with Midinfrared Quantum Cascade Lasers", Phys. Rev. Res. **5**, 013047 (2023).

[2] K. N. Komagata, A. Parriaux, M. Bertrand, J. Hillbrand, M. Beck, V. J. Wittwer, J. Faist, and T. Südmeyer, "Coherent Control of Mid-Infrared Frequency Comb by Optical Injection of Near-Infrared Light", ArXiv230501508 Phys., `10.48550/arXiv.2305.01508` (2023).

[3] K. N. Komagata, M. Gianella, P. Jouy, F. Kapsalidis, M. Shahmohammadi, M. Beck, R. Matthey, V. J. Wittwer, A. Hugi, J. Faist, L. Emmenegger, T. Südmeyer, and S. Schilt, "Absolute Frequency Referencing in the Long Wave Infrared Using a Quantum Cascade Laser Frequency Comb", Opt. Express **30**, 12891 (2022).

[4] A. Tikan, A. Tusnin, J. Riemensberger, M. Churaev, X. Ji, K. N. Komagata, R. N. Wang, J. Liu, and T. J. Kippenberg, "Protected Generation of Dissipative Kerr Solitons in Supermodes of Coupled Optical Microresonators", Sci. Adv. **8**, eabm6982 (2022).

[5] A. K. Tusnin, A. M. Tikan, K. Komagata, and T. J. Kippenberg, "Spatio-Temporal Dissipative Kerr Solitons and Regularized Wave-Collapses in Chains of Nonlinear Microresonators", ArXiv210411731 Phys., `10.48550/arXiv.2104.11731` (2022).

[6] K. Komagata, A. Shehzad, G. Terrasanta, P. Brochard, R. Matthey, M. Gianella, P. Jouy, F. Kapsalidis, M. Shahmohammadi, M. Beck, V. J. Wittwer, J. Faist, L. Emmenegger, T. Südmeyer, A. Hugi, and S. Schilt, "Coherently-Averaged Dual Comb Spectrometer at 7.7 µm with Master and Follower Quantum Cascade Lasers", Opt. Express **29**, 19126 (2021).

[7] K. Komagata, A. Tusnin, J. Riemensberger, M. Churaev, H. Guo, A. Tikan, and T. J. Kippenberg, "Dissipative Kerr Solitons in a Photonic Dimer on Both Sides of Exceptional Point", Commun. Phys. **4**, 1 (2021).

[8] A. Tikan, J. Riemensberger, K. Komagata, S. Hönl, M. Churaev, C. Skehan, H. Guo, R. N. Wang, J. Liu, P. Seidler, and T. J. Kippenberg, "Emergent Nonlinear Phenomena in a Driven Dissipative Photonic Dimer", Nat. Phys. **17**, 604 (2021).

[9] D. Cruz, R. Fournier, F. Gremion, A. Jeannerot, K. Komagata, T. Tosic, J. Thiesbrummel, C. L. Chan, N. Macris, M.-A. Dupertuis, and C. Javerzac-Galy, "Efficient Quantum Algorithms for GHZ and W States, and Implementation on the IBM Quantum Computer", Adv. Quantum Techol. **2**, 1900015 (2019).

Patents

[1] S. Schilt, P. Brochard, K. Komagata, G. Terrasanta, and A. Hugi, "Dual-Comb Spectroscopy", U.S. pat. 20220146312A1 (Irsweep AG, May 12, 2022).

Conference papers

[1] K. N. Komagata, V. J. Wittwer, T. Südmeyer, L. Emmenegger, and M. Gianella, "Sub-MHz Accuracy Current-Tuned Quantum Cascade Laser Dual-Comb Spectroscopy", Field Laser Application in Industry and Research 2022, (Sept. 12, 2022).

[2] K. N. Komagata, S. Vogel, V. J. Wittwer, M. Bertrand, S. Schilt, J. Faist, T. Südmeyer, L. Emmenegger, and M. Gianella, "Fast and Accurate Dual-Comb Spectroscopy with Mid-Infrared Quantum Cascade Laser Frequency Combs", in Proceedings of the 2022 Conference on Lasers and Electro-Optics Pacific Rim (Aug. 31, 2022), CTuP6B_03.

[3] K. N. Komagata, M. Gianella, P. Jouy, F. Kapsalidis, M. Shahmohammadi, M. Beck, R. Matthey, V. J. Wittwer, A. Hugi, J. Faist, L. Emmenegger, T. Südmeyer, and S. Schilt, "Quantum Cascade Laser Frequency Comb for Comb-Calibrated Spectroscopy in the Long-Wave Infrared", in Proceedings of the 2022 Conference on Lasers and Electro-Optics Pacific Rim (Aug. 31, 2022), CTuP6B_02.

[4] M. Gianella, K. N. Komagata, S. Vogel, V. J. Wittwer, M. Bertrand, S. Schilt, J. Faist, T. Südmeyer, and L. Emmenegger, "Frequency Scale Calibration for High-Resolution Quantum Cascade Laser Dual-Comb Spectroscopy", in Optical Sensors and Sensing Congress 2022 (AIS, LACSEA, Sensors, ES) (July 11, 2022), EM3D.1.

[5] M. Gianella, K. Komagata, S. Vogel, V. J. Wittwer, M. Bertrand, S. Schilt, J. Faist, T. Südmeyer, and L. Emmenegger, "High-Resolution Quantum Cascade Laser Dual-Comb Spectroscopy with Accurate, Absolute Frequency Scale", in Conference on Lasers and Electro-Optics (May 15, 2022), ATu5K.5.

[6] A. Tikan, K. N. Komagata, A. Tusnin, J. Riemensberger, M. Churaev, H. Guo, and T. J. Kippenberg, “Dissipative Kerr Solitons in a Photonic Dimer on Both Sides of an Exceptional Point”, in Conference on Lasers and Electro-Optics (May 15, 2022), FM4B.4.

[7] K. N. Komagata, M. Gianella, P. Jouy, F. Kapsalidis, M. Shahmohammadi, M. Beck, R. Matthey, V. J. Wittwer, A. Hugi, J. Faist, L. Emmenegger, T. Südmeyer, and S. Schilt, “Comb-Calibrated Spectroscopy Using a Quantum Cascade Laser Frequency Comb in the Long-Wave Infrared”, in Optica High-brightness Sources and Light-driven Interactions Congress (Mar. 21, 2022), MW6C.2.

[8] M. Gianella, K. N. Komagata, S. Vogel, V. J. Wittwer, M. Bertrand, S. Schilt, J. Faist, T. Südmeyer, and L. Emmenegger, “High-Resolution Quantum Cascade Laser Dual-Comb Spectroscopy with Accurate Absolute Frequency Scale”, in Optica High-brightness Sources and Light-driven Interactions Congress (Mar. 21, 2022), MW6C.4.

[9] P. Allmendinger, K. Komagata, A. Shehzad, R. Matthey, V. Wittwer, A. Hugi, P. Jouy, M. Mangold, S. Dal Cin, G. Strasser, B. Schwarz, M. Gianella, L. Emmenegger, T. Südmeyer, and S. Schilt, “Demonstration of Frequency-Stabilized Quantum Cascade Laser Dual-Comb Spectroscopy”, SPIE Photonics Europe Conferences, Optical Sensing and Detection VII, (Apr. 3, 2022).

[10] K. N. Komagata, V. J. Wittwer, and T. Südmeyer, “Quantum cascade laser stabilization and optimized coating solutions for mid-infrared precision spectroscopy”, Searching for New Physics at the Quantum Technology Frontier, ETH Zurich, (Jan. 21, 2022).

[11] K. Komagata, A. Shehzad, M. Hamrouni, R. Matthey, F. Kapsalidis, P. Jouy, M. Beck, V. J. Wittwer, A. Hugi, J. Faist, T. Südmeyer, and S. Schilt, “Frequency Control of a Mid-Infrared Quantum Cascade Laser Frequency Comb by Near-Infrared Light Injection and Intensity Modulation”, in 2021 Conference on Lasers and Electro-Optics Europe and European Quantum Electronics Conference (June 21, 2021), cb_4_4.

[12] K. Komagata, A. Shehzad, G. Terrasanta, P. Brochard, R. Matthey, M. Gianella, P. Jouy, F. Kap-salidis, M. Shahmohammadi, M. Beck, V. J. Wittwer, J. Faist, L. Emmenegger, T. Südmeyer, A. Hugi, and S. Schilt, “Coherently-Averaged Dual-Comb Spectrometer at 7.7 µm with Master and Follower Quantum Cascade Lasers”, in 2021 Conference on Lasers and Electro-Optics Europe and European Quantum Electronics Conference (June 21, 2021), cb_8_2.

[13] M. Gianella, S. Vogel, K. Komagata, J. Hillbrand, F. Kapsalidis, B. Tuzson, A. Nataraj, M. Beck, A. Hugi, M. Mangold, P. Jouy, T. Südmeyer, J. Faist, and L. Emmenegger, “Gapless High-Resolution QCL Dual-Comb Spectroscopy with Real-Time Data Processing for Dynamic Gas-Phase Measurements”, in 2021 Conference on Lasers and Electro-Optics Europe and European Quantum Electronics Conference (June 21, 2021), ed_1_5.

[14] K. Komagata, A. Shehzad, M. Hamrouni, P. Jouy, F. Kapsalidis, M. Shahmohammadi, M. Beck, R. Matthey, V. J. Wittwer, J. Faist, T. Südmeyer, A. Hugi, and S. Schilt, “All-Mid-Infrared Stabilized Quantum Cascade Laser Frequency Comb with 30-kHz Frequency Stability at 7.7 µm”, in Conference on Lasers and Electro-Optics (May 9, 2021), STu1H.3.

[15] A. Tikan, A. Tusnin, J. Riemensberger, M. Churaev, K. Komagata, K. Komagata, X. Ji, R. N. Wang, J. Liu, and T. J. Kippenberg, “Symmetry Protection against Mode Crossings in Multimode Photonic Resonator Chains”, in Conference on Lasers and Electro-Optics (May 9, 2021), FTu4E.4.

[16] A. Shehzad, P. Brochard, K. Komagata, R. Matthey, F. Kapsalidis, M. Shahmohammadi, M. Beck, A. Hugi, P. Jouy, J. Faist, T. Südmeyer, and S. Schilt, “Noise Correlation Between the Two Degrees of Freedom of a Mid-Infrared Quantum Cascade Laser Frequency Comb”, in Conference on Lasers and Electro-Optics (May 10, 2020), SF2G.2.

[17] A. Tikan, J. Riemensberger, K. Komagata, S. Honl, M. Churaev, C. Skehan, H. Guo, R. N. Wang, J. Liu, P. Seidler, and T. J. Kippenberg, “Dissipative Kerr Solitons in a Photonic Dimer”, in Conference on Lasers and Electro-Optics (May 10, 2020), FTh1A.5.

Chapter 1

Introduction

The mid-infrared (MIR) is a part of the electromagnetic spectrum characterized by strong interaction of molecules with light. Indeed, the fundamental vibrational modes of many molecular bonds are resonant in this wavelength range that can be defined between 3 µm and 20 µm. These modes are hybridized with the rotation of the molecule to form bands of so-called ro-vibrational transitions, whose eigen-frequencies depend on various parameters such as atomic mass and intramolecular bond strength. As a result, each molecule has a characteristic absorption spectrum stemming from the ro-vibrational transitions, and this spectrum can be likened to a fingerprint that uniquely defines atomic arrangements up to isotopic differences.

Thus, the intense and specific response of molecules to MIR light make the latter particularly interesting for sensing and non-destructive measurements by laser spectroscopy. Indeed, accurate and sensitive molecular detection offers many enticing perspectives such as breath-based health analysis [1], imaging of biological samples [2], environmental monitoring [3], or industrial process control, from plant cultivation [4] to drug content verification [5]. MIR spectroscopy satisfies the acquisition speed, standoff and nondestructive detection, and miniaturization potential to meet these applications. Other technologies such as mass spectrometers fall short of those criteria.

Besides this family of applications, the MIR is strategic for at least two enterprises. The first is the study of molecular physics and chemistry due to the strong light-matter interaction. For example, accurate measurement of the transition frequencies are paramount for refining the quantum model of molecules [6], and they can, in the most extreme cases, even contribute to frontier research in fundamental physics [7]. Another example are time-resolved measurements, which allow the study of chemical reaction dynamics and transient states [8]. This knowledge is precious for extending our comprehension of the universe and creating new solutions. Second, transmission of MIR light in the presence of scattering (e.g. fog or dust) is far superior than the near-infrared (NIR) [9]. Thus, the MIR atmospheric transmission windows, found between 3–4 µm, 4.5–5.5 µm, and 8–14 µm, are relevant for free-space telecommunication, when fiber infrastructures are not present.

All these prospects and their potential disruptive impact on society have been inspirations for the development of MIR optical technologies and spectroscopy. However, the MIR still lacks the technological maturity of the NIR region, specifically near 1.55 µm, which has been driven by the telecommunication motives stirred by the available ultra-low-loss fibers. One could also argue that nature privileges optics and photonics in the NIR over the MIR. This was true for lasers at least, with the difficulty of finding satisfactory gain materials for the MIR. The problem was solved with the invention of quantum cascade lasers (QCLs) [10], for which the gain is induced by cascades of quantum wells set with specific energy level differences.

Another key component in optical technologies is an optical frequency comb (OFC or FC). It is a source of coherent light constituted by a set of discrete and equidistant frequency lines:

$$f_n = f_0 + n f_r, \tag{1.1}$$

where n is an integer for the index of the line, f_r is the equidistant spacing between each line, and f_0 is a global offset [11]. It follows from Equation 1.1, called the comb equation, that the optical frequency of each comb line can be determined accurately if both f_0 and f_r are linked to radio-frequency (RF) standards. This is possible because they typically lie in the RF domain. In the time domain, f_r is named the repetition rate and relates to the periodicity of the emitted light. The electric field is indeed periodic up to a phase shift from period to period that is related to f_0, also called the (carrier-envelope) offset frequency.

In the first applications of OFCs, optical frequencies were compared using knowledge of f_r [12]. Then, in the year 2000, the direct measurement and control of f_0 in addition f_r was demonstrated [13]. Thus, OFCs replaced the complex frequency division links [14] and became a tool for microwave to optical frequency linking and optical frequency synthesis [15–17]. They have also revolutionized optical spectroscopy through frequency comb spectroscopy [18, 19], which combines fast acquisition, large optical bandwidths, high frequency accuracy, and high sensitivity. Moreover, OFCs have opened or enhanced countless other applications [20], due to the convenience of the comb equation (Equation 1.1) and the fact that it can translate to ultra-short pulses in the time domain. As a result, a share of the 2005 Nobel prize in physics was awarded for the invention of the OFC [21, 22].

OFCs are thus highly relevant. In the MIR, they can be generated, among other methods, by QCLs designed with broad gain and small dispersion [23, 24]. Typically, the laser Fabry-Perot cavity is simply the laser waveguide of a few millimeters in length. While various mechanism are involved, it is finally the inherent Kerr nonlinearity that phase-locks the multimode emission into an equidistant frequency grid. Thus, an OFC is generated simply by electrically driving the laser and maintaining it at a constant temperature. The time domain emission is characterized by a repeating (at f_r) saw-tooth instantaneous frequency and a weakly-modulated amplitude profile [25], which can be compressed to sub-picosecond pulses by correcting the chirp [26].

An outstanding advantage and potential of QCLs is that they are compatible with mass fabrication at low unit-cost. Indeed, they are fabricated on wafers and have a small volume. In fact, QCLs and other integrated comb sources such as interband cascade lasers [27] and soliton microcomb lasers [28] have this upper hand compared to all other comb sources regardless of wavelength. The other FC sources in the long-wave infrared (LWIR, 8–14 µm window) are based on the nonlinear frequency conversion of an OFC from another wavelength (typically in the NIR) by difference frequency generation (DFG) or in a optical parametric oscillator (OPO). These sources cannot be integrated on chip as of now.

Furthermore, the optical power emitted by QCL FCs ranges from 100 mW to 1 W [29], which is unrivaled in the LWIR. Typical DFG sources emit less than 10 mW (e.g. [30–33]). The 100 mW range can be reached by increasing the power and shortening the pulse driving the DFG process at the cost of added complexity [34, 35]. OPOs also can reach 100 mW of MIR radiation [36] but the requirement of cavity synchronization makes them more complex than DFG sources. Aside power and integration, a distinctive asset for many application is the high repetition rate in the 10 GHz range, which results from the short cavity round-trip time. Such repetition rate is hardly attained by the other aforementioned sources, with the exception of two reports at 1 GHz [37] and 10 GHz [38] based on DFG. The reason is that higher f_r leads to weaker peak power for a given and limited average power, and thus decreased nonlinear conversion efficiency.

However, the bandwidth of QCL FCs is comparatively narrow, currently reaching about 7% of the center wavelength (90 cm^{-1} in the 8 µm range) [29, 39]. In conjunction with the absence of natural ultrashort pulse emission, this hinders the detection of the offset frequency by nonlinear interferometry [40]. Therefore, the comb lines could not simply be linked to RF references as with other types of OFCs. Moreover, methods for full and tight comb stabilization were not investigated in depth. Instead, QCL FCs have been mainly operated in free-running operation. Their range of application lingered on dual comb spectroscopy (DCS) alone, in cases where stabilization was not strictly necessary as high frequency accuracy was secondary; QCL-based DCS filled a strong demand for spectroscopic data in the MIR, especially in time-resolved measurement of molecular dynamics occurring in microsecond time scales [8]. The mutual coherence required for DCS could be retrieved through post-processing at the cost of reduced duty-cycle and computational power.

Nevertheless, other MIR applications require and profit from high-quality stabilization of the QCL FC parameters and not all necessitate offset frequency detection. In comb calibrated spectroscopy [41, 42] for example, the OFC allows the accurate determination of the probing frequency of a scanning laser. It requires the full stabilization of the OFC, which can be achieved by locking f_n, at a given n, to a known molecular transition and locking f_r to an RF reference, i.e. the direct measurement of f_0 is not needed. Therefore, stabilization techniques are relevant and feasible in spite of the limited bandwidth and absence of pulse emission. These will require investigation to develop or adapt specific stabilization technique that take advantage of the distinct properties of MIR QCL FCs. One challenge is to find suitable handles for the feedback control of the comb frequencies: actuation on the drive current lacks the bandwidth to reach a high spectral purity [43]. Moreover, the techniques should ideally be compatible with the compactness of the laser. An accurate understanding of the frequency noise [44, 45] as well as the characterization of the locks will also benefit the development of the techniques. Most importantly, the conformity to the comb equation (Equation 1.1), which is the essence and power of an OFC, needs to be assessed when applying the stabilization techniques. Last but not least, proof-of-principles experiments are needed to evaluate and demonstrate the suitability of QCL OFCs for MIR comb-based applications.

I tackle these relevant questions in this thesis. In chapter 2, I investigate mutual stabilization in the context of DCS. Because the actuation bandwidth of the drive current is not high enough, I implement an analog processing scheme that ensures high coherence and largely reduces the computational load related to post-processing corrections. In chapter 3, I characterize an alternative stabilization method that has a higher response bandwidth and thus achieves the high spectral purity required for most applications. I also study the phase noise of the comb lines and show evidence for the conformity to the comb equation across a broad bandwidths. Applications are explored next. In chapter 4, the comb equidistance is exploited for comb calibrated spectroscopy. High frequency accuracy is obtained, as limited by the reference laser, but not by the QCL FC.

In chapter 5, I present a scheme for the accurate retrieval of the frequency axis in high-resolution DCS. The results demonstrate a remarkable combination of high speed, high sensitivity, and high frequency accuracy. They are granted by the unique marriage of high power and high repetition frequency of QCL FCs. Finally, I review the results and give an outlook in chapter 6: MIR QCL FCs do have a large potential of transforming our society for the better. The progress in stabilization and the proof-of-principle experiments presented in this thesis are small but necessary steps towards that direction.

Each chapter, except the conclusion and introduction, are based on an article published in a peer-review journal or in submission. While the articles constitute the core results of the thesis, I found it fitting to write enclosing chapters and reproduce the articles in the appendix of each chapter. In this way, I can introduce each topic from the perspective of the thesis and offer extensive discussion of elements, which the article could not sustain for matter of space, or which, at the time of the original redaction, did not occur to me. While a minimal summary of the article is also included in order to smooth the reading, direct study of the article in addition to the chapters is recommended. An approach of minimal reiteration between chapters and articles was pursued for the sake of the reader.

References

[1] B. Henderson, A. Khodabakhsh, M. Metsälä, I. Ventrillard, F. M. Schmidt, D. Romanini, G. A. D. Ritchie, S. Te Lintel Hekkert, R. Briot, T. Risby, N. Marczin, F. J. M. Harren, and S. M. Cristescu, “Laser Spectroscopy for Breath Analysis: Towards Clinical Implementation”, Appl. Phys. B **124**, 161 (2018).

[2] R. Bhargava and A. Madabhushi, “Emerging Themes in Image Informatics and Molecular Analysis for Digital Pathology”, Annu. Rev. Biomed. Eng. **18**, 387 (2016).

[3] S. Henne, D. Brunner, B. Oney, M. Leuenberger, W. Eugster, I. Bamberger, F. Meinhardt, M. Steinbacher, and L. Emmenegger, “Validation of the Swiss Methane Emission Inventory by Atmospheric Observations and Inverse Modelling”, Atmospheric Chem. Phys. **16**, 3683 (2016).

[4] M. Yumoto, Y. Kawata, T. Abe, T. Matsuyama, and S. Wada, “Non-Destructive Mid-IR Spectroscopy with Quantum Cascade Laser Can Detect Ethylene Gas Dynamics of Apple Cultivar ‘Fuji’ in Real Time”, Sci. Rep. **11**, 20695 (2021).

[5] V. Villanueva-López, L. C. Pacheco-Londoño, R. Villarreal-González, J. R. Castro-Suarez, A. Román-Ospino, W. Ortiz-Rivera, N. J. Galán-Freyle, and S. P. Hernandez-Rivera, “API Content and Blend Uniformity Using Quantum Cascade Laser Spectroscopy Coupled with Multivariate Analysis”, Pharmaceutics **13**, 985 (2021).

[6] M. Germann, A. Hjältén, V. Boudon, C. Richard, K. Krzempek, A. Hudzikowski, A. Głuszek, G. Soboń, and A. Foltynowicz, “A Methane Line List with Sub-MHz Accuracy in the 1250 to 1380 cm^{-1} Range from Optical Frequency Comb Fourier Transform Spectroscopy”, J. Quant. Spectrosc. Radiat. Transf. **288**, 108252 (2022).

[7] S. K. Tokunaga, C. Stoeffler, F. Auguste, A. Shelkovnikov, C. Daussy, A. Amy-Klein, C. Chardonnet, and B. Darquié, “Probing Weak Force-Induced Parity Violation by High-Resolution Mid-Infrared Molecular Spectroscopy”, Mol. Phys. **111**, 2363 (2013).

[8] J. L. Klocke, M. Mangold, P. Allmendinger, A. Hugi, M. Geiser, P. Jouy, J. Faist, and T. Kottke, “Single-Shot Sub-microsecond Mid-infrared Spectroscopy on Protein Reactions with Quantum Cascade Laser Frequency Combs”, Anal. Chem. **90**, 10494 (2018).

[9] A. K. Majumdar and J. C. Ricklin, eds., *Free-Space Laser Communications: Principles and Advances*, Optical and Fiber Communications Reports 2 (Springer, New York, NY, 2008), 417 pp.

[10] J. Faist, F. Capasso, D. L. Sivco, C. Sirtori, A. L. Hutchinson, and A. Y. Cho, “Quantum Cascade Laser”, Science **264**, 553 (1994).

[11] T. Udem, R. Holzwarth, and T. W. Hänsch, “Optical Frequency Metrology”, Nature **416**, 233 (2002).

[12] Th. Udem, J. Reichert, R. Holzwarth, and T. W. Hänsch, “Absolute Optical Frequency Measurement of the Cesium D_1 Line with a Mode-Locked Laser”, Phys. Rev. Lett. **82**, 3568 (1999).

[13] J. Reichert, M. Niering, R. Holzwarth, M. Weitz, Th. Udem, and T. W. Hänsch, “Phase Coherent Vacuum-Ultraviolet to Radio Frequency Comparison with a Mode-Locked Laser”, Phys. Rev. Lett. **84**, 3232 (2000).

[14] J. E. Bernard, A. A. Madej, L. Marmet, B. G. Whitford, K. J. Siemsen, and S. Cundy, “Cs-Based Frequency Measurement of a Single, Trapped Ion Transition in the Visible Region of the Spectrum”, Phys. Rev. Lett. **82**, 3228 (1999).

[15] S. A. Diddams, D. J. Jones, J. Ye, S. T. Cundiff, J. L. Hall, J. K. Ranka, R. S. Windeler, R. Holzwarth, T. Udem, and T. W. Hänsch, "Direct Link between Microwave and Optical Frequencies with a 300 THz Femtosecond Laser Comb", Phys. Rev. Lett. **84**, 5102 (2000).

[16] D. J. Jones, S. A. Diddams, J. K. Ranka, A. Stentz, R. S. Windeler, J. L. Hall, and S. T. Cundiff, "Carrier-Envelope Phase Control of Femtosecond Mode-Locked Lasers and Direct Optical Frequency Synthesis", Science **288**, 635 (2000).

[17] J. D. Jost, J. L. Hall, and J. Ye, "Continuously Tunable, Precise, Single Frequency Optical Signal Generator", Opt. Express **10**, 515 (2002).

[18] N. Picqué and T. W. Hänsch, "Frequency Comb Spectroscopy", Nat. Photonics **13**, 146 (2019).

[19] M. L. Weichman, P. B. Changala, J. Ye, Z. Chen, M. Yan, and N. Picqué, "Broadband Molecular Spectroscopy with Optical Frequency Combs", Journal of Molecular Spectroscopy **355**, 66 (2019).

[20] T. Fortier and E. Baumann, "20 Years of Developments in Optical Frequency Comb Technology and Applications", Commun. Phys. **2**, 1 (2019).

[21] T. W. Hänsch, "Nobel Lecture: Passion for Precision", Rev. Mod. Phys. **78**, 1297 (2006).

[22] J. L. Hall, "Nobel Lecture: Defining and Measuring Optical Frequencies", Rev. Mod. Phys. **78**, 1279 (2006).

[23] A. Hugi, G. Villares, S. Blaser, H. C. Liu, and J. Faist, "Mid-Infrared Frequency Comb Based on a Quantum Cascade Laser", Nature **492**, 229 (2012).

[24] J. Faist, G. Villares, G. Scalari, M. Rösch, C. Bonzon, A. Hugi, and M. Beck, "Quantum Cascade Laser Frequency Combs", Nanophotonics **5**, 272 (2016).

[25] M. Singleton, P. Jouy, M. Beck, and J. Faist, "Evidence of Linear Chirp in Mid-Infrared Quantum Cascade Lasers", Optica **5**, 948 (2018).

[26] P. Täschler, M. Bertrand, B. Schneider, M. Singleton, P. Jouy, F. Kapsalidis, M. Beck, and J. Faist, "Femtosecond Pulses from a Mid-Infrared Quantum Cascade Laser", Nat. Photonics **15**, 919 (2021).

[27] M. Bagheri, C. Frez, L. A. Sterczewski, I. Gruidin, M. Fradet, I. Vurgaftman, C. L. Canedy, W. W. Bewley, C. D. Merritt, C. S. Kim, M. Kim, and J. R. Meyer, "Passively Mode-Locked Interband Cascade Optical Frequency Combs", Sci. Rep. **8**, 3322 (2018).

[28] C. Xiang, J. Liu, J. Guo, L. Chang, R. N. Wang, W. Weng, J. Peters, W. Xie, Z. Zhang, J. Riemensberger, J. Selvidge, T. J. Kippenberg, and J. E. Bowers, "Laser Soliton Microcombs Heterogeneously Integrated on Silicon", Science **373**, 99 (2021).

[29] P. Jouy, J. M. Wolf, Y. Bidaux, P. Allmendinger, M. Mangold, M. Beck, and J. Faist, "Dual Comb Operation of $\lambda \sim 8.2$ µm Quantum Cascade Laser Frequency Comb with 1 W Optical Power", Appl. Phys. Lett. **111**, 141102 (2017).

[30] A. Ruehl, A. Gambetta, I. Hartl, M. E. Fermann, K. S. E. Eikema, and M. Marangoni, "Widely-Tunable Mid-Infrared Frequency Comb Source Based on Difference Frequency Generation", Opt. Lett. **37**, 2232 (2012).

[31] A. Gambetta, N. Coluccelli, M. Cassinerio, D. Gatti, P. Laporta, G. Galzerano, and M. Marangoni, "Milliwatt-Level Frequency Combs in the 8–14 Mm Range via Difference Frequency Generation from an Er: Fiber Oscillator", Opt. Lett. **38**, 1155 (2013).

[32] K. Krzempek, D. Tomaszewska, A. Głuszek, T. Martynkien, P. Mergo, J. Sotor, A. Foltynowicz, and G. Soboń, "Stabilized All-Fiber Source for Generation of Tunable Broadband f_{CEO}-Free Mid-IR Frequency Comb in the 7 – 9 µm Range", Opt. Express **27**, 37435 (2019).

[33] T. Nakamura, V. Ramaiah Badarla, K. Hashimoto, P. G. Schunemann, and T. Ideguchi, "Simple Approach to Broadband Mid-Infrared Pulse Generation with a Mode-Locked Yb-doped Fiber Laser", Opt. Lett. **47**, 1790 (2022).

[34] I. Pupeza, D. Sánchez, J. Zhang, N. Lilienfein, M. Seidel, N. Karpowicz, T. Paasch-Colberg, I. Znakovskaya, M. Pescher, W. Schweinberger, V. Pervak, E. Fill, O. Pronin, Z. Wei, F. Krausz, A. Apolonski, and J. Biegert, "High-Power Sub-Two-Cycle Mid-Infrared Pulses at 100 MHz Repetition Rate", Nat. Photonics **9**, 721 (2015).

[35] S. Vasilyev, I. S. Moskalev, V. O. Smolski, J. M. Peppers, M. Mirov, A. V. Muraviev, K. Zawilski, P. G. Schunemann, S. B. Mirov, K. L. Vodopyanov, and V. P. Gapontsev, "Super-Octave Longwave Mid-Infrared Coherent Transients Produced by Optical Rectification of Few-Cycle 2.5-µm Pulses", Optica **6**, 111 (2019).

[36] K. Iwakuni, G. Porat, T. Q. Bui, B. J. Bjork, S. B. Schoun, O. H. Heckl, M. E. Fermann, and J. Ye, "Phase-Stabilized 100 mW Frequency Comb near 10 µm", Appl. Phys. B **124**, 128 (2018).

[37] N. Hoghooghi, S. Xing, P. Chang, D. Lesko, A. Lind, G. Rieker, and S. Diddams, "Broadband 1-GHz Mid-Infrared Frequency Comb", Light Sci. Appl. **11**, 264 (2022).

[38] A. S. Kowligy, D. R. Carlson, D. D. Hickstein, H. Timmers, A. J. Lind, P. G. Schunemann, S. B. Papp, and S. A. Diddams, "Mid-Infrared Frequency Combs at 10 GHz", Opt. Lett. **45**, 3677 (2020).

[39] Q. Lu, D. Wu, S. Slivken, and M. Razeghi, "High Efficiency Quantum Cascade Laser Frequency Comb", Sci. Rep. **7**, 43806 (2017).

[40] H. R. Telle, G. Steinmeyer, A. E. Dunlop, J. Stenger, D. H. Sutter, and U. Keller, "Carrier-Envelope Offset Phase Control: A Novel Concept for Absolute Optical Frequency Measurement and Ultrashort Pulse Generation", Appl. Phys. B **69**, 327 (1999).

[41] P. Del'Haye, O. Arcizet, M. L. Gorodetsky, R. Holzwarth, and T. J. Kippenberg, "Frequency Comb Assisted Diode Laser Spectroscopy for Measurement of Microcavity Dispersion", Nat. Photonics **3**, 529 (2009).

[42] A. Nishiyama, D. Ishikawa, and M. Misono, "High Resolution Molecular Spectroscopic System Assisted by an Optical Frequency Comb", J. Opt. Soc. Am. B **30**, 2107 (2013).

[43] F. Cappelli, G. Campo, I. Galli, G. Giusfredi, S. Bartalini, D. Mazzotti, P. Cancio, S. Borri, B. Hinkov, J. Faist, and P. De Natale, "Frequency Stability Characterization of a Quantum Cascade Laser Frequency Comb", Laser Photonics Rev. **10**, 623 (2016).

[44] L. Tombez, S. Schilt, J. Di Francesco, P. Thomann, and D. Hofstetter, "Temperature Dependence of the Frequency Noise in a Mid-IR DFB Quantum Cascade Laser from Cryogenic to Room Temperature", Opt. Express **20**, 6851 (2012).

[45] A. Shehzad, P. Brochard, R. Matthey, F. Kapsalidis, M. Shahmohammadi, M. Beck, A. Hugi, P. Jouy, J. Faist, T. Südmeyer, and S. Schilt, "Frequency Noise Correlation between the Offset Frequency and the Mode Spacing in a Mid-Infrared Quantum Cascade Laser Frequency Comb", Opt. Express **28**, 8200 (2020).

Chapter 2

Coherently-Averaged Dual Comb Spectroscopy

At the moment, DCS [1] is the most common use of MIR QCL combs, with the existence of commercial products sold by Irsweep AG. This is due to the hardly-matched ability of QCL-based DCS to make broadband MIR measurements with microsecond time resolutions. This unprecedented capability matched existing needs in various fields, notably chemistry and biology [2, 3].

The commercial spectrometers use free-running lasers with an involved software for computational correction, such as computational coherent averaging [4]. This solution is suitable for many applications, but has two main disadvantages. The software requires large computing power and the computing time reduces the measurement duty-cycle, i.e., either the results are not available right away or the measurements have to wait that the computation is complete before continuing [5]. These drawbacks are especially important for DCS with QCLs, due to the large typical RF bandwidth compared to other frequency comb sources.

Another option is to mutually lock the lasers to obtain stable and periodic time domain signals that can be coherently averaged in real-time, i.e., the signal is co-added so that only the periodic component remains [6, 7]. The result is a short signal comprising only one period whereas the noise has been reduced according to the total measurement time. The advantage of this option is that the computational part is straightforward and quick, i.e. can be done in real time. Moreover, mutual locking is an intermediate step towards stabilization to a reference which is a further step in taming QCL FCs (chapter 4).

In a first work published in Optics Express [8] and patented [9], we demonstrated the mutual stabilization of QCLs and the coherent averaging of the DCS signal in a proof of principle experiment. The publication is reproduced at the end of the chapter with permission from the publisher. Here is a short summary of the article.

2.1 Summary of the article

Partial locks (i.e. only one degree of freedom) of QCL combs had been shown before [10, 11], but a full lock had only been shown for THz QCLs [12]. Therefore, we devised a scheme for the full mutual locking (see Fig. 1). In particular, we developed a QCL-specific solution for the mutual lock of the repetition rate difference which does not require costly low noise 10 GHz synthesizers. The phase noise measurements [see Fig. 2(a)] proved that all comb lines were phase-locked, while also showing that the actuation bandwidth was insufficient to achieve a high purity lock (see chapter 3). We therefore developped an analog scheme for common mode noise subtraction (CMNS, Fig. 6) which was effective in reducing the phase noise of all comb lines [see Fig. 3(a)]. Finally, we characterized spectroscopic results in terms of Allan-Werle variance and compared the free-running (corrected with a basic algorithm) to the mutually-stabilized system [Fig. 5(a,b)]. The comparison showed that the spectroscopic performances are similar.

2.2 Further discussion

2.2.1 Locking bandwidth

After this work was over, I realized that the locking bandwidth had not been solely limited by the internal dynamics of the QCL when working on the stabilization of QCLs using NIR light (see chapter 3). The laser driver and the phase detection unit also did contribute to decreasing the bandwidth from approximately 400 kHz to the measured 150 kHz.

2.2.2 Phase noise dependence on the comb line

We commented in the paper that the residual phase noise increased with the offset from the locked line. This is expected and follows from the phase coherence of the comb as also demonstrated in different ways in [13–15]. However, the increase in phase noise was larger than it should, had it originated only from the synthesizer. I suspect that the excess noise originates in the imperfect injection locking, due to insufficient RF power. The study of the phase noise as a function of comb lines at different RF injection power could give more insights in the phase locking performances of RF injection locking.

2.2.3 Repetition rate difference

We had used two lasers with a repetition rate difference of about 45 MHz, which is much larger than usual values on the order of 5 MHz. The reason was simply that we did not have a matched pair of lasers. The large difference in repetition rates made it easier to filter out a single beat thanks to the excess bandwidth. That being said, I expect that reducing the mismatch to 5 MHz would have still been possible with only minor adaptations. Further reduction of the mismatch would at some point require an auxiliary laser [16] for optically filtering the two comb lines to be phase locked.

For the mutual lock of the repetition rate, care would be required to achieve a high sideband suppression in the frequency shifting process in the case of a small difference of repetition rate. A double shifting process, e.g. shifting by +105 MHz and shifting by -100 MHz, could be applied with a pair of narrow bandpass filters. Alternatively, a voltage controlled oscillator phase locked to the repetition rate of the master QCL with the correct frequency offset could generate the signal to be injected in the follower QCL.

2.2.4 Subsampling of the multiheterodyne signal

While working on this project, I also investigated the use of a RF frequency comb to down-sample the multiheterodyne beat. This works similarly to subsampling via aliasing [17], with the objective to reduce the sampling frequency of the digitizer. In our case, we mixed the RF frequency comb with the multiheterodyne beat in order to reduce the effective repetition rate mismatch to a synthetic value between 100 kHz and 2 MHz. We removed these results during the review process, because although the scheme worked, more investigations would have been required to properly assess the performances.

2.3 Conclusion

We developed a mutual locking scheme for MIR QCLs combs, demonstrated coherent averaging, and characterized its positive implications for the signal-to-noise ratio (SNR). Besides, this work revealed the phase noise dependence on the comb line, which is an important characteristic for comb applications requiring high spectral purity. This work is important for highly-sensitive MIR

DCS as well as for the development of further mutual stabilization techniques, in particular, on ways to achieve high spectral purity without correction schemes, which is discussed in the next chapter.

References

[1] I. Coddington, N. Newbury, and W. Swann, "Dual-Comb Spectroscopy", Optica **3**, 414 (2016).

[2] E. Lins, S. Read, B. Unni, S. M. Rosendahl, and I. J. Burgess, "Microsecond Resolved Infrared Spectroelectrochemistry Using Dual Frequency Comb IR Lasers", Anal. Chem. **92**, 6241 (2020).

[3] J. L. Klocke, M. Mangold, P. Allmendinger, A. Hugi, M. Geiser, P. Jouy, J. Faist, and T. Kottke, "Single-Shot Sub-microsecond Mid-infrared Spectroscopy on Protein Reactions with Quantum Cascade Laser Frequency Combs", Anal. Chem. **90**, 10494 (2018).

[4] L. A. Sterczewski, J. Westberg, and G. Wysocki, "Computational Coherent Averaging for Free-Running Dual-Comb Spectroscopy", Opt. Express **27**, 23875 (2019).

[5] M. Gianella, S. Vogel, K. Komagata, J. Hillbrand, F. Kapsalidis, B. Tuzson, A. Nataraj, M. Beck, A. Hugi, M. Mangold, P. Jouy, T. Südmeyer, J. Faist, and L. Emmenegger, "Gapless High-Resolution QCL Dual-Comb Spectroscopy with Real-Time Data Processing for Dynamic Gas-Phase Measurements", in 2021 Conference on Lasers and Electro-Optics Europe and European Quantum Electronics Conference (June 21, 2021), Paper Ed_1_5.

[6] O. Rompelman and H. H. Ros, "Coherent Averaging Technique: A Tutorial Review Part 1: Noise Reduction and the Equivalent Filter", J. Biomed. Eng. **8**, 24 (1986).

[7] Z. Chen, M. Yan, T. W. Hänsch, and N. Picqué, "A Phase-Stable Dual-Comb Interferometer", Nat. Commun. **9**, 3035 (2018).

[8] K. Komagata, A. Shehzad, G. Terrasanta, P. Brochard, R. Matthey, M. Gianella, P. Jouy, F. Kapsalidis, M. Shahmohammadi, M. Beck, V. J. Wittwer, J. Faist, L. Emmenegger, T. Südmeyer, A. Hugi, and S. Schilt, "Coherently-Averaged Dual Comb Spectrometer at 7.7 µm with Master and Follower Quantum Cascade Lasers", Opt. Express **29**, 19126 (2021).

[9] S. Schilt, P. Brochard, K. Komagata, G. Terrasanta, and A. Hugi, "Dual-Comb Spectroscopy", U.S. pat. 20220146312A1 (Irsweep AG, May 12, 2022).

[10] F. Cappelli, G. Campo, I. Galli, G. Giusfredi, S. Bartalini, D. Mazzotti, P. Cancio, S. Borri, B. Hinkov, J. Faist, and P. De Natale, "Frequency Stability Characterization of a Quantum Cascade Laser Frequency Comb", Laser Photonics Rev. **10**, 623 (2016).

[11] J. Westberg, L. A. Sterczewski, and G. Wysocki, "Mid-Infrared Multi-heterodyne Spectroscopy with Phase-Locked Quantum Cascade Lasers", Appl. Phys. Lett. **110**, 141108 (2017).

[12] L. Consolino, M. Nafa, F. Cappelli, K. Garrasi, F. P. Mezzapesa, L. Li, A. G. Davies, E. H. Linfield, M. S. Vitiello, P. De Natale, and S. Bartalini, "Fully Phase-Stabilized Quantum Cascade Laser Frequency Comb", Nat. Commun. **10**, 2938 (2019).

[13] G. Villares, A. Hugi, S. Blaser, and J. Faist, "Dual-Comb Spectroscopy Based on Quantum-Cascade-Laser Frequency Combs", Nat. Commun. **5**, 5192 (2014).

[14] M. Singleton, P. Jouy, M. Beck, and J. Faist, "Evidence of Linear Chirp in Mid-Infrared Quantum Cascade Lasers", Optica **5**, 948 (2018).

[15] F. Cappelli, L. Consolino, G. Campo, I. Galli, D. Mazzotti, A. Campa, M. Siciliani de Cumis, P. Cancio Pastor, R. Eramo, M. Rösch, M. Beck, G. Scalari, J. Faist, P. De Natale, and S. Bartalini, "Retrieval of Phase Relation and Emission Profile of Quantum Cascade Laser Frequency Combs", Nat. Photonics **13**, 562 (2019).

[16] T. Ideguchi, A. Poisson, G. Guelachvili, N. Picqué, and T. W. Hänsch, "Adaptive Real-Time Dual-Comb Spectroscopy", Nat. Commun. **5**, 3375 (2014).

[17] L. A. Sterczewski and M. Bagheri, "Subsampling Dual-Comb Spectroscopy", Opt. Lett. **45**, 4895 (2020).

Research Article | Vol. 29, No. 12 / 7 June 2021 / *Optics Express* 19126
Optics EXPRESS

Coherently-averaged dual comb spectrometer at 7.7 µm with master and follower quantum cascade lasers

K. KOMAGATA,[1,*] A. SHEHZAD,[1] G. TERRASANTA,[2] P. BROCHARD,[1] R. MATTHEY,[1] M. GIANELLA,[3] P. JOUY,[2] F. KAPSALIDIS,[4] M. SHAHMOHAMMADI,[4] M. BECK,[4] V. J. WITTWER,[1] J. FAIST,[4] L. EMMENEGGER,[3] T. SÜDMEYER,[1] A. HUGI,[2] AND S. SCHILT[1]

[1] *Laboratoire Temps-Fréquence, Institut de Physique, Université de Neuchâtel, Avenue de Bellevaux 51, 2000 Neuchâtel, Switzerland*
[2] *IRsweep AG, Laubisrütistrasse 44, 8712 Stäfa, Switzerland*
[3] *Empa, Laboratory for Air Pollution / Environmental Technology, 8600 Dübendorf, Switzerland*
[4] *Institute for Quantum Electronics, ETH Zurich, 8093 Zurich, Switzerland*
[*] *kenichi.komagata@unine.ch*

Abstract: We demonstrate coherent averaging of the multi-heterodyne beat signal between two quantum cascade laser frequency combs in a master-follower configuration. The two combs are mutually locked by acting on the drive current to control their relative offset frequency and by radio-frequency extraction and injection locking of their intermode beat signal to stabilize their mode spacing difference. By implementing an analog common-noise subtraction scheme, a reduction of the linewidth of all heterodyne beat notes by five orders of magnitude is achieved compared to the free-running lasers. We compare stabilization and post-processing corrections in terms of amplitude noise. While they give similar performances in terms of signal-to-noise ratio, real-time processing of the stabilized signal is less demanding in terms of computational power. Lastly, a proof-of-principle spectroscopic measurement was performed, showing the possibility to reduce the amount of data to be processed by three orders of magnitude, compared to the free-running system.

© 2021 Optical Society of America under the terms of the OSA Open Access Publishing Agreement

1. Introduction

In recent years, dual comb spectroscopy (DCS) has emerged as a new solution for fast and broadband spectroscopy [1]. Mid-infrared (MIR) quantum cascade laser (QCL) frequency combs [2] are an appealing and thriving technology for DCS [3,4], as they cover strong spectroscopic absorption bands of many relevant molecules in the MIR region. Dual QCL comb spectrometers have become commercially available as a table-top instrument, which is leading to new discoveries in many fields of science including biology and chemistry [5–12]. One key advantage of QCL-based DCS is the ability to perform studies with up to sub-microsecond time-resolution [11].

Moreover, QCL combs are very compact electrically-driven semiconductor light sources. Their longitudinal modes can be locked together through a four-wave mixing process [2] similar to the case of micro-resonator combs [13], leading to an equidistant comb spectrum, but which is not associated to the generation of soliton pulses in contrast to micro-resonators. QCLs do not require optical pumping, in contrast to other optical frequency comb (OFC) sources, which are based on optically-pumped gain [14] or nonlinear materials [15]. Thus, the comb properties can be directly controlled through the laser driving current, the chip temperature [3] or by radio-frequency (RF) injection of the repetition frequency [16–18]. These are key advantages for system integration.

#425480 https://doi.org/10.1364/OE.425480
Journal © 2021 Received 7 Apr 2021; revised 12 May 2021; accepted 18 May 2021; published 4 Jun 2021

Furthermore, the control with the laser driving current and by RF injection is fast, enabling high locking bandwidths to be achieved or the possibility of fast frequency scanning of the comb spectrum [4].

In state-of-the-art DCS with MIR QCL combs, the multi-heterodyne beat signal is typically composed of 100 to 250 lines and spans an RF bandwidth of 400 MHz to 900 MHz [3,4,8,19,20]. The linewidth of the optical modes in free-running operation is in the megahertz range, which is largely sufficient to resolve relevant spectroscopic features in many applications [4,8,11]. The interferogram is then typically digitized with 12-bit to 16-bit resolution at 1.6 GS/s to 2.5 GS/s [3,4,11]. The reported implementations use two detectors for the sample and reference signals, respectively, such that the size of the data to be processed is between 4.8 GB/s and 8 GB/s. As a comparison, with fiber mode-locked lasers in the near-infrared (NIR), the data rate is on the order of 400 MB/s [1] with typically more than 100'000 lines comprised in an RF bandwidth of 50 MHz [21]. We note that NIR fiber mode-locked lasers typically have repetition rates of a few hundred MHz compared to multiple GHz for QCL combs.

The large data rate encountered with QCL DCS is cumbersome for storage and processing, and may lead to low measurement duty cycles. A solution to this issue that is widely used with NIR systems is real-time coherent averaging. Coherent averaging is a processing method used to isolate the periodic components of a signal [22], which can reduce the amount of data to handle in some conditions. Coherent averaging of the digitized signal can be implemented with different (and potentially combined) approaches: full or relative locking of the two combs [23–29], correction of the noise of the multi-heterodyne signal using various types of error signals [21,23,24,30–32], or computational processing without requiring additional information on the system other than the interferogram [33–36]. The last approach has been used with MIR QCL frequency combs, but remains challenging to implement in real-time due to the large data rate, even if recent works have shown that it is possible using adequate hardware and parallel processing on graphics processing unit (GPU) [37].

Regarding the two other approaches that are routinely used with NIR lasers (i.e., full or relative locking of the two combs, correction using error signals), the known solutions cannot be implemented in a straightforward manner with MIR QCL-based DCS because of the lack or poorer availability of required optical components in the MIR. Moreover, the specificity of QCLs is also an opportunity to implement other techniques to achieve a mutual lock between the two combs, such as RF injection locking. Although the mutual lock of one degree of freedom between two QCL combs has been reported [38], it has not been the case so far for a full mutual lock to the best of our knowledge. One further interest to apply a mutual lock is that it represents an intermediate step towards a full independent stabilization of the two combs, which is highly desirable in a high-resolution spectrometer [4].

In this work, we mutually locked a pair of QCL combs in their two degrees of freedom in a master-follower scheme (also known as master-slave scheme). To further reduce the relative offset-frequency fluctuations, a common-mode noise subtraction (CMNS) scheme was implemented as an alternative approach from Refs. [21,39]. This allowed us to perform coherent averaging of the spectroscopic signal, and to compare those performances with post-processing corrections using the signal from the reference photodiode.

The outline of the paper is as follows: The experimental setup with the implemented relative frequency stabilization and noise compensation scheme is described in Section 2. The performance of the system in terms of frequency stability is reported in Section 3 and a proof-of-principle spectroscopic demonstration with coherent averaging is presented in Section 4. Finally, Section 5 presents the conclusion and outlook of this work.

2. Experimental setup

In this section, we describe the experimental setup of our DCS system. Notably, we implemented a mutual lock of two QCL combs. We used an all-RF scheme to further lower the phase fluctuations of the interferogram and remove its offset frequency in order to fulfill the conditions necessary for coherent averaging, which is to have a harmonic comb in which the frequency of each comb line is an exact multiple of their spacing.

2.1. Dual QCL comb system

The experimental setup implemented for dual-QCL-comb spectroscopy and frequency stabilization of the multi-heterodyne signal is schematized in Fig. 1. Two mid-infrared QCL combs emitting in the 8-μm spectral range are heterodyned on two fast photodiodes (Vigo models PV-3TE-10.6-0.05 × 0.05 and PV-4TE-10.6-0.1 × 0.1 with 1-GHz bandwidth) for sample and reference measurements. The sample is placed in one of the combined beam paths for absorption DCS, whereas the signal from the second detector is used for normalization.

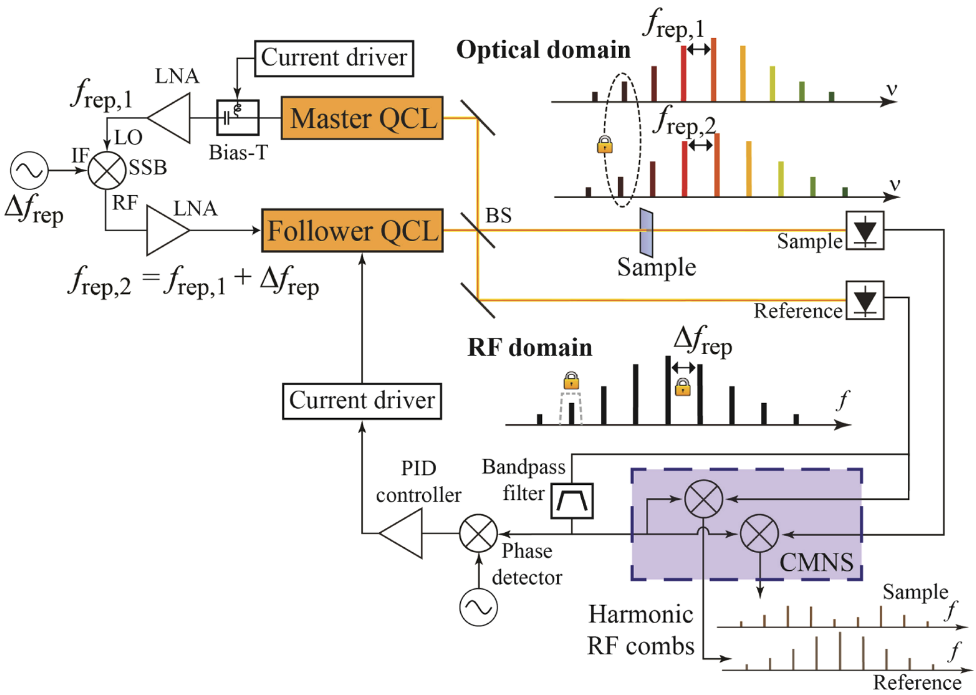

Fig. 1. DCS setup and master-follower stabilization. Two QCL combs are heterodyned on two photodiodes (reference and measurement channels), leading to RF combs in the photodiode output signals. The injection of the frequency-shifted intermode beat frequency from the master to the follower QCL locks the mode spacing of the RF comb. In addition, an optical line of the follower QCL comb is locked to one line of the master QCL comb by stabilizing the frequency of their heterodyne beat. The beat frequency is compared in phase to a reference oscillator and a correction signal is fed back to the follower QCL as a modulation of the driving current. The common-mode noise subtraction scheme (CMNS) is schematized in the dashed box and is described in detail in the Appendix. LNA: low noise amplifier, SSB: single sideband mixer.

The first QCL acts as a master comb. It is operated at a temperature of 23°C and is driven at an average current of ∼1420 mA. The resulting comb spectrum centered around 1275 cm^{-1} spans over about 40 cm^{-1}. The spacing between the comb modes is $f_{rep,1}$ = 9.70 GHz. The beating of the modes in the laser cavity modulates the current in the QCL and produces a so-called intermode beat signal at $f_{rep,1}$ [40]. A bias-tee is used to enable simultaneous direct current drive of the QCL and RF extraction of the electrical intermode beat signal. The extracted signal has a power of roughly −80 dBm. The second QCL acts as a follower laser that is phase-locked to the master to achieve their relative stabilization (see Section 2.2). It is operated at ~1050 mA and 24°C and emits a comb spectrum spanning from 1290 cm^{-1} to 1300 cm^{-1}. Its mode spacing is typically 45 MHz higher than for the master QCL. The operation points of the two QCLs are slightly varied depending on the time of the measurement to ensure a low-noise comb operation for each of them (characterized by a narrow intermode beat signal < 10 kHz), as the same operating point did not always result in the same comb state. The comb state is also chosen to limit the bandwidth of the generated multi-heterodyne beat signal, shown in Fig. 2, to less than 1 GHz with approximately 15 comb lines (11 lines in a 25-dB bandwidth). The incident power on the photodiodes is attenuated to approximately 1 mW with neutral density filters and wire grid polarizers. The follower QCL is mounted in a dedicated package with an RF port connected to the laser that is distinct from the driving current port and is optimized for efficient RF extraction/injection. Injecting an RF signal with a frequency that is close to the native mode spacing of the QCL can force it to operate at the injected frequency (RF injection locking), therefore locking its mode spacing [2,16–18].

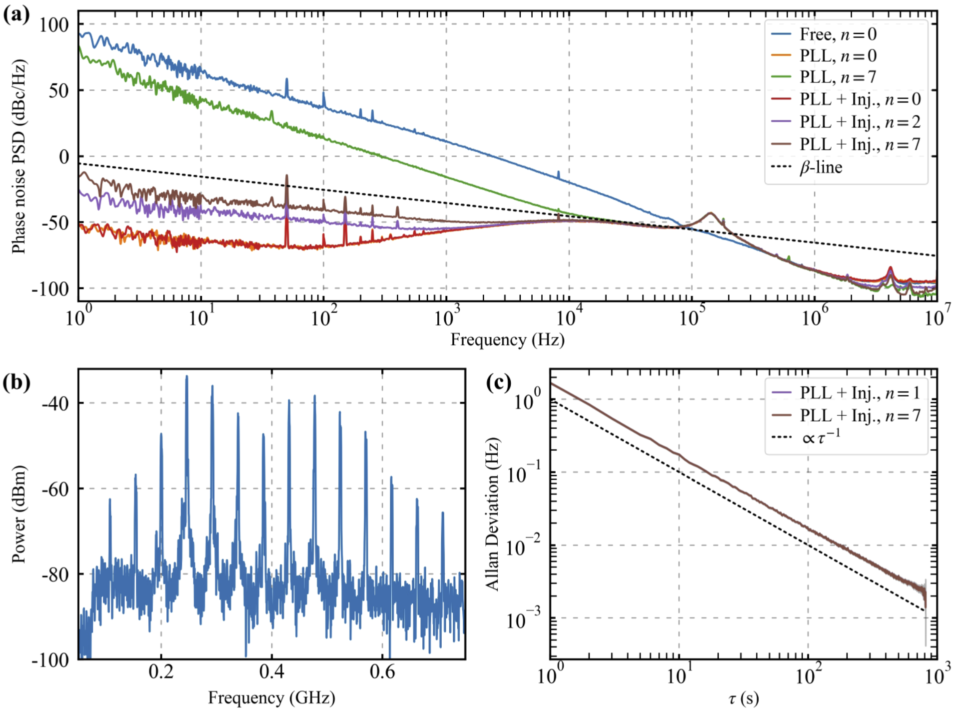

Fig. 2. Evaluation of the master-follower stabilization. (a) Phase noise PSD of different lines of the RF comb in the free-running case (Free), with the PLL activated (PLL) or with both PLL and RF injection locking (PLL + Inj.). The orange line (PLL only for $n = 0$) is almost exactly hidden by the red line (PLL + Inj. for $n = 0$). (b) Typical spectrum of the multi-heterodyne beat. The exact shape may vary. (c) Allan deviation of the frequency of two different lines that show a high overlap.

2.2. Master-follower QCL stabilization

RF injection is used to lock one degree of freedom of the follower QCL to the master QCL. This is achieved by extracting the intermode beat signal from the master QCL using a bias-tee. The extracted signal is then amplified, up-shifted by approximately 45 MHz using a single sideband (SSB) mixer and injected in the follower QCL after further amplification to ~5 dBm. To achieve a full relative phase lock of the follower QCL to the master QCL, its second degree of freedom is stabilized by phase-locking one line of the multi-heterodyne beat signal to a reference RF oscillator. A comb line at ~200 MHz in the reference RF comb is filtered with a narrowband filter and compared in phase to a reference oscillator in a digital phase detector (DXD200 from Menlo Systems). The resulting phase error signal is amplified in a proportional-integral-derivative (PID) servo-controller (Vescent D2-125) and corrects the follower QCL by feedback to the driving current. All electronic oscillators used in the locking scheme are referenced to a hydrogen maser to ensure their long-term stability.

2.3. Common mode noise subtraction scheme

An analog CMNS scheme is used to remove the offset frequency of the RF combs and the remaining common frequency noise among their lines [21,39]. Removing the offset frequency is necessary for coherent averaging [24]. The principle is to isolate one spectral line of the multi-heterodyne signal and to mix it with the entire RF comb to produce their frequency difference. The resulting RF comb is offset-free, i.e., it constitutes a harmonic comb, in which the common noise between all lines has been furthermore removed. We implemented a different CMNS scheme than reported in Refs. [21,39], which is described in the Appendix. We note that unlike Ref. [21], this scheme does not require additional optical components, which is possible as the RF comb modes are well resolved.

3. Evaluation of the stabilization schemes

3.1. Master-follower stabilization

The master-follower scheme described in Fig. 1 was implemented by first stabilizing one line of the RF comb at 200 MHz to a reference signal using a phase-lock loop (PLL). The phase noise of different lines of the reference RF comb was measured using a phase noise analyzer (Rohde & Schwarz FSWP-26) and is displayed in Fig. 2(a). The line $n = 0$ at 200 MHz used for the phase-lock shows a noise reduction of 140 dBc/Hz at 1-Hz Fourier frequency as a result of the stabilization. The locking bandwidth is 100 kHz, assessed from the servo bump in the noise spectrum. Other lines, e.g., $n = 7$ (the 7^{th} line from the locked line) showed only ~15 dBc/Hz noise reduction when solely the PLL was activated. The remaining noise likely results from the relative frequency fluctuations between the mode spacing of the two QCL combs.

In a second step, we added a relative stabilization between the mode spacing of the two QCL combs by RF extraction/injection as described in Section 2.2. The locking range was in the order of 200 kHz, enabling small tuning of Δf_{rep}. The RF injection sometimes led to a state change of the follower comb. We believe that the injection of the RF power heats the laser, which can cause a change of state.

With the combined RF injection locking of the mode spacing of the follower QCL and phase-lock of the RF comb line at 200 MHz, the other lines of the multi-heterodyne spectrum showed a large phase noise reduction compared to the case of the PLL only [see Fig. 2(a)]. We used the β-separation line approximation [41] to estimate the linewidth of the RF comb modes from their corresponding phase noise power spectral density (PSD). The free-running linewidth of 1 MHz (at 1-s integration time) calculated for the line $n = 0$ is reduced to 700 kHz with the master-follower stabilization scheme. This marginal linewidth reduction relative to the large decrease observed for the phase noise PSD results from the phase noise bump added by the

Optics EXPRESS

PLL, which has a large impact on the linewidth as it occurs at high Fourier frequencies (~100 kHz) [42].

Even with RF injection-locking of the mode spacing, the phase noise of the RF comb modes at Fourier frequencies between 1 Hz and 1 kHz increases with the mode index. We infer that that it is due to the residual noise of the mode spacing difference Δf_{rep} between the two QCL combs. Neglecting the correlations between the frequency fluctuations of Δf_{rep} and of the locked line frequency f_0, the frequency noise (FN) PSD of Δf_{rep} can be estimated as $S_{f_{\text{rep}}} = (S_0 - S_n)/n^2$, where S_0 and S_n are the FN-PSD of the locked line f_0, and of the analyzed line of index n, respectively. The results are consistent when computed from lines 1, 3, and 6 [data from Fig. 3(a)], leading to an FN-PSD of Δf_{rep} of $5.3 \cdot 10^{-4}$ Hz^2/Hz at 1-Hz Fourier frequency.

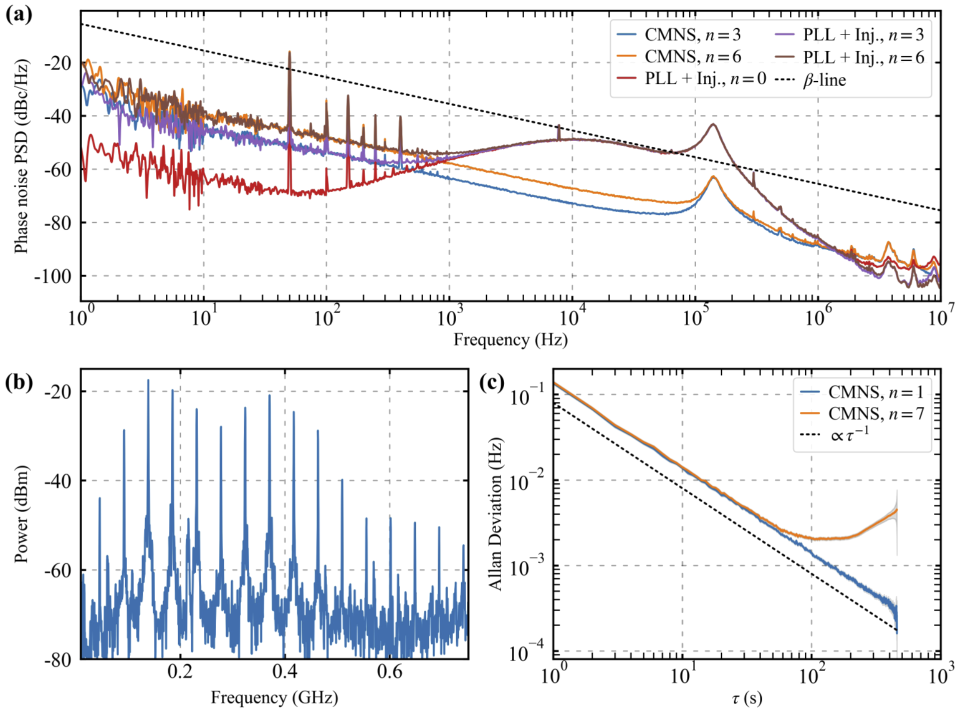

Fig. 3. Evaluation of the CMNS. (a) Phase noise PSD of different lines of the RF comb in the master-follower configuration with CMNS and without (PLL + Inj.). (b) Typical spectrum of the multi-heterodyne beat. The exact shape may vary. (c) Allan deviation of two different lines of the RF comb.

The long-term frequency stability of the fully-stabilized RF comb was investigated by measuring the frequency of different lines using a multi-channel Π-type frequency counter (FXM-50 from Menlo Systems). Lines $n = 1$ and $n = 7$ were frequency down-converted to < 50 MHz within the counter bandwidth so that they can be simultaneously measured. Allan deviations calculated from the recorded time series of these lines show Hz-level fluctuations at 1-s averaging time, averaging down to below 10 mHz at integration times longer than 200 s [see Fig. 2(c)].

3.2. Common-mode noise subtraction

The phase noise of the RF comb lines was further lowered using the CMNS scheme in addition to the mutual stabilization. The frequency fluctuations of the phase-locked RF comb line at ~200 MHz were subtracted from the entire comb spectrum as described in Section 2.3.

The noise-compensated spectrum displayed in Fig. 3(b) has the same overall envelope as the original one within 3 dB. This does not compromise spectroscopic measurements to be achieved, even if the sample and reference measurements can be affected slightly differently, as a time-sequential calibration scheme is usually used in QCL DCS (sample and background spectra successively measured) [4]. Furthermore, the reference channel is mainly used for amplitude noise compensation by normalization. Some spurious weaker lines appear between the main comb lines in the common-noise-compensated spectrum, resulting from different mixing products that may occur in the noise compensation scheme. These spurious lines are not problematic as their contribution to the processed spectrum is made negligible by the coherent averaging process.

The phase noise measured for lines $n = 3$ and $n = 6$ of the noise-compensated spectrum is displayed in Fig. 3(a). These lines correspond to components at 342 MHz and 485 MHz of the initial RF comb and are shifted to 142 MHz and 285 MHz by the CMNS scheme, with $\Delta f_{rep} =$ 47.46 MHz. A strong reduction of the phase noise of all modes is observed in the frequency range of 1 kHz to 1 MHz that was weakly affected by the PLL. At low Fourier frequencies below ~1 kHz, the phase noise of all lines coincides with the level achieved with the PLL and RF injection scheme alone. This results from the residual noise of the comb mode spacing, as shown in Section 3.1. A linewidth of 10 Hz, which mainly originates from the contribution of 50-Hz noise components, is obtained for the RF comb line n =3 with both master-follower and CMNS schemes. As the free-running linewidth of 1 MHz was reduced to only 700 kHz by the mutual stabilization between the two QCL combs, the CMNS brings a linewidth reduction of the RF comb lines by almost 5 orders of magnitude (from 700 kHz to 10 Hz).

The long-term frequency stability of the harmonic RF comb obtained with the CMNS was also assessed by recording the frequency of two lines $n = 1$ and $n = 7$ using a frequency counter and by processing the corresponding Allan deviation (see Fig. 3(c)). We observed sub-Hz frequency fluctuations at 1-s integration time for both lines. At a longer averaging time of 200 s, the frequency stability reaches a sub-mHz level for the line $n = 1$, while the other line achieves a value of 3 mHz. We believe that the increase of the Allan deviation observed for averaging times longer than 100 s is due to an improper referencing of the synthesizer used to frequency down-convert the line $n = 7$ to fit in the frequency range of the frequency counter. However, the achieved stability is fully suitable for the implementation of coherent averaging.

4. Proof-of-principle spectroscopic measurement with coherent averaging

We compared multiple measurements of the dual comb multi-heterodyne beat signal with and without stabilization. The former includes the full mutual lock between the two QCL combs and the CMNS scheme. We acquired time traces of the sample and reference signals at 2 GS/s and 16-bit resolution using the acquisition unit of the IRis-F1 spectrometer from IRsweep. The measurements are limited by the internal memory to 16-ms acquisition time, corresponding to 2^{25} samples per acquisition and channel. The conditions for coherent averaging requires the interferogram to be offset-free with the spacing between the modes well matched to the sampling rate [24,28]. These conditions also prevent spectral leakage in other systems based on Fourier-transform spectrometers [43]. They are fulfilled with the CMNS that leads to an offset-free RF comb and by setting Δf_{rep} so that 3 interferograms are contained in exactly 128 data samples, corresponding to $\Delta f_{rep} = 46.875$ MHz. However, the data acquisition unit was not referenced to the reference clock during the experiment, such that coherent averaging was limited to measurement times of approximately 100 µs, after which the sampling and the interferogram lose their coherence.

4.1. FFT spectra and coherent averaging

In Fig. 4(a)-(b), we show the fast Fourier transform (FFT) of the 16-ms time trace acquired without frequency stabilization and a zoom on a line. The typical linewidth is in the MHz range. The highest signal-to-noise ratio (SNR) in terms of power spectrum is approximately 50 dB. In Fig. 4(c), we show a fraction of the time trace containing 3 periods with different phase offsets (blue). We also draw the coherently-averaged signal (orange) with 2048 co-added slices of 128 samples. As the conditions for coherent averaging are not fulfilled, the coherently averaged signal averages to zero.

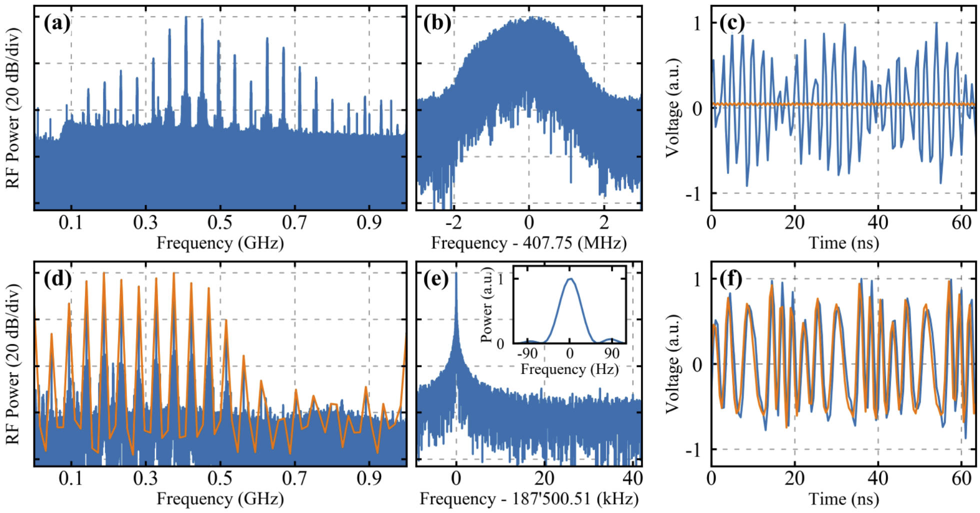

Fig. 4. (a) – (c) DCS results obtained without stabilization nor signal correction of the RF comb. (a) Spectrum obtained from the FFT of a 16-ms time trace. (b) Zoom of a line of panel (a). (c) Example time trace including approximatively 3 periods (blue). The signal averages out to zero when coherent averaging is performed (orange). (d) – (f) DCS results with master-follower and common-mode noise subtraction schemes. (d) Spectrum from a 0.13-ms time trace (blue) compared to that obtained with coherent averaging (orange). (e) Zoom of a comb line from a 16-ms time trace. The inset shows the linewidth of the comb line in linear scale, limited by the measurement time. The signal was zero-padded. (f) Example time trace (blue) compared to the coherent average of 2048 traces (0.13 ms). The phase slip led to losses of the high frequency components.

In Fig. 4(d), we show the FFT of a 130-µs time trace of the noise-compensated signal of the dual comb, and in orange, the spectrum obtained by coherently averaging the same time trace as 2048 slices of 128 samples. As the RF comb is harmonic and three interferograms are contained in 128 samples (Δf_{rep} = 46.875 MHz), every third bin of the spectrum lies on a comb line. We note that the SNR is much higher than in panel (a) even in a 10-times shorter measurement time as a result of the spectral stability. Panel (e) shows a closer view on the 4$^{\text{th}}$ line of the comb. Here the 16-ms signal was zero-padded to show the linewidth below 100 Hz (inset), as limited by the measurement time. The center frequency of 187,500,510 Hz is 510 Hz above the expected value of $4{\cdot}\Delta f_{\text{rep}}$ because of the mismatch between the internal clock of the acquisition unit and the reference clock used in the stabilization scheme. Figure 4(f) compares a single slice containing exactly 3 periods and the coherent average of 2048 slices. We notice a good correspondence, due to the high frequency stability of the RF comb. A difference is induced by the small phase slip occurring between the sampling frequency and Δf_{rep}, which can be seen as a small delay of the average with respect to the single slice, or as a filter on the higher frequency components (fast changes), which are more sensitive to this mismatch.

4.2. Amplitude noise characterization

The fractional Allan deviation $\sigma_a(\tau)$ of the amplitude of different lines was computed for different integration times τ by slicing the time traces into segments of duration τ. For the CMNS, coherent averaging was applied (in the time domain) on each segment using slices of 128 samples and the amplitude of a line was obtained at specified bins of the Fourier transform of the coherently-averaged data, for each segment. A similar computation was performed in the free-running case. However, for a given segment and a given line, the amplitude was obtained by averaging the complex peak amplitudes obtained by a standard peak finder algorithm applied to the Fourier transform of all consecutive slices of 2048 samples contained in the segment. This method is labeled as SFT.

For comparison, computational phase corrections (PC) or phase and amplitude corrections (PAC) were implemented on the signals. For this purpose, the slices were co-averaged in the spectral domain, after the signal bins of the sample photodiode were divided by the phase factor or by the complex amplitude of the respective bin of the reference photodiode. This correction was applied similarly to the complex peak amplitude in the free-running case.

Moreover, to emulate an application where the signal is coherently-averaged in the data acquisition unit without software corrections at short timescales and corrected over longer timescales, we perform the following processing:

1. Segments of 66-µs duration of the signal (1024 slices of 128 samples) are coherently averaged without correction. Each segment is thus condensed into 128 samples by the coherent averaging.
2. We take the Fourier transform of each condensed 128-sample segment.
3. The Fourier transforms of the condensed segments are co-averaged by dividing the signal bins as with the above-mentioned PAC.

We label this method as HCA (hybrid coherent averaging). In practice, it would lead to a reduction by 3 orders of magnitude in the amount of data to be transferred, which could be further improved by referencing the clock of the acquisition unit.

The fractional Allan deviation of the amplitude of selected lines is shown in Fig. 5(a). CMNS with coherent averaging shows an improvement of the fractional amplitude noise as a function of the integration time τ as $\tau^{-1/2}$ (dot-dashed line). However, the phase slip resulting from the clock mismatch introduces a decrease in performance at integration times longer than 1 ms. Moreover, ground loops with noise peak frequencies of ~100 kHz add frequency noise which converts into amplitude noise in Fig. 5(a) at approximately 1-µs averaging times.

When PC or PAC is applied, the Allan deviation decreases as $\tau^{-1/2}$ up to the millisecond-range. These corrections effectively attenuate the effects of phase slips and ground loops. The corrections are also effective for HCA, where the compensation was done at time scales longer than the effect of the noise source. We note that the Allan deviation is computed from integration times of 66 µs for HCA, as it is the shortest time unit available for this processing method. In the free-running case [Fig. 5(b)], PAC corrections enable the same performance to be reached as with the other schemes. The limit in the ms-range is believed to arise from uncorrelated amplitude fluctuations in the signals from the two photodiodes, which originates from mechanical vibrations, e.g. induced by the fan of the photodetectors.

According to the Allan deviation at 8 ms, the short-term noise equivalent absorption (NEA) for the chosen line is estimated to $10^{-5}/\sqrt{\text{Hz}}$ for HCA using the CMNS and master-follower schemes, which is similar to the NEA reported in Ref. [38]. Free-running lasers with PAC yield

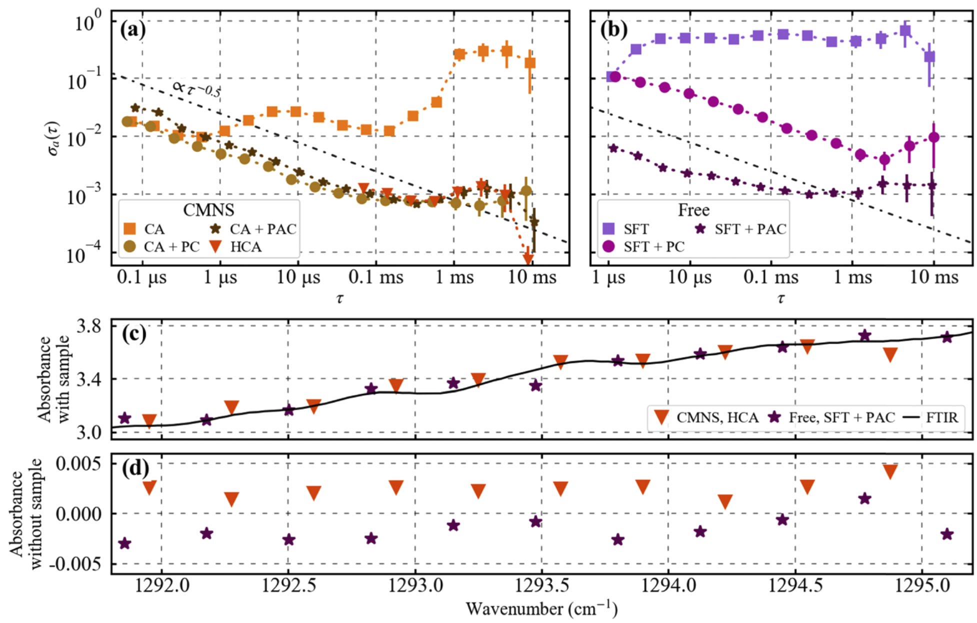

Fig. 5. Fractional amplitude Allan deviation σ_a and spectroscopic results. (a,b) Allan deviation of the amplitude of a selected line. Data points are offset horizontally for clarity. (a) Results with mutual stabilization and CMNS, with coherent averaging (CA), phase (and amplitude) correction (PC/PAC) and hybrid temporal and spectral averaging with correction (HCA). (b) Results without any stabilization of the QCL combs, where the amplitude of the RF comb lines is determined using a peak finder algorithm on Fourier transforms of slices (SFT). (c) Spectroscopic measurement of PP, compared to a spectrum measured with a standard FTIR. (d) Reference measurement with no sample showing accuracy better than 0.005, when the background measurement immediately follows the sample measurement.

approximately one order of magnitude higher NEA. These values are better than the value of $10^{-3}/\sqrt{\text{Hz}}$ reported in Ref. [20], where however the number of spectral components is one order of magnitude higher than in this study.

4.3. Spectroscopic measurements

A proof-of-principle spectroscopic measurement of polypropylene (PP) was made in order to demonstrate the suitability of the implemented schemes. A PP sheet with a thickness of 500 ± 5 µm was placed in the path of the combined QCL beams. The two fast photodiodes were used to provide sample and reference signals, respectively. The two photodiodes have different sensitivities, such that a background measurement was recorded in the absence of the sample to calibrate the respective photodiode signals.

The transmission of a given comb line was calculated as follows

$$T = \left| \frac{A_s B_r}{A_r B_s} \right|, \tag{1}$$

where A_i, B_i are the complex amplitudes of the line of the sample and background measurements, respectively. The subscripts denote the signal from the sample photodiode (s) or from the reference photodiode (r). The absorbance is calculated from the natural logarithm of T.

Results of the DCS experiment are shown in Fig. 5(c) for an acquisition time of 16 ms. We adjusted the frequency axis to match the absorption spectrum measured by DCS to an FTIR reference measurement of the same sample, as no absolute optical frequency reference was available during the experiment to calibrate the optical frequency axis. The CMNS with HCA provides similar results as in free-running operation with PAC. They are consistent with the FTIR measurement within an error in the order of 0.05 in absorbance unit.

In the measurement without PP sample [Fig. 5(d)], two background measurements were performed immediately one after the other and compared using Eq. (1). The standard deviation of the absorbance is 0.0008 and 0.004 for the CMNS and free-running measurements respectively, consistent with the Allan deviation of approximately 0.001 in panels (a) and (b) of Fig. 5. However, a mean offset of 0.0024 and −0.0016, respectively, is observed from the theoretical value of 0 absorbance.

These results show that digital correction of phase noise and amplitude noise of the interferogram gives similar performance, whether the two QCLs are locked together or not. However, the mutual locking and the CMNS enable real time coherent averaging to be applied, which is a key condition to data reduction. Here, coherent averaging was successfully applied over up to 66 µs, which would lead to a data size reduction by 3 orders of magnitude if implemented in real-time. These results were limited by the phase slip of the data acquisition unit. Therefore, we expect that the amount of data can be further reduced by synchronizing the clocks to achieve longer real-time averaging.

5. Conclusion and outlook

We implemented a dual-QCL comb setup in a master-follower configuration. The offset frequency difference between the two combs was corrected by acting on the drive current of the follower QCL, while the repetition frequency difference was locked by electrical extraction from the master QCL, up-shifting, and injection in the follower QCL. We thus showed that two QCL combs can be mutually locked in both degrees of freedom simultaneously.

We observed that the actuation bandwidth for the stabilization of the offset frequency did not allow a significant reduction of the linewidth of the beat notes. Therefore, the frequency noise of the RF comb was further reduced using an all-RF common-mode noise subtraction scheme, which strongly reduced the common phase noise at Fourier frequencies between 1 kHz and 1 MHz.

These steps enabled fast and efficient sampling of the harmonic RF comb through coherent averaging using a minimum number of optical components for DCS. This allowed for reduced data handling and computational time in a proof-of-principle experiment, which promises real-time computation of the absorption spectra. It was shown that the amplitude noise of the comb lines is similar for both the frequency-stabilized and free-running systems, if computational corrections are implemented. The achieved short-term noise equivalent absorption is comparable with other studies such as reported in Ref. [38]. Therefore, the main motivation for the implemented mutual stabilization is to enable real-time data processing.

We expect that the multiple methods presented in this work will benefit QCL-based DCS by enabling more accurate measurements, owing to the increased possible averaging time. Also, the relative lock between the two QCLs is a steppingstone to a fully-referenced dual QCL comb system, where additionally, the accuracy of the frequency grid can be improved by the use of an optical reference in the mid-infrared.

The CMNS and the master-follower stabilization could be integrated in existing commercial systems, offering higher quality dual comb spectrometers. A next step is to apply the methods while scanning the offset frequency of the QCL combs to perform gapless spectroscopic measurements [4], where the challenge resides in the change of repetition rates during the scan.

Appendix

Common-mode noise subtraction scheme

An analog common-mode noise subtraction (CMNS) scheme is used to remove the offset frequency of the RF combs and the remaining common noise among their lines. The principle is to isolate one spectral line and to mix it with the entire RF comb to produce their frequency difference. The resulting RF comb is offset-free, i.e., it constitutes a harmonic comb, in which the common noise between all lines is removed. In practice, an RF mixer outputs both the sum and difference frequency of the input signals, resulting in two RF combs shifted from each other. SSB mixers, which produce only either the sum (SSB+) or the difference (SSB-) frequency of the two input signals, could be used to generate a single noise-compensated comb, but they are not available in the frequency range required here. Therefore, we first up-converted both the filtered single RF comb line by 2.5 GHz and the full RF comb by 2.5 GHz $+ m \cdot \Delta f_{rep}$ as schematized in Fig. 6, where m is an integer number and Δf_{rep} is the mode spacing of the RF comb. The single line is up-converted using an SSB+ mixer, while the comb is up-converted using a double balanced mixer followed by a high-pass filter to suppress the difference-frequency signal. The up-converted RF comb line and RF comb are then mixed, and the difference frequency component is selected using an appropriate filter. The resulting signal is a low-noise harmonic RF comb, as the frequency noise of the selected RF comb mode that was common to all comb lines has been subtracted.

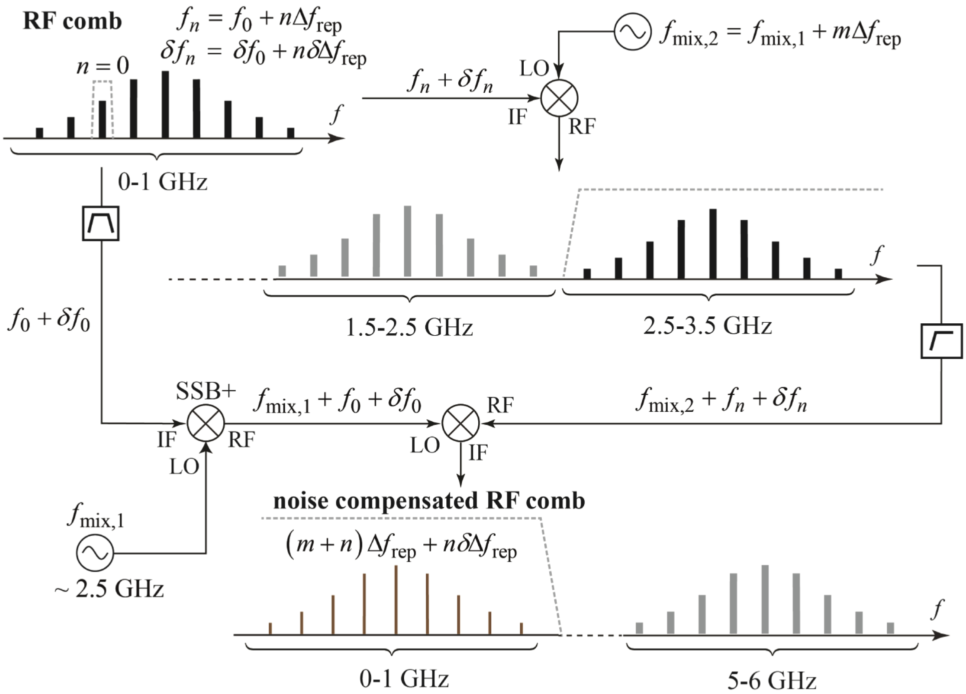

Fig. 6. Common-mode noise subtraction scheme. One line (indexed with $n = 0$) of the multi-heterodyne beat signal is filtered, and its frequency is shifted by $f_{mix,1}$ using an SSB mixer. The entire RF comb is also shifted by $f_{mix,1} + m \cdot \Delta f_{rep}$ using a mixer and a high-pass filter. The two signals are mixed, such that their common noise is compensated, and the resulting low-noise RF comb is harmonic.

Funding. Swiss Space Office (MdP COSMICS); Schweizerischer Nationalfonds zur Förderung der Wissenschaftlichen

Forschung (2000020_178864, 20B2-1_176584); Horizon 2020 Framework Programme (871529).

Disclosures. The authors declare no conflicts of interest.

Data availability. Data underlying the results presented in this paper are available in Ref. [44].

References

1. I. Coddington, N. Newbury, and W. Swann, "Dual-comb spectroscopy," Optica **3**(4), 414–426 (2016).
2. A. Hugi, G. Villares, S. Blaser, H. C. Liu, and J. Faist, "Mid-infrared frequency comb based on a quantum cascade laser," Nature **492**(7428), 229–233 (2012).
3. G. Villares, A. Hugi, S. Blaser, and J. Faist, "Dual-comb spectroscopy based on quantum-cascade-laser frequency combs," Nat. Commun. **5**(1), 5192 (2014).
4. M. Gianella, A. Nataraj, B. Tuzson, P. Jouy, F. Kapsalidis, M. Beck, M. Mangold, A. Hugi, J. Faist, and L. Emmenegger, "High-resolution and gapless dual comb spectroscopy with current-tuned quantum cascade lasers," Opt. Express **28**(5), 6197–6208 (2020).
5. M. J. Norahan, R. Horvath, N. Woitzik, P. Jouy, F. Eigenmann, K. Gerwert, and C. Kötting, "Microsecond resolved infrared spectroscopy on non-repetitive protein reactions by applying caged-compounds and quantum cascade laser frequency combs," bioRxiv 2021.01.04.425172 (2021).
6. P. Fjodorow, P. Allmendinger, R. Horvath, J. Herzler, F. Eigenmann, M. Geiser, M. Fikri, and C. Schulz, "Monitoring formaldehyde in a shock tube with a fast dual-comb spectrometer operating in the spectral range of 1740–1790cm –1," Appl. Phys. B **126**(12), 193 (2020).
7. N. H. Pinkowski, S. J. Cassady, C. L. Strand, and R. K. Hanson, "Quantum-cascade-laser-based dual-comb thermometry and speciation at high temperatures," Meas. Sci. Technol. **32**(3), 035501 (2021).
8. N. H. Pinkowski, Y. Ding, C. L. Strand, R. K. Hanson, R. Horvath, and M. Geiser, "Dual-comb spectroscopy for high-temperature reaction kinetics," Meas. Sci. Technol. **31**(5), 055501 (2020).
9. G. Zhang, R. Horvath, D. Liu, M. Geiser, and A. Farooq, "QCL-Based Dual-Comb Spectrometer for Multi-Species Measurements at High Temperatures and High Pressures," Sensors **20**(12), 3602 (2020).
10. E. Lins, S. Read, B. Unni, S. M. Rosendahl, and I. J. Burgess, "Microsecond Resolved Infrared Spectroelectrochemistry Using Dual Frequency Comb IR Lasers," Anal. Chem. **92**(9), 6241–6244 (2020).
11. J. L. Klocke, M. Mangold, P. Allmendinger, A. Hugi, M. Geiser, P. Jouy, J. Faist, and T. Kottke, "Single-Shot Sub-microsecond Mid-infrared Spectroscopy on Protein Reactions with Quantum Cascade Laser Frequency Combs," Anal. Chem. **90**(17), 10494–10500 (2018).
12. U. Szczepaniak, S. H. Schneider, R. Horvath, J. Kozuch, and M. Geiser, "Vibrational Stark Spectroscopy of Fluorobenzene Using Quantum Cascade Laser Dual Frequency Combs," Appl. Spectrosc. **74**(3), 347–356 (2020).
13. T. J. Kippenberg, A. L. Gaeta, M. Lipson, and M. L. Gorodetsky, "Dissipative Kerr solitons in optical microresonators," Science **361**(6402), eaan8083 (2018).
14. S. Droste, G. Ycas, B. R. Washburn, I. Coddington, and N. R. Newbury, "Optical Frequency Comb Generation based on Erbium Fiber Lasers," Nanophotonics **5**(2), 196–213 (2016).
15. T. J. Kippenberg, R. Holzwarth, and S. A. Diddams, "Microresonator-Based Optical Frequency Combs," Science **332**(6029), 555–559 (2011).
16. J. Hillbrand, A. M. Andrews, H. Detz, G. Strasser, and B. Schwarz, "Coherent injection locking of quantum cascade laser frequency combs," Nat. Photonics **13**(2), 101–104 (2019).
17. F. Kapsalidis, B. Schneider, M. Singleton, M. Bertrand, E. Gini, M. Beck, and J. Faist, "Mid-infrared quantum cascade laser frequency combs with a microstrip-like line waveguide geometry," Appl. Phys. Lett. **118**(7), 071101 (2021).
18. M. R. St-Jean, M. I. Amanti, A. Bernard, A. Calvar, A. Bismuto, E. Gini, M. Beck, J. Faist, H. C. Liu, and C. Sirtori, "Injection locking of mid-infrared quantum cascade laser at 14 GHz, by direct microwave modulation," Laser Photonics Rev. **8**(3), 443–449 (2014).
19. P. Jouy, J. M. Wolf, Y. Bidaux, P. Allmendinger, M. Mangold, M. Beck, and J. Faist, "Dual comb operation of λ ~ 8.2 μm quantum cascade laser frequency comb with 1 W optical power," Appl. Phys. Lett. **111**(14), 141102 (2017).
20. J. Westberg, L. A. Sterczewski, F. Kapsalidis, Y. Bidaux, J. M. Wolf, M. Beck, J. Faist, and G. Wysocki, "Dual-comb spectroscopy using plasmon-enhanced-waveguide dispersion-compensated quantum cascade lasers," Opt. Lett. **43**(18), 4522–4525 (2018).
21. T. Ideguchi, A. Poisson, G. Guelachvili, N. Picqué, and T. W. Hänsch, "Adaptive real-time dual-comb spectroscopy," Nat. Commun. **5**(1), 3375 (2014).
22. O. Rompelman and H. H. Ros, "Coherent averaging technique: A tutorial review Part 1: Noise reduction and the equivalent filter," J. Biomed. Eng. **8**(1), 24–29 (1986).
23. I. Coddington, W. C. Swann, and N. R. Newbury, "Coherent dual-comb spectroscopy at high signal-to-noise ratio," Phys. Rev. A **82**(4), 043817 (2010).
24. E. Baumann, F. R. Giorgetta, W. C. Swann, A. M. Zolot, I. Coddington, and N. R. Newbury, "Spectroscopy of the methane ν 3 band with an accurate midinfrared coherent dual-comb spectrometer," Phys. Rev. A **84**(6), 062513 (2011).

25. A. M. Zolot, F. R. Giorgetta, E. Baumann, W. C. Swann, I. Coddington, and N. R. Newbury, "Broad-band frequency references in the near-infrared: Accurate dual comb spectroscopy of methane and acetylene," J. Quant. Spectrosc. Radiat. Transfer **118**, 26–39 (2013).
26. S. Okubo, K. Iwakuni, H. Inaba, K. Hosaka, A. Onae, H. Sasada, and F.-L. Hong, "Ultra-broadband dual-comb spectroscopy across 1.0–1.9 µm," Appl. Phys. Express **8**(8), 082402 (2015).
27. G.-W. Truong, E. M. Waxman, K. C. Cossel, E. Baumann, A. Klose, F. R. Giorgetta, W. C. Swann, N. R. Newbury, and I. Coddington, "Accurate frequency referencing for fieldable dual-comb spectroscopy," Opt. Express **24**(26), 30495–30504 (2016).
28. N. Hoghooghi, R. J. Wright, A. S. Makowiecki, W. C. Swann, E. M. Waxman, I. Coddington, and G. B. Rieker, "Broadband coherent cavity-enhanced dual-comb spectroscopy," Optica **6**(1), 28–33 (2019).
29. H. Guo, W. Weng, J. Liu, F. Yang, W. Hänsel, C. S. Brès, L. Thévenaz, R. Holzwarth, and T. J. Kippenberg, "Nanophotonic supercontinuum-based mid-infrared dual-comb spectroscopy," Optica **7**(9), 1181–1188 (2020).
30. J.-D. Deschênes, P. Giaccarri, and J. Genest, "Optical referencing technique with CW lasers as intermediate oscillators for continuous full delay range frequency comb interferometry," Opt. Express **18**(22), 23358–23370 (2010).
31. T. Ideguchi, A. Poisson, G. Guelachvili, T. W. Hänsch, and N. Picqué, "Adaptive dual-comb spectroscopy in the green region," Opt. Lett. **37**(23), 4847–4849 (2012).
32. J. Roy, J.-D. Deschênes, S. Potvin, and J. Genest, "Continuous real-time correction and averaging for frequency comb interferometry," Opt. Express **20**(20), 21932–21939 (2012).
33. D. Burghoff, Y. Yang, and Q. Hu, "Computational multiheterodyne spectroscopy," Sci. Adv. **2**(11), e1601227 (2016).
34. N. B. Hébert, J. Genest, J.-D. Deschênes, H. Bergeron, G. Y. Chen, C. Khurmi, and D. G. Lancaster, "Self-corrected chip-based dual-comb spectrometer," Opt. Express **25**(7), 8168–8179 (2017).
35. L. A. Sterczewski, J. Westberg, and G. Wysocki, "Computational coherent averaging for free-running dual-comb spectroscopy," Opt. Express **27**(17), 23875–23893 (2019).
36. Ł. A. Sterczewski, A. Przewłoka, W. Kaszub, and J. Sotor, "Computational Doppler-limited dual-comb spectroscopy with a free-running all-fiber laser," APL Photonics **4**(11), 116102 (2019).
37. M. Gianella, S. Vogel, K. Komagata, J. Hillbrand, F. Kapsalidis, B. Tuzson, A. Nataraj, A. Hugi, M. Mangold, P. Jouy, T. Südmeyer, S. Schilt, J. Faist, and L. Emmenegger, "Gapless high-resolution QCL dual-comb spectroscopy with real-time data processing for dynamic gas-phase measurements," Submitted to CLEO/Europe (2021).
38. J. Westberg, L. A. Sterczewski, and G. Wysocki, "Mid-infrared multiheterodyne spectroscopy with phase-locked quantum cascade lasers," Appl. Phys. Lett. **110**(14), 141108 (2017).
39. F. Cappelli, L. Consolino, G. Campo, I. Galli, D. Mazzotti, A. Campa, M. Siciliani de Cumis, P. Cancio Pastor, R. Eramo, M. Rösch, M. Beck, G. Scalari, J. Faist, P. De Natale, and S. Bartalini, "Retrieval of phase relation and emission profile of quantum cascade laser frequency combs," Nat. Photonics **13**(8), 562–568 (2019).
40. M. Piccardo, D. Kazakov, N. A. Rubin, P. Chevalier, Y. Wang, F. Xie, K. Lascola, A. Belyanin, and F. Capasso, "Time-dependent population inversion gratings in laser frequency combs," Optica **5**(4), 475–478 (2018).
41. G. Di Domenico, S. Schilt, and P. Thomann, "Simple approach to the relation between laser frequency noise and laser line shape," Appl. Opt. **49**(25), 4801–4807 (2010).
42. P. Brochard, S. Bilicki, A. Shehzad, S. Schilt, and T. Südmeyer, "Laser Linewidth Optimization in a Feedback Loop," in *2017 European Conference on Lasers and Electro-Optics and European Quantum Electronics Conference* (Optical Society of America, 2017), p. CH_4_3.
43. P. Maslowski, K. F. Lee, A. C. Johansson, A. Khodabakhsh, G. Kowzan, L. Rutkowski, A. A. Mills, C. Mohr, J. Jiang, M. E. Fermann, and A. Foltynowicz, "Surpassing the path-limited resolution of Fourier-transform spectrometry with frequency combs," Phys. Rev. A **93**(2), 021802 (2016).
44. K. Komagata, A. Shehzad, G. Terrasanta, P. Brochard, R. Matthey, M. Gianella, P. Jouy, F. Kapsalidis, M. Shahmohammadi, M. Beck, V. J. Wittwer, J. Faist, L. Emmenegger, T. Südmeyer, A. Hugi, and S. Schilt, "Data underlying the results presented in this paper are available at the EUDAT B2SHARE repository," b2share (2021)http://doi.org/10.23728/b2share.1ceecd3c598a420d8aba7254dae4ae2f

Chapter 3

Achieving High Spectral Purity

In chapter 2, the issue of insufficient locking bandwidth was solved by a common-mode noise subtraction scheme. This worked well since the coherence was only required in the RF domain. However, some applications necessitate a high spectral purity in the optical domain, e.g., locking the FC to an enhancement cavity [1], providing a pure frequency reference, etc. Therefore, other approaches are required.

Apart from active feedback, there are two passive solutions: optical injection and optical feedback. Optical injection has demonstrated the mutual phase lock between two lasers [2]. Moreover, optical feedback, i.e., self-optical injection, was demonstrated to lock a distributed feedback (DFB) QCL to a cavity, e.g., Ref. [3], or to stabilize the repetition rate of a QCL comb [4]. Active solutions arguably offer more flexibility, such as the ability to choose the frequency offset between two locked lasers, or generally, the freedom of gain and locking bandwidth. However, they require an actuator that is faster than the noise source, which for QCLs is the internal current noise and its conversion to heat [5]. Thus, stabilization by the drive current, which relies on the same process [6], is not satisfactory.

Therefore, I investigated the use of NIR light to stabilize QCL FC with a larger bandwidth than drive current actuation. We are currently submitting an article that synthesizes these results. The Arxiv preprint is reproduced at the end of the chapter in accordance with its CC-BY 4.0 license [7].

3.1 Summary of the article

We measured the response of a QCL FC as a function of illuminated NIR power on the front facet in terms of offset, repetition, and optical frequency (i.e., the frequency of a comb line). The transfer functions of these quantities reveal a bandwidth larger than 1 MHz, which is the limit of the accurate measurement (Fig. 4). In particular, NIR light seems adequate for locking the offset frequency while the frequency of a comb line suffers from the reversal of the sign of the response near 33 Hz. We show that the comb line can nevertheless be phase locked using a combination of drive current and NIR light intensity modulation, with a servo bandwidth over 2 MHz enabled by the optical actuator. The residual phase noise integrated between 1 Hz and 10 MHz is then 200 mrad (Fig. 5). Lastly, we demonstrate the versatility of NIR light for the coherent control of QCL FCs with preliminary results on the injection locking of the repetition rate by modulation of the NIR power (Fig. 6).

3.2 Additional results

In the article, we wrote that all comb lines are phase locked, but did not provide proofs for it. It is generally necessary to characterize the effectiveness of phase locking schemes as phase noise can never completely be suppressed. In the specific case of OFCs, the noise of the repetition rate is multiplied [8], such that a small residual can become significant with increased mode number. Moreover, the cross-coupling between the two comb degrees of freedom affects the achievable noise reduction and shifts the mode with the smallest noise [9]. We thus continued the investigation in a dual comb scheme, which allows to asses the mutual phase noise of multiple lines. Most of the analysis is complete, but some details may be missing as the results are very recent.

We mutually locked two comb lines of a pair of QCL FCs using combined electrical and optical actuation, while the repetition frequencies were locked by injection locking of two RF references. Moreover, the intermode beat note (IBN) [10] of each FC was extracted in parallel to the injection. Their frequency difference, Δf_{rep}, was compared in phase with an RF reference at 5 MHz. This generated a phase error signal that was fed back via a servo controller to the synthesizer injecting in the follower QCL. The motivation was to avoid the large phase noise of signals at 11 GHz, by having Δf_{rep} inherit the spectral properties of a 5 MHz signal.

By beating the two combs, we can access, as in chapter 2, the mutual coherence of different comb lines. The preliminary results are found in Figure 3.1.

The multiheterodyne spectrum with the highlighted comb lines used for analysis are in Figure 3.1(a). The RF comb lines are designated with index n, where $n = 0$ denotes the line that is used in the phase lock loop (PLL). The phase noise of RF comb line n at frequency $\Delta f_n = \Delta f_0 + n\Delta f_{\text{rep}}$ shows an increase as a function of n [Figure 3.1(b)]. The phase noise of a comb line should follow the equation

$$S_n = S_0 + n^2 S_{\text{rep}} + n S_{\text{corr}}, \tag{3.1}$$

$S_n \equiv S_{\Delta f_n, \Delta f_n}$ is the phase noise power spectral density (PSD) of RF comb line n, $S_{\text{rep}} \equiv S_{\Delta f_{\text{rep}}, \Delta f_{\text{rep}}}$ is that of the difference in repetition rate, and $S_{\text{corr}} = S_{\Delta f_0, \Delta f_{\text{rep}}} + S_{f_{\text{rep}}, \Delta f_0}$ captures the correlation between Δf_{rep} and Δf_0. Thus, using line 0, and two other lines (here $k = -20$, and $l = 15$), the values

$$S_{\text{rep}} = \frac{1}{k-l}\left[\frac{S_k}{k} - \frac{S_l}{l} + S_0\left(\frac{1}{l} - \frac{1}{k}\right)\right] \tag{3.2}$$

$$S_{\text{corr}} = \frac{1}{l-k}\left[l\frac{S_k}{k} - k\frac{S_l}{l} + S_0\left(\frac{k}{l} - \frac{l}{k}\right)\right] \tag{3.3}$$

can be computed and the noise of the other comb lines can be predicted. The difference between the measured and predicted phase noise PSD is represented in Figure 3.1(c). Good correspondence is obtained within the measurement uncertainty, except near 4 kHz, which is discussed below. However, the retrieved noise on Δf_{rep} [Figure 3.1(d)] shows discrepancy with the phase noise retrieved from the mixing product of the two IBNs, which inherited the high spectral purity of the 5 MHz source. Actually, the retrieved S_{rep} follows the noise of the incoherent sum of the two IBNs phase noise when they are not locked between 100 Hz and 1 kHz. Above 1 kHz, the retrieved noise is higher and is reminiscent of a servo bump. It stipulates that the injection locking of the 15 dBm signal is only effective up to 1 kHz of Fourier frequency. The noise bump is clearly seen in Figure 3.1(b,c). I expect that the discrepancy in Figure 3.1(c) near 4 kHz is an artifact caused by the slow evolution of the noise bump during the sequential measurement of each line (about 20 minutes in total). For frequencies above the servo bump, S_{rep} remains higher than the incoherent sums of the phase noise of the IBNs under RF injection but lower than the free-running case. Below 100 Hz, the mutual lock of the synthesizers proved useful to reduce the noise below the incoherent sum, although it is not as low as the detected phase noise of the mixing product.

Figure 3.1(d) also features S_{corr}, which closely follows S_{rep}. The correlation causes a minor asymmetry in the integrated phase noise ϕ_{rms} as a function of comb index, shown in Figure 3.1(e). The inset shows that in this condition, ϕ_{rms} at 1-s integration time is projected to remain below 1 rad for more than

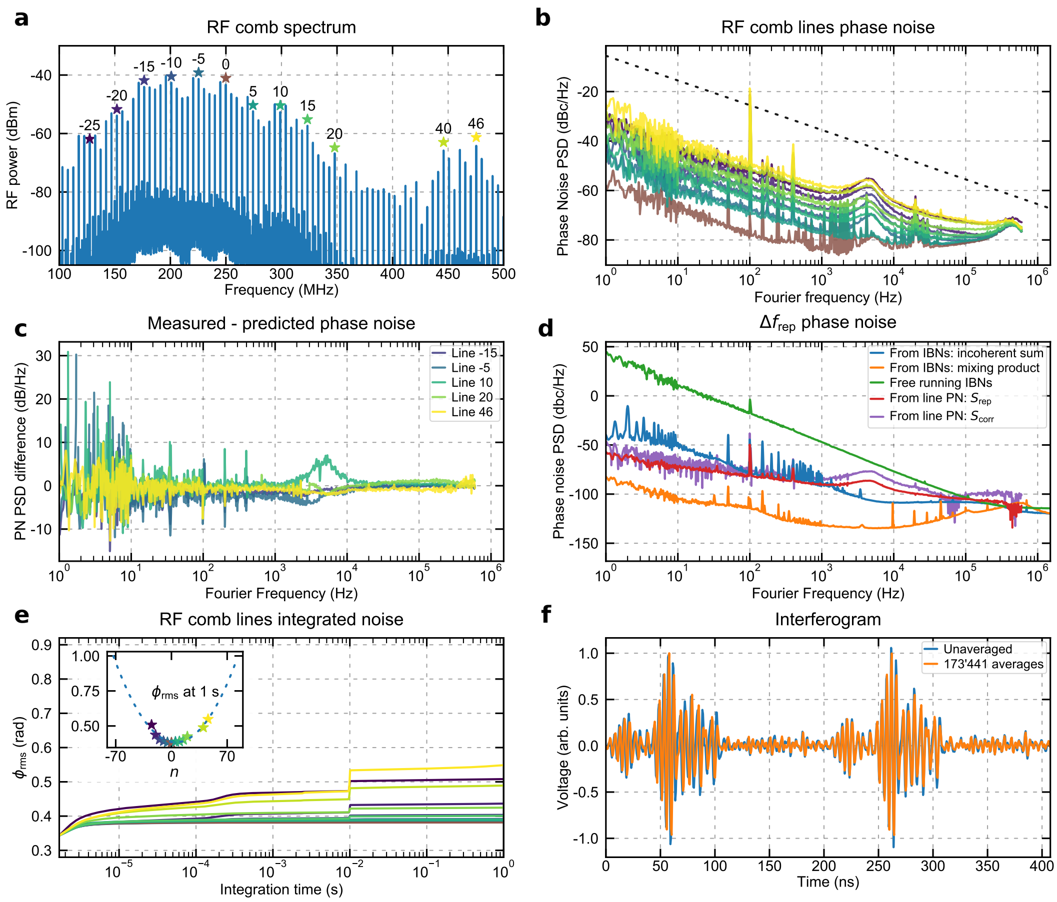

Figure 3.1: Analysis of the mutual coherence of the comb lines. (a) Dual comb multiheterodyne spectrum at 50 Hz resolution bandwidth (auto peak mode). (b) Phase noise of individual lines highlighted in (a) with a star of the same color. (c) Measured - predicted phase noise using lines 0, -20, and 15. (d) Phase noise of Δf_{rep} determined from different methods and estimation of S_{corr}. (e) Integrated phase noise of each line. The inset shows the value at an integration time of 1 s as a function of comb line number and a quadratic fit. (f) Two interferograms (blue) compared to their average over 72 ms.

150 lines between $n = -73$ and $n = 83$. Finally, Figure 3.1(f) demonstrates that the locking scheme allows the coherent averaging of single interferograms (two are shown) during 72 ms, limited by the memory of the digitizer (Zurich instruments, UHF, DIG option).

We are now writing a paper to report these results, which prove that a QCL OFC can be phase-locked tightly across a large bandwidth. They also highlight the phase coherence of the comb (read discussion below), and the difficulty of assessing the noise when performing RF injection locking.

3.3 Further discussion

3.3.1 Phase coherence

The comb nature of QCL combs has been proved in different ways. Shifted wave interference Fourier transform spectroscopy was used in the first demonstration of a MIR QCL comb [11]. Villares *et al.* [12] demonstrated the equidistance of two pairs of comb modes on a time scale from 10 ms to 25 s in a dual comb setup. Further evidences are the repetitive linear chirp of the emission [13], the ability to compress it to a pulse [14], the ability to perform computational coherent averaging [15], and the results in chapter 2 on the coherent averaging of a QCL-based dual comb spectrometer [16]. Note that the results of chapter 4 set only a loose upper bound of 100 kHz on the equidistance [17] so that it is not a critical evidence compared to other results. Here, compared to the other works, we delve deeper into the phase coherence at short time scales. Although these timescales were investigated in chapter 2, the noise on the repetition rate was much larger than expected and only about 3 lines were studied, with a maximum index of 7. With now more than 3 lines, phase noise predictions were made and compared to the measurement. The correspondence between measurement and prediction demonstrate that the QCL FC satisfies the comb equation not only on average, i.e., equidistance, but also in phase, between 1 Hz and 600 kHz of offset frequencies. On this point, I agree that equidistance generally implies phase-locking, as there is a lack of explanation as to what physical process would generate the former in absence of the latter. In QCLs, the phase-locking Kerr-nonlinearity [18] is by many orders of magnitude faster than this 600 kHz measurement.

3.3.2 Sideband generation

Although this was not investigated, I believe that the NIR light could also be used to create sidebands on the QCL FC. An application would be cavity enhanced spectroscopy [1], where locking the comb to a cavity requires frequency modulation for the Pound-Drever-Hall lock [19]. Then, the same NIR source could be used to correct the QCL FC for locking to the cavity. Moreover, modulation at subharmonics of the repetition rate could decrease the spacing of the QCL FC for specific applications. Modulation bandwidths and residual amplitude modulation will have to be characterized and compared to drive current modulation.

3.3.3 Other stabilization schemes

Using two actuators and the RF injection locking is not thrifty. I have tried two other locking schemes, where the repetition rate is locked by RF injection or in a PLL using the drive current as actuator, before one comb line is locked with the NIR light. The first did not work and the latter showed some signs of success but suffered from the frequency noise increase on the comb line due to the locking of the repetition rate [20]. Hopefully, the prospect of self-referencing QCL FC has been made more tangible by the generation of sub-picosecond pulse [14] and the development of MIR nonlinear waveguides [21]. When the offset frequency is detected, NIR light should be a good actuator, according to the measured transfer function. Then the drive current could stabilize the repetition frequency [20]. However, an analysis using a coupled-loop model could already reveal, from the transfer functions and the free-running frequency noise [20], the suitability of this scheme [9]. In the negative case, other wavelengths would have to be explored as actuators. Moreover, two-point locking to an enhancement cavity could also be explored [1]. One potential solution is to actuate on one side of the spectrum using drive current and on the other side using NIR light.

As of now, feedforward correction is not a good option. They offer high actuation bandwidth in the NIR [22], but require an additional modulator. In the MIR, there are acoustic-optic frequency shifters whose actuation bandwidth is only about 100 kHz [23], and electro-optic modulators suffering from low efficiency [24]. However, the recent progresses in MIR amplitude modulators (e.g. [25]) promise the same for frequency modulators.

I note that RF injection locking of the repetition rate is very practical and has been exploited in nearly all of my works. However, it is not an ideal solution for the most demanding applications due to the natural multiplication of the noise with the mode number, and as seen here the difficulty in estimating the the performance of the lock. It is conceivable that the latter is dependent on the injected RF power, and requires more investigations. Injection locking mediated by NIR light could lead to different conclusions.

3.4 Conclusion

To conclude, QCL FCs respond faster to NIR light than to drive current modulation. Thus, the former can be used to lock QCL FCs with low residual phase noise unattainable with electrical modulation alone. Moreover, the study of the phase noise of multiple RF comb lines demonstrated (1) the tight phase-lock and the phase coherence of the comb lines in times scales ranging between 1 s to 1.7 µs, (2) that the phase lock of the repetition rate by RF injection is limited in bandwidth, and (3) that the performance of RF injection should be monitored via optical means. Thus, RF injection locking is not satisfactory for the most stringent applications. However, it is still useful, as will be seen in chapter 4. Achieving high spectral purity of all comb lines is essential for many OFC applications. Therefore, these results, in particular, the phase coherence of the comb lines, further establish the fitness of QCLs as MIR FCs. This phase coherence also promises that better locking schemes will allow ultra-low phase noise for all comb lines.

References

[1] A. Foltynowicz, P. Masłowski, A. J. Fleisher, B. J. Bjork, and J. Ye, “Cavity-Enhanced Optical Frequency Comb Spectroscopy in the Mid-Infrared Application to Trace Detection of Hydrogen Peroxide”, Appl. Phys. B **110**, 163 (2013).

[2] J. Hillbrand, M. Bertrand, V. Wittwer, N. Opačak, F. Kapsalidis, M. Gianella, L. Emmenegger, B. Schwarz, T. Südmeyer, M. Beck, and J. Faist, “Synchronization of Frequency Combs by Optical Injection”, Opt. Express **30**, 36087 (2022).

[3] E. Fasci, N. Coluccelli, M. Cassinerio, A. Gambetta, L. Hilico, L. Gianfrani, P. Laporta, A. Castrillo, and G. Galzerano, “Narrow-Linewidth Quantum Cascade Laser at 8.6 µm”, Opt. Lett. **39**, 4946 (2014).

[4] C. C. Teng, J. Westberg, and G. Wysocki, “Gapless Tuning of Quantum Cascade Laser Frequency Combs with External Cavity Optical Feedback”, Opt. Lett. **48**, 363 (2023).

[5] L. Tombez, S. Schilt, J. Di Francesco, P. Thomann, and D. Hofstetter, “Temperature Dependence of the Frequency Noise in a Mid-IR DFB Quantum Cascade Laser from Cryogenic to Room Temperature”, Opt. Express **20**, 6851 (2012).

[6] L. Tombez, F. Cappelli, S. Schilt, G. Di Domenico, S. Bartalini, and D. Hofstetter, "Wavelength Tuning and Thermal Dynamics of Continuous-Wave Mid-Infrared Distributed Feedback Quantum Cascade Lasers", Appl. Phys. Lett. **103**, 031111 (2013).

[7] K. N. Komagata, A. Parriaux, M. Bertrand, J. Hillbrand, M. Beck, V. J. Wittwer, J. Faist, and T. Südmeyer, "Coherent Control of Mid-Infrared Frequency Comb by Optical Injection of Near-Infrared Light", ArXiv230501508 Phys., `10.48550/arXiv.2305.01508` (2023).

[8] T. Fortier and E. Baumann, "20 Years of Developments in Optical Frequency Comb Technology and Applications", Commun. Phys. **2**, 1 (2019).

[9] V. Dolgovskiy, N. Bucalovic, P. Thomann, C. Schori, G. Di Domenico, and S. Schilt, "Cross-Influence between the Two Servo Loops of a Fully Stabilized Er: Fiber Optical Frequency Comb", J. Opt. Soc. Am. B **29**, 2944 (2012).

[10] M. Piccardo, D. Kazakov, N. A. Rubin, P. Chevalier, Y. Wang, F. Xie, K. Lascola, A. Belyanin, and F. Capasso, "Time-Dependent Population Inversion Gratings in Laser Frequency Combs", Optica **5**, 475 (2018).

[11] A. Hugi, G. Villares, S. Blaser, H. C. Liu, and J. Faist, "Mid-Infrared Frequency Comb Based on a Quantum Cascade Laser", Nature **492**, 229 (2012).

[12] G. Villares, A. Hugi, S. Blaser, and J. Faist, "Dual-Comb Spectroscopy Based on Quantum-Cascade-Laser Frequency Combs", Nat. Commun. **5**, 5192 (2014).

[13] M. Singleton, P. Jouy, M. Beck, and J. Faist, "Evidence of Linear Chirp in Mid-Infrared Quantum Cascade Lasers", Optica **5**, 948 (2018).

[14] P. Täschler, M. Bertrand, B. Schneider, M. Singleton, P. Jouy, F. Kapsalidis, M. Beck, and J. Faist, "Femtosecond Pulses from a Mid-Infrared Quantum Cascade Laser", Nat. Photonics **15**, 919 (2021).

[15] L. A. Sterczewski, J. Westberg, and G. Wysocki, "Computational Coherent Averaging for Free-Running Dual-Comb Spectroscopy", Opt. Express **27**, 23875 (2019).

[16] K. Komagata, A. Shehzad, G. Terrasanta, P. Brochard, R. Matthey, M. Gianella, P. Jouy, F. Kapsalidis, M. Shahmohammadi, M. Beck, V. J. Wittwer, J. Faist, L. Emmenegger, T. Südmeyer, A. Hugi, and S. Schilt, "Coherently-Averaged Dual Comb Spectrometer at 7.7 µm with Master and Follower Quantum Cascade Lasers", Opt. Express **29**, 19126 (2021).

[17] K. N. Komagata, M. Gianella, P. Jouy, F. Kapsalidis, M. Shahmohammadi, M. Beck, R. Matthey, V. J. Wittwer, A. Hugi, J. Faist, L. Emmenegger, T. Südmeyer, and S. Schilt, "Absolute Frequency Referencing in the Long Wave Infrared Using a Quantum Cascade Laser Frequency Comb", Opt. Express **30**, 12891 (2022).

[18] N. Opačak, S. D. Cin, J. Hillbrand, and B. Schwarz, "Frequency Comb Generation by Bloch Gain Induced Giant Kerr Nonlinearity", Phys. Rev. Lett. **127**, 093902 (2021).

[19] R. Jason Jones, I. Thomann, and J. Ye, "Precision Stabilization of Femtosecond Lasers to High-Finesse Optical Cavities", Phys. Rev. A **69**, 051803 (2004).

[20] A. Shehzad, P. Brochard, R. Matthey, F. Kapsalidis, M. Shahmohammadi, M. Beck, A. Hugi, P. Jouy, J. Faist, T. Südmeyer, and S. Schilt, "Frequency Noise Correlation between the Offset Frequency and the Mode Spacing in a Mid-Infrared Quantum Cascade Laser Frequency Comb", Opt. Express **28**, 8200 (2020).

[21] M. Montesinos-Ballester, C. Lafforgue, J. Frigerio, A. Ballabio, V. Vakarin, Q. Liu, J. M. Ramirez, X. Le Roux, D. Bouville, A. Barzaghi, C. Alonso-Ramos, L. Vivien, G. Isella, and D. Marris-Morini, "On-Chip Mid-Infrared Supercontinuum Generation from 3 to 13 µm Wavelength", ACS Photonics **7**, 3423 (2020).

[22] Z. Chen, M. Yan, T. W. Hänsch, and N. Picqué, "A Phase-Stable Dual-Comb Interferometer", Nat. Commun. **9**, 3035 (2018).

[23] M. Lamperti, B. AlSaif, D. Gatti, M. Fermann, P. Laporta, A. Farooq, and M. Marangoni, "Absolute Spectroscopy near 7.8 µm with a Comb-Locked Extended-Cavity Quantum-Cascade-Laser", Sci. Rep. **8**, 1 (2018).

[24] V. Bernard, C. Daussy, G. Nogues, L. Constantin, P. E. Durand, A. Amy-Klein, A. Van Lerberghe, and C. Chardonnet, "CO_2 Laser Stabilization to 0.1-Hz Level Using External Electrooptic Modulation", IEEE J. Quantum Electron. **33**, 1282 (1997).

[25] H. Dely, M. Joharifar, X. Pang, D. Gacemi, T. Salgals, R. Schatz, Y.-T. Sun, T. Bonazzi, E. Rodriguez, Y. Todorov, A. Vasanelli, A. Udalcovs, S. Spolitis, V. Bobrovs, O. Ozolins, S. Popov, and C. Sirtori, "High Bitrate Data Transmission in the 8-14 µm Atmospheric Window Using an External Stark-effect Modulator with Digital Equalization", Opt. Express **31**, 7259 (2023).

arXiv:2305.01508v2 [physics.optics] 15 May 2023

Coherent Control of Mid-Infrared Frequency Comb by Optical Injection of Near-Infrared Light

Kenichi N. Komagata,[1,*] Alexandre Parriaux,[1] Mathieu Bertrand,[2] Johannes Hillbrand,[2] Mattias Beck,[2] Valentin J. Wittwer,[1] Jérôme Faist,[2] and Thomas Südmeyer[1]

[1] *Laboratoire Temps-Fréquence, Institut de Physique, Université de Neuchâtel, Avenue de Bellevaux 51, 2000 Neuchâtel, Switzerland*

[2] *Institute for Quantum Electronics, ETH Zurich, Auguste-Piccard-Hof 1, 8093 Zurich, Switzerland*

(Dated: May 16, 2023)

We demonstrate the use of a low power near-infrared laser illuminating the front facet of a quantum cascade laser (QCL) as an optical actuator for the coherent control of a mid-infrared frequency comb. We show that by appropriate current control of the QCL comb and intensity modulation of the near-infrared laser, a tight phase lock of a comb line to a distributed feedback laser is possible with 2 MHz of locking bandwidth and 200 mrad of residual phase noise. A characterization of the whole scheme is provided showing the limits of the electrical actuation which we bypassed using the optical actuation. Both comb degrees of freedom can be locked by performing electrical injection locking of the repetition rate in parallel. However, we show that the QCL acts as a fast near-infrared light detector such that injection locking can also be achieved through modulation of the near-infrared light. These results on the coherent control of a quantum cascade laser frequency comb are particularly interesting for coherent averaging in dual-comb spectroscopy and for mid-infrared frequency comb applications requiring high spectral purity.

I. INTRODUCTION

Quantum cascade lasers (QCL) emitting frequency combs were first demonstrated in 2012 [1] and have since then become an established technology for fast and broadband mid-infrared (MIR) spectroscopic applications, such as time-resolved studies of microsecond-scale molecular dynamics [2], high-pressure and temperature thermometry in shock tubes [3], or high-resolution measurements of molecular spectra [4–6]. Some of their key assets are their low footprint and large optical power compared to other types of MIR combs, especially in the 8–10 µm spectral range that is usually reached via nonlinear frequency conversion [7–9]. Indeed, QCLs are electrically-driven devices that directly emit frequency combs in the MIR with a power that can reach 1 W [10].

In the context of comb spectroscopy, the use of two mutually coherent combs with slightly different repetition rates, namely dual-comb spectroscopy (DCS), has shown great potential for ultra fast and high resolution measurements without the need of complex and expensive instruments [11, 12]. DCS has been well demonstrated with mode-locked lasers in the near-infrared (NIR), but the MIR is more interesting as molecules generally have stronger absorption features, which is advantageous for many applications such as trace gas detection [13], or isotope ratio measurements [14]. DCS with QCLs is then highly interesting as it provides a compact, low footprint and high-resolution spectrometer [4–6].

In DCS, Comb stabilization is not strictly necessary thanks to the availability of computational phase correction of free-running lasers [15]. Nevertheless, stabilization of the combs allows accurate frequency referencing and arguably more flexibility, e.g., smaller repetition rates. Moreover, to properly establish QCLs as a source of choice for MIR comb applications such as optical frequency synthesis [16–18], demonstrating high spectral purity and coherent control can be considered as important as increasing their bandwidth and detecting their offset frequency [19].

For QCLs, actuation on the drive-current is the most straightforward way to phase-lock a comb line [20–22], while the other degree of freedom, namely the repetition rate, is locked by electrically injecting a radio-frequency (RF) signal close to the round-trip frequency [23]. These two handles allow the coherent control of QCL combs and can be used together [18]. However, as for distributed feedback (DFB) QCLs [24, 25], we expect the intrinsic frequency noise of the QCL comb and the stabilization by drive current to involve the same physical process, i.e., current to temperature to refractive index change. In that case, the time scale of the stabilization will always be close to the cutoff of the noise process, thus limiting the performance of the lock. A solution adopted for other types of lasers is to employ another actuator bound by time scales much faster than the noise source such as opto-optical modulation [26].

For QCLs, light illumination at another wavelength also enables its control and can play as an actuator. The technique has been used on DFB-QCLs emitting a single wavelength for applications such as fast switching [27], gain enhancement [28], stabilization [29], and frequency modulation [30]. More recently, a QCL comb emitting in the THz range was locked via the intensity modulation of a white LED [31]. We also note that illumination of resonant light enabled the mutual lock between two MIR QCL combs via injection locking [32]. However, this only allows mutual locking at the same optical fre-

* Corresponding author: kenichi.komagata@unine.ch

quency, whereas modulation by off-resonant light offers more possibilities.

Indeed, light illumination at a different wavelength can influence various parameters with different strengths, for example to allow pure frequency modulation of a DFB-QCL [33]. Moreover, multiple locking-scheme could be possible for combs, such as the locking of the repetition rate via current actuation [34, 35] combined with locking of the comb line frequency with NIR light. Finally, the NIR is supported by mature technologies allowing a wide range of possibilities. Among others, the high modulation bandwidths reaching a few tens of GHz could enable the injection locking of the QCL comb repetition frequency. In light of the above, there is a compelling interest to investigate the potential of NIR light illumination for the coherent control of MIR QCL combs.

In this work, we characterize the influence of NIR light illuminating the front facet of a MIR QCL comb emitting in the 8 µm range. We measure its transfer function on the comb frequencies and compare it to the more conventional electrical actuation. We demonstrate that the limits of electrical actuation for phase-locks can be bypassed using the intensity modulated NIR light by tightly locking a QCL comb to a DFB-QCL. Lastly, we show that the repetition rate of the QCL can also be injection-locked by intensity modulation of the NIR light.

II. EXPERIMENTAL SETUP

The experimental setup considered here is presented in Figure 1 and pivots around a QCL comb. The laser is controlled in current and temperature with a custom-made driver that sets the operation point of the laser to 1200 mA (1.45 times the lasing threshold) and 0°C. A frequency comb centered around 1305 cm^{-1} is emitted, with approximately 80 lines, a total power of 126 mW, and a repetition frequency of 11.057 GHz. In QCL combs, the comb modes beating together in the Fabry-Perot cavity lead to a measurable voltage oscillating at the repetition frequency [36]. Thus, two wire bonds connect the top of the QCL waveguide near the front and back facet of the laser to RF waveguides on a PCB chip to efficiently inject and extract the repetition rate independently of the drive current.

A custom-made dichroic mirror produced by ion beam sputtering is placed in the optical comb path to direct NIR light from a continuous wave (CW) laser at 1.55 µm (Optilab, DFB-1550-EAM-12-K) to the front facet of the QCL via the collimation lens (Thorlabs, C037TME-F). The NIR laser has an output power around 1 mW and can be modulated up to 12 GHz using an integrated electro-absorption modulator (EAM). The beam is aligned into the QCL so as to maximize the frequency response (see Sect. III). The amount of light effectively reaching the front facet is 55% of the emitted power of the NIR laser and these losses are mainly due to the transmission of the QCL collimation lens at 1.55 µm. The polarization

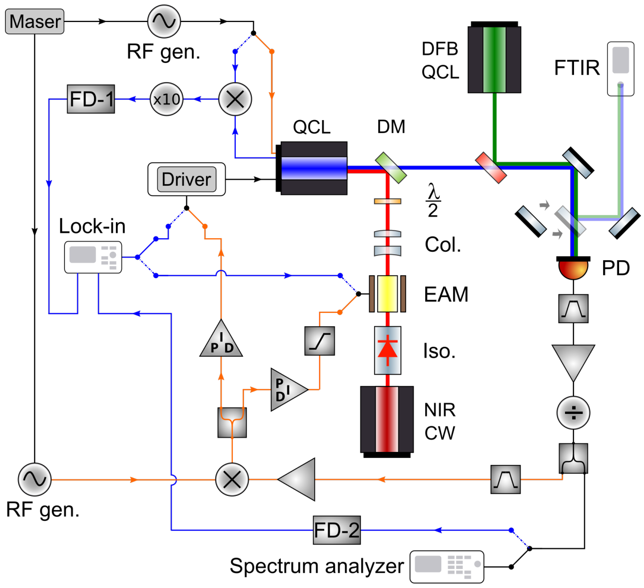

FIG. 1. Schematic showing the experimental setup used to phase lock a line from a QCL comb to a DFB-QCL using an intensity modulated NIR CW laser, and for characterization. The electrical blue wires represent the path for characterizing the repetition frequency and a comb line, whereas the orange wires represent the path for phase locking. CW: continuous wave, EAM: electro-absorption modulator, DM: dichroic mirror, FD: Frequency discriminator, PD: Photodetector, FTIR: Fourier transform infrared spectrometer.

of the NIR light was fixed, however, it did not seem to change the experimental results.

After passing through the dichroic mirror, the comb is mixed on a 50/50 beam splitter with a CW MIR light generated by a DFB-QCL (Alpes Laser). The latter is driven at a current of 191 mA and a temperature of 0 °C, to emit at a frequency $f_{\mathrm{cw}} = 1309.79$ cm^{-1}, which is within the spectral range of the frequency comb. A typical optical spectrum of the comb and the DFB recorded with a Fourier transform infrared spectrometer (Bristol 771A-MIR) is presented in Figure 2. The beating f_b between the comb and the DFB-QCL is recorded on a fast photodetector (VIGO, PV-4TE-10.6).

In the following section we will start with studying the frequency response of the QCL comb when NIR light illuminates its front facet

III. RESPONSE CHARACTERIZATION

We start with the static response before moving on to the frequency dependent response.

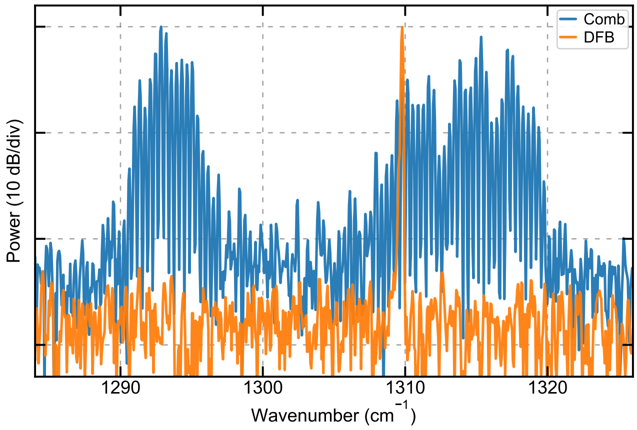

FIG. 2. Typical optical spectrum generated by the QCL comb and the continuous wave generated by the DFB-QCL.

A. Static response

First, we slowly vary the NIR power reaching the QCL from 0 mW to 0.6 mW, and measure on a RF spectrum and phase noise analyzer (Rohde & Schwarz, FSWP26) the frequency shift of a comb line f_n via its beating with the DFB-QCL, and of the repetition rate f_r, measured directly via the independent channel for RF extraction on the QCL comb. For comparison, we also measure the frequency shifts when the drive current of the QCL comb is varied over 1 mA. These results are presented in Figure 3(a, b), where the shift in f_r is scaled by the mode number $n = 3550$ for better comparability with f_n.

For a small variations (1 mA) of the QCL drive currents, the frequencies shift linearly with a superimposed sinusoidal modulation on f_r due to back-reflections [37]. The fitted functions to the experimental data (dashed lines in Figure 3) using a linear model supplemented by a sine wave give an average slope of -210 MHz/mA and -85 kHz/mA for f_n and f_r respectively, although the slope for f_r is dependent on the drive current (position within the modulation) due to the back reflections. The response to low power NIR light suggests a quadratic trend. Moreover, the shift ratio between f_n and nf_r depends on the alignment of the NIR light on the active region of the QCL comb. The main alignment method used in this article (alignment 1, described in section III B) is to maximize the dynamic response of f_n at modulation frequencies of 100 kHz. Another method would be to maximize the static shift of f_n (alignment 2). In the latter case, f_r shows a sinusoidal modulation that is nearly nonexistent for alignment 1, and varies far less than for alignment 1. For alignment 1, the slope interpolated at zero power are -315 MHz/mW and -570 kHz/mW for f_n and f_r respectively.

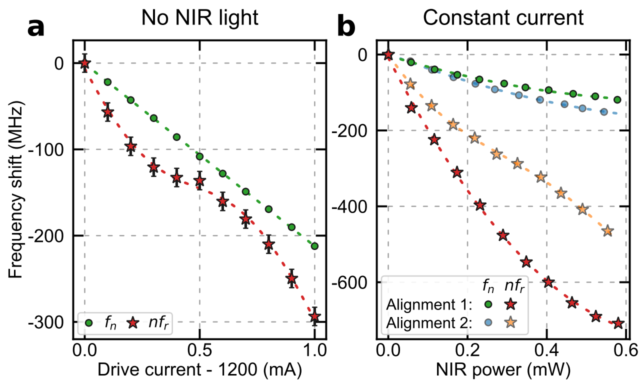

FIG. 3. Static response of the QCL comb frequencies to a change in (a) drive current or (b) illuminated NIR power. The shift in f_r is scaled by n. In (b), the response is reported for two alignment conditions (see main text). Dashed lines are fitted functions to the experimental data. Error bars are plotted when larger than the data marker.

B. Dynamic response

We now take an interest in the frequency-dependent response of the QCL comb. A lock-in amplifier (LIA, Zurich Instruments, UHFLI) modulates the power of the NIR light via the EAM or the comb drive current through the laser driver, see the blue path in Figure 1. We study the response of three comb characteristic frequencies, namely, the offset frequency f_0, f_r, and f_n. Naturally, the three frequencies are coupled to each other through the comb equation:

$$f_n = f_0 + nf_r \quad , \tag{1}$$

where n is an integer. Due to the modulation of the drive current or the NIR power set by the LIA at frequency ω, the comb, i.e., its frequencies respond as:

$$f_i = f_i^{(0)} + \Delta f_i \sin(\omega t + \theta_i) \quad , \tag{2}$$

where $i = \{0; r; n\}$ indexes the three comb frequencies under study, $f_i^{(0)}$ is the average value of f_i, Δf_i the peak amplitude of f_i due to the modulation, and θ_i is the phase of the response. To measure the amplitudes and phases, we convert the frequency modulation of f_i to a voltage modulation using a frequency discriminator (FD) and demodulate this voltage on the LIA.

For this purpose, the repetition rate of the comb is extracted electrically as before, amplified and down-mixed to 60 MHz. As Δf_r is only on the order of 20 kHz, we take the 10$^{\text{th}}$ harmonic and down-mix it to 21 MHz before sending it to FD-1 (Miteq, FMDM-21.4/4-2, see Figure 1), whose output is connected to the LIA. As for the comb line n, the amplitude and phase response of the comb line f_n is encoded in the beating signal with the DFB-QCL as:

$$f_b = f_n^{(0)} + \Delta f_n \sin(\omega t + \theta_n) - f_{\text{cw}} \quad . \tag{3}$$

The signal f_b detected on the photodetector is then filtered, amplified, divided by 15 and 3 (RF bay, FPS-15-8, FPS-3-8), up-mixed to 60 MHz (not shown), and fed to a FD (Miteq, FMDM-60/16-4BC), whose output is connected to the LIA, as shown in Figure 1. The division step allows a larger frequency excursion to be measured than the linear range of the FD. The frequency to voltage conversion ratios, including all division and multiplication steps for Δf_r and Δf_n are respectively (8.2 ± 0.4) V/MHz and (5.93 ± 0.06) mV/MHz.

Regarding f_0, this frequency can not be directly detected in practice since f–to–$2f$ interferometry [19] is currently unavailable to QCL combs but fluctuations thereof can be detected [35], which allows the measurement of its transfer function. However, for experimental simplicity, we can compute it from the transfer function of f_n and f_r. Indeed, according to Eq. (1), (2) and the elastic tape model [38, 39], we have:

$$\begin{aligned} \Delta f_0 \sin(\omega t + \theta_0) = &\Delta f_n \sin(\omega t + \theta_n) \\ &- n\Delta f_r \sin(\omega t + \theta_r) \end{aligned} . \qquad (4)$$

Therefore, Eq. (4) yields that Δf_0 and θ_0 are respectively the modulus and phase of the complex value $\Delta f_n \exp(i\theta_n) - n\Delta f_r \exp(i\theta_r)$. Here, $n = 3551$ is set by the wavenumber of the DFB-QCL at 1309.79 cm^{-1}, and by the repetition rate.

Figure 4 shows the resulting phase θ_i and amplitude responses Δf_i of the frequencies (f_n, nf_r, f_0) to modulation of the electrical drive current, $\Delta I = 200$ µA, and the NIR power, $\Delta P = 50$ µW, where Δ represents the peak amplitude of the modulation. Note that Δf_r is scaled by n for better comparison with Δf_n. Also, the contributions of various components of the characterization scheme (i.e. the FDs and the laser driver) were measured and deducted in order to obtain the laser response as faithfully as possible. Moreover, the responses were measured with two different settings for the ranges [1 Hz, 100 Hz] and [100 Hz, 10 MHz], leading to negligible mismatches at 100 Hz.

Focusing first on the electrical actuation in Figure 4(a, c), we observe that the amplitude response Δf_n decreases steadily with the modulation frequency setting the 3-dB modulation bandwidth to 30 kHz, before decreasing sharply after about 200 kHz. The phase response remains flat up to 10 kHz with a 90° modulation bandwidth at 420 kHz, which is coherent with previous tight-locking results [20]. Moreover, the response of f_n closely mimic that of DFB-QCLs [25, 40]. f_r follows a similar behavior as f_n with a 3-dB and 90° modulation bandwidth of 80 kHz and 840 kHz respectively. The dashed line in Figure 4(c) is the phase response of f_n with the laser driver, and has an 90° modulation bandwidth of 280 kHz. The difference between Δf_n and $n\Delta f_r$ gives the response f_0, which has a flatter response in amplitude with a 3-dB modulation bandwidth of 160 kHz. The uncertainty on the measurements of Δf_n and $n\Delta f_r$, in particular, the slope of the FDs which depend on the input RF power induces a large absolute uncertainty on Δf_0. As

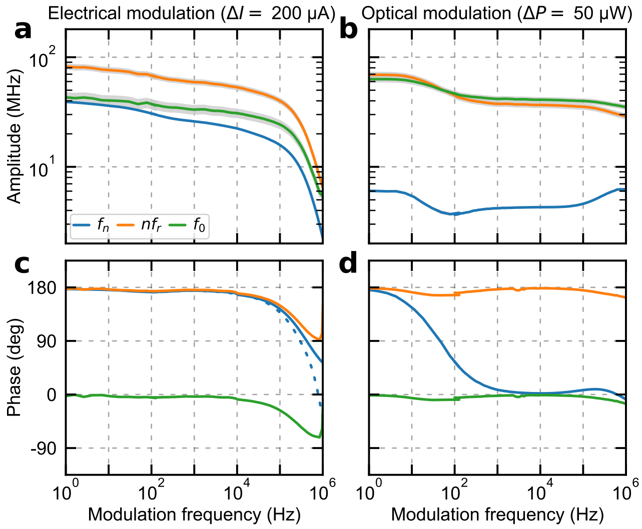

FIG. 4. Response of the comb frequencies (f_n, nf_r, f_0) to modulation of the drive current (a, c) and of the intensity of the NIR light (b, d). Panels (a, b) present the frequency excursions Δf_i while panels (c, d) show the phase response θ_i. The dashed line in (c) is the phase response of f_n with the laser driver.

for the phase, its response is also flatter, reaching $-70°$ near 1 MHz, after which the measurement is no longer accurate due to the lack of sensitivity. The (quasi-)fix point [38, 39] increases with modulation frequency from mode number 1850 at 1 Hz to mode number 2200 at 100 kHz.

Although the transfer function of a MIR QCL frequency comb has already been reported in Ref. [35], our measurements highlight a 90° modulation bandwidth one order of magnitude above what was previously shown. This is in agreement with the response of DFB-QCLs [25, 40, 41] and other QCL combs, measured directly [42] or demonstrated in a phase-lock loop [20, 22]. This discrepancy with the measured modulation bandwidth could be attributed to the frequency response of the bias-tee used in Ref. [35]. Furthermore, we observed in Figure 3 that modulations of f_r due to back reflections locally change the slope, such that the ratio between Δf_0 and Δf_n and the fix points are expected to be modulated as well.

We now turn to the optical actuation shown in Figure 4(b, d). For this measurement, the NIR laser was aligned on the QCL to the maximize the dynamic response of f_n at a 100 kHz modulation. We observe a nearly flat phase response for f_r up to 1 MHz, with a small resonance near 33 Hz and a start of a roll-off near 1 MHz. At the resonance near 33 Hz the amplitude response decreases by a factor 2, and then remains nearly flat apart from the onset of the roll-off near 1 MHz. The 33-Hz resonance also marks a change of regime for f_n, due to the crossing of $n\Delta f_r$ with Δf_0, the latter having a similar response as f_r, although a smaller relative change in amplitude response, and an opposite phase response. Thus, for modulation frequencies lower (higher) than 33 Hz, Δf_0 is smaller (higher) than $n\Delta f_r$, such that the response of f_n flips sign from 180° to 0° from 1 Hz to 1 kHz. The respective (quasi-)fixed points are at mode numbers 3250 and 3950. An associated dip in the amplitude response of f_n is also visible. Above 1 kHz, the response is flat up to about 50 kHz, where the response increases in phase and magnitude before showing a signature of a roll-off near 1 MHz.

The mechanism causing frequency modulation due to the drive current change is, identically to DFB-QCLs, a change of the refractive index [25]. In the case of a NIR injection, the strong inter-band absorption in the InGaAs quantum wells (the absorption coefficient $\alpha = 6000$ cm^{-1} at 1550 nm), that are part of the active region of the QCL, is responsible for the modulation of the refractive index through the generation of carriers in the vicinity of the NIR injection point. Also, we believe that the response below 30 Hz is dominated by thermal processes (heating of the QCL), as the sign of the responses are equal to drive current modulation and as the optimization of maximum static shift of f_n causes modulation of f_r as with drive current changes.

From the perspective of locking the QCL comb, the actuation via the NIR power is advantageous as it offers a higher bandwidth than the drive current actuation for all comb frequencies, even when the driver response has been accounted for. It is especially well suited for the stabilization of f_0 if it can be measured. The stabilization of f_n will require a countermeasure against the sign reversal as detailed in the next section. As for f_r, the increased actuation bandwidth is not as interesting given that it can be tightly-locked by actuation on the drive current [35].

IV. MUTUAL STABILIZATION

We now seek to implement a mutual lock between one comb line f_n of the QCL comb and a DFB-QCL as a proof-of-principle demonstration. The electrical part of the setup is adapted according to the orange path in Figure 1. The phase fluctuations between the two lasers are obtained by mixing the signal f_b after division by 15 with a synthesized reference frequency locked to the maser. This error signal is injected into two PID controllers (Vescent, D2-125). The output of one PID controller is fed back to the driver of the QCL comb to modulate the electrical current. The output of the second PID controller is fed back, after high-pass filtering with a 2$^{\text{nd}}$-order custom-designed filter with a cutoff at 1 kHz, to the EAM to modulate the intensity of the NIR CW laser. We also monitor the beatnote with the RF spectrum and phase noise analyzer. In this way, slow (< 100 kHz) corrections of f_n, which cannot be handled by the NIR light due to the sign reversal, are done by the drive current, while the NIR light extends the available bandwidth and

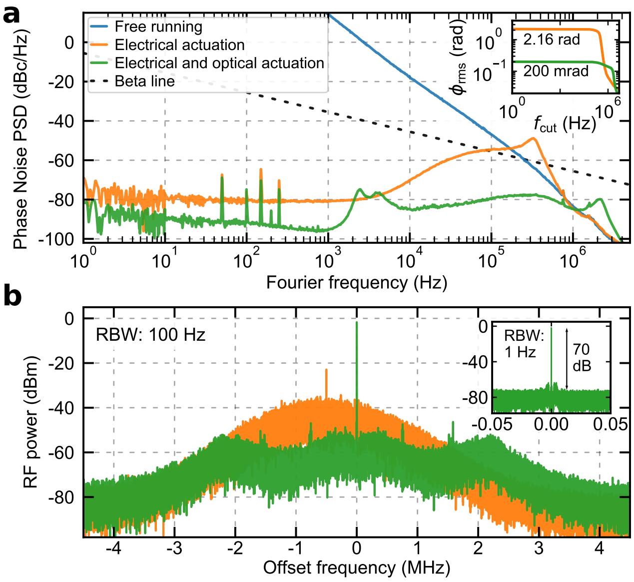

FIG. 5. Tight-locking of a QCL comb to a DFB-QCL. (a) Phase noise power spectral density (PSD) of the mutual beatnote in free-running mode, electrical actuation, and both electrical and optical actuation. (b) RF power spectrum at 100 Hz RBW of the beatnote between one line of the QCL comb and the DFB-QCL depending on the stabilization scheme used. Inset: Zoom on the beatnote at 1 Hz RBW.

cancels added noise from the drive current, i.e. the servo bump.

Figure 5 (a) and (b) respectively show the results of the stabilization of f_b in terms of phase noise and RF power spectrum. When only the electrical actuation is considered, we observe two bumps in the phase noise power spectral density (PSD). The first is due to the limit of the integrator at about 100 kHz, while the second near 300 kHz is the servo bump, which nearly coincides with the 90° modulation bandwidth of the combined driver and laser (see dashed blue line in Figure 4(c)). The white phase noise from 1 Hz to about 100 Hz is due to the reference oscillator, which due to the division by 15, has its contribution increased by 23 dB. The resulting RF spectrum shows a Gaussian shape topped with a coherent peak.

The addition of the optical actuation reduces the phase noise PSD to a value in the order of -80 dBc/Hz, below the β-line [43], for all Fourier frequencies. As a result, the integrated phase noise is decreased from 2.16 rad to 200 mrad (see inset in Figure 5(a)). The electrical servo bump is eliminated, while a new servo bump appears at 2 MHz. This fast bandwidth allows to employ a lower division ratio of 4: the residual phase noise from 1 Hz to 3 kHz is set by the reference oscillator. At higher frequencies, we believe that the mismatch between the reference voltages of the two different servo controller added noise to the system. Moreover, the bumps near 3 kHz coincide with the cutoff frequency of the high-pass filter. Further optimization of the electronic components could improve the lock and decrease the integrated phase noise further, including the use of a single dual-output servo controller. We also believe the stabilization bandwidth could be increased by shortening all the cables, fibers, and free-space paths. In terms of spectrum (Figure 5(b)), the power in the coherent peak improves by 20 dB. The height of the pedestal is decreased by 15 dB, such that the difference between the coherent peak and the top of the pedestal is 50 dB at a RBW of 100 Hz, or about 25 dB more than in Ref. [20] at 500 Hz RBW. The inset shows a zoom over the peak at a 1 Hz resolution bandwidth (RBW) with an SNR of 70 dB.

In parallel, the repetition frequency of the comb is stabilized by RF injection locking using a resonant RF signal with 15 dBm of power delivered by a signal generator (Rohde & Schwarz, SMF100A) referenced to a maser. This RF signal is sent to the QCL via the dedicated channel for RF injection. Thus both degrees of freedom are tightly-locked simultaneously with low residual phase noise. The electrical injection of the repetition rate is the usual approach for its stabilization. However, the previous results suggest that the repetition rate could also be injection-locked by modulating the NIR light.

V. REPETITION RATE INJECTION VIA NIR ILLUMINATION

We thus modulated the EAM of the NIR laser near the repetition frequency near 11.06 GHz while monitoring the generated voltage modulation of the QCL via the dedicated RF extraction port on a RF spectrum analyzer. At low NIR power and close to resonance (1 MHz offset), the modulation frequency was picked up by the QCL, which thus acted as a NIR detector (see Figure 6(a)). By slightly increasing the average NIR power with an amplifier to 1.5 mW at the QCL and the RF power on the EAM to 17 dBm (estimated modulation depth close to 100%), we were able to injection-lock the repetition frequency to the synthesizer and obtain the resolution-limited signal shown in Figure 6(b) at 50 Hz RBW. We obtained a lock range of a few kHz when scanning the modulation frequency across the free running repetition frequency (see Figure 6(c)). The phase noise PSD was reduced up to a Fourier frequency of about 3 kHz compared to the free-running case (Figure 6(d)). We expect that larger locking ranges could be achieved when using more NIR power, which will be one of the study we will present in another dedicated article.

VI. DISCUSSION

In this article, we used a low power NIR CW light illuminating the front facet of a MIR QCL frequency comb as an optical actuator for the phase stabilization of a comb line and as a mean to achieve coherent injection locking of the repetition rate. First, by characterizing the response of the QCL, we showed that intensity modulation of the NIR light offers a higher modulation bandwidth compared to conventional drive current modulation. Then, we implemented a stabilization scheme exploiting the NIR light to extend the locking-bandwidth from 300 kHz to over 2 MHz, which resulted in an increase of the SNR by 35 dB and an integrated phase noise as low as 200 mrad. Finally, we showed that the QCL can act as a detector of NIR light modulated at a frequency of 11 GHz, and that it can be injection-locked in such a way.

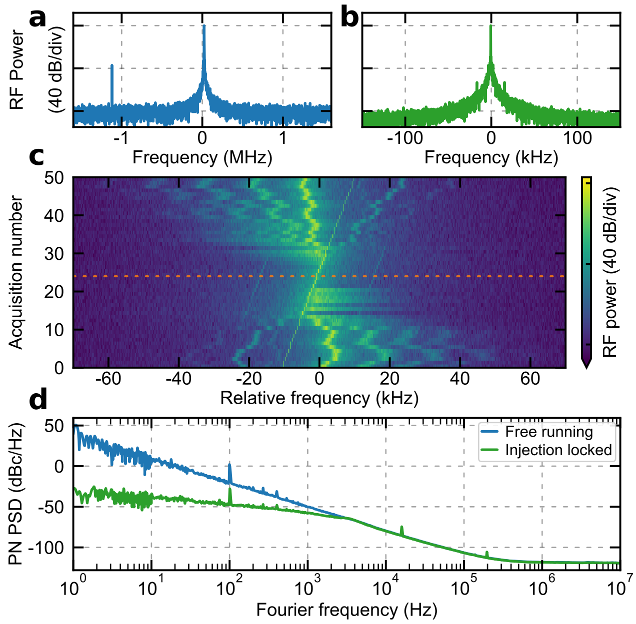

FIG. 6. Injection locking of the repetition rate by the NIR laser. (a, b) Electrically measured RF spectrum of the QCL with (a) the free running intermode beat and the detection of a weak off-resonant NIR modulation near −1 MHz, and (b) the injection-locked intermode beat using 1.5 mW of NIR light with 100% modulation depth. (c) Stacked RF spectra (50 Hz RBW) with the increasing modulation frequency crossing the natural repetition frequency and causing injection-locking over a range of a few kHz. The dashed horizontal line indexes the acquisition shown in (b). (d) Phase noise power spectral density (PN PSD) of the intermode beat signal in the free-running and injection locked regime.

We believe that the tighter mutual stabilization enabled by the high bandwidth of the NIR light could lead to higher sensitivities through coherent averaging in DCS [22, 44], which is currently one of the main applications of QCL combs. In this regard, a comprehensive comparison with the performance of computational coherent averaging [15] is necessary. The high bandwidth could also allow locking to enhancement cavities for further improvement of the sensitivity [45]. Moreover, high spectral purity in the MIR is relevant for a variety of applications such as quantum control of molecules [46], tests of fundamental physics [47, 48], and generally for the study of molecules via high-resolution spectroscopy [5, 49, 50]. Thus, we expect our results to facilitate the application of QCL frequency combs in the MIR.

As a further outlook, we anticipate that other wavelengths [33] could be more suitable for orthogonal control without sign reversal of the comb properties such as the offset and repetition frequencies, while perhaps they could also be used to dynamically tune laser parameters such as dispersion, gain, or nonlinearity. Faster modulations from 10 MHz to a few GHz could be investigated as a way to achieve (pure) frequency modulation of the comb. Then, full optical control of the QCL comb merely driven by a battery could be envisaged. To keep the compactness of the device and its low footprint, light could be delivered by fiber or directly generated and modulated on the same chip if low power is sufficient. Optical control could also be investigated in interband cascade lasers [51]. Moreover, the recent work on free-space communications using QCL combs [42] inspires the adaptation of injection locking of the QCL by NIR light for direct conversion of NIR telecommunication streams to MIR signals. We believe that increasing the injected optical power could increase the locking range of the repetition rate to a sufficient level for this application. Further work including theoretical and numerical investigations of the laser dynamics [52, 53] are necessary to understand the full potential of controlling QCLs via optical means.

ACKNOWLEDGMENTS

We thank Stéphane Schilt for support in the early stage of the investigation. We thank Alpes Laser for providing the DFB-QCL used in this work.

We acknowledge fundings from the Schweizerischer Nationalfonds zur Förderung der Wissenschaftlichen Forschung (40B2-1_176584).

Data underlying the results presented in this paper will be made available on an open server.

[1] A. Hugi, G. Villares, S. Blaser, H. C. Liu, and J. Faist, Mid-infrared frequency comb based on a quantum cascade laser, Nature **492**, 229 (2012).

[2] J. L. Klocke, M. Mangold, P. Allmendinger, A. Hugi, M. Geiser, P. Jouy, J. Faist, and T. Kottke, Single-Shot Sub-microsecond Mid-infrared Spectroscopy on Protein Reactions with Quantum Cascade Laser Frequency Combs, Anal. Chem. **90**, 10494 (2018).

[3] N. H. Pinkowski, P. Biswas, J. Shao, C. L. Strand, and R. K. Hanson, Thermometry and speciation for high-temperature and -pressure methane pyrolysis using shock tubes and dual-comb spectroscopy, Meas. Sci. Technol. **32**, 125502 (2021).

[4] M. Lepère, O. Browet, J. Clément, B. Vispoel, P. Allmendinger, J. Hayden, F. Eigenmann, A. Hugi, and M. Mangold, A mid-infrared dual-comb spectrometer in step-sweep mode for high-resolution molecular spectroscopy, J. Quant. Spectrosc. Radiat. Transf. **287**, 108239 (2022).

[5] J. A. Agner, S. Albert, P. Allmendinger, U. Hollenstein, A. Hugi, P. Jouy, K. Keppler, M. Mangold, F. Merkt, and M. Quack, High-resolution spectroscopic measurements of cold samples in supersonic beams using a QCL dual-comb spectrometer*, Mol. Phys. **120**, e2094297 (2022).

[6] K. N. Komagata, V. J. Wittwer, T. Südmeyer, L. Emmenegger, and M. Gianella, Absolute frequency referencing for swept dual-comb spectroscopy with midinfrared quantum cascade lasers, Phys. Rev. Res. **5**, 013047 (2023).

[7] K. Iwakuni, G. Porat, T. Q. Bui, B. J. Bjork, S. B. Schoun, O. H. Heckl, M. E. Fermann, and J. Ye, Phase-stabilized 100 mW frequency comb near 10 µm, Appl. Phys. B **124**, 128 (2018).

[8] K. Krzempek, D. Tomaszewska, A. Głuszek, T. Martynkien, P. Mergo, J. Sotor, A. Foltynowicz, and G. Soboń, Stabilized all-fiber source for generation of tunable broadband f_{CEO}-free mid-IR frequency comb in the 7 – 9 µm range, Opt. Express **27**, 37435 (2019).

[9] N. Hoghooghi, S. Xing, P. Chang, D. Lesko, A. Lind, G. Rieker, and S. Diddams, Broadband 1-GHz mid-infrared frequency comb, Light Sci. Appl. **11**, 264 (2022).

[10] P. Jouy, J. M. Wolf, Y. Bidaux, P. Allmendinger, M. Mangold, M. Beck, and J. Faist, Dual comb operation of $\lambda \sim 8.2$ µm quantum cascade laser frequency comb with 1 W optical power, Appl. Phys. Lett. **111**, 141102 (2017).

[11] I. Coddington, N. Newbury, and W. Swann, Dual-comb spectroscopy, Optica **3**, 414 (2016).

[12] N. Picqué and T. W. Hänsch, Frequency comb spectroscopy, Nat. Photonics **13**, 146 (2019).

[13] F. R. Giorgetta, J. Peischl, D. I. Herman, G. Ycas, I. Coddington, N. R. Newbury, and K. C. Cossel, Open-Path Dual-Comb Spectroscopy for Multispecies Trace Gas Detection in the 4.5–5 µm Spectral Region, Laser Photonics Rev. **15**, 2000583 (2021).

[14] A. Parriaux, K. Hammani, C. Thomazo, O. Musset, and G. Millot, Isotope ratio dual-comb spectrometer, Phys. Rev. Res. **4**, 023098 (2022).

[15] L. A. Sterczewski, J. Westberg, and G. Wysocki, Computational coherent averaging for free-running dual-comb spectroscopy, Opt. Express **27**, 23875 (2019).

[16] J. D. Jost, J. L. Hall, and J. Ye, Continuously tunable, precise, single frequency optical signal generator, Opt. Express **10**, 515 (2002).

[17] B. Argence, B. Chanteau, O. Lopez, D. Nicolodi, M. Abgrall, C. Chardonnet, C. Daussy, B. Darquié, Y. Le Coq, and A. Amy-Klein, Quantum cascade laser frequency stabilization at the sub-Hz level, Nat. Photonics **9**, 456 (2015).

[18] K. N. Komagata, M. Gianella, P. Jouy, F. Kapsalidis, M. Shahmohammadi, M. Beck, R. Matthey, V. J. Wittwer, A. Hugi, J. Faist, L. Emmenegger, T. Südmeyer, and S. Schilt, Absolute frequency referencing in the long wave infrared using a quantum cascade laser frequency

comb, Opt. Express **30**, 12891 (2022).

[19] H. R. Telle, G. Steinmeyer, A. E. Dunlop, J. Stenger, D. H. Sutter, and U. Keller, Carrier-envelope offset phase control: A novel concept for absolute optical frequency measurement and ultrashort pulse generation, Appl. Phys. B **69**, 327 (1999).

[20] F. Cappelli, G. Campo, I. Galli, G. Giusfredi, S. Bartalini, D. Mazzotti, P. Cancio, S. Borri, B. Hinkov, J. Faist, and P. De Natale, Frequency stability characterization of a quantum cascade laser frequency comb, Laser Photonics Rev. **10**, 623 (2016).

[21] J. Westberg, L. A. Sterczewski, and G. Wysocki, Mid-infrared multiheterodyne spectroscopy with phase-locked quantum cascade lasers, Appl. Phys. Lett. **110**, 141108 (2017).

[22] K. Komagata, A. Shehzad, G. Terrasanta, P. Brochard, R. Matthey, M. Gianella, P. Jouy, F. Kapsalidis, M. Shahmohammadi, M. Beck, V. J. Wittwer, J. Faist, L. Emmenegger, T. Südmeyer, A. Hugi, and S. Schilt, Coherently-averaged dual comb spectrometer at 7.7 µm with master and follower quantum cascade lasers, Opt. Express **29**, 19126 (2021).

[23] J. Hillbrand, A. M. Andrews, H. Detz, G. Strasser, and B. Schwarz, Coherent injection locking of quantum cascade laser frequency combs, Nat. Photonics **13**, 101 (2019).

[24] L. Tombez, S. Schilt, J. Di Francesco, P. Thomann, and D. Hofstetter, Temperature dependence of the frequency noise in a mid-IR DFB quantum cascade laser from cryogenic to room temperature, Opt. Express **20**, 6851 (2012).

[25] L. Tombez, F. Cappelli, S. Schilt, G. Di Domenico, S. Bartalini, and D. Hofstetter, Wavelength tuning and thermal dynamics of continuous-wave mid-infrared distributed feedback quantum cascade lasers, Appl. Phys. Lett. **103**, 031111 (2013).

[26] M. Hoffmann, S. Schilt, and T. Südmeyer, CEO stabilization of a femtosecond laser using a SESAM as fast opto-optical modulator, Opt. Express **21**, 30054 (2013).

[27] C. Zervos, M. D. Frogley, C. C. Phillips, D. O. Kundys, L. R. Wilson, M. Hopkinson, and M. S. Skolnick, All-optical switching in quantum cascade lasers, Appl. Phys. Lett. **90**, 053505 (2007).

[28] G. Chen, C. G. Bethea, and R. Martini, Quantum cascade laser gain enhancement by front facet illumination, Opt. Express **17**, 24282 (2009).

[29] L. Tombez, S. Schilt, D. Hofstetter, and T. Südmeyer, Active linewidth-narrowing of a mid-infrared quantum cascade laser without optical reference, Opt. Lett. **38**, 5079 (2013).

[30] C. Peng, G. Chen, J. Tang, L. Wang, Z. Wen, H. Zhou, and R. Martini, High-Speed Mid-Infrared Frequency Modulation Spectroscopy Based on Quantum Cascade Laser, IEEE Photonics Technol. Lett. **28**, 1727 (2016).

[31] L. Consolino, A. Campa, M. De Regis, F. Cappelli, G. Scalari, J. Faist, M. Beck, M. Rösch, S. Bartalini, and P. De Natale, Controlling and phase-locking a THz quantum cascade laser frequency comb by small optical frequency tuning, Laser Photonics Rev. **15**, 2000417 (2021).

[32] J. Hillbrand, M. Bertrand, V. Wittwer, N. Opačak, F. Kapsalidis, M. Gianella, L. Emmenegger, B. Schwarz, T. Südmeyer, M. Beck, and J. Faist, Synchronization of frequency combs by optical injection, Opt. Express **30**, 36087 (2022).

[33] C. Peng, H. Zhou, L. Zhu, T. Chen, Q. Liu, D. Wang, J. Li, Q. Peng, G. Chen, and Z. Li, Purified frequency modulation of a quantum cascade laser with an all-optical approach, Opt. Lett. **42**, 4506 (2017).

[34] F. Cappelli, L. Consolino, G. Campo, I. Galli, D. Mazzotti, A. Campa, M. Siciliani de Cumis, P. Cancio Pastor, R. Eramo, M. Rösch, M. Beck, G. Scalari, J. Faist, P. De Natale, and S. Bartalini, Retrieval of phase relation and emission profile of quantum cascade laser frequency combs, Nat. Photonics **13**, 562 (2019).

[35] A. Shehzad, P. Brochard, R. Matthey, F. Kapsalidis, M. Shahmohammadi, M. Beck, A. Hugi, P. Jouy, J. Faist, T. Südmeyer, and S. Schilt, Frequency noise correlation between the offset frequency and the mode spacing in a mid-infrared quantum cascade laser frequency comb, Opt. Express **28**, 8200 (2020).

[36] M. Piccardo, D. Kazakov, N. A. Rubin, P. Chevalier, Y. Wang, F. Xie, K. Lascola, A. Belyanin, and F. Capasso, Time-dependent population inversion gratings in laser frequency combs, Optica **5**, 475 (2018).

[37] C. C. Teng, J. Westberg, and G. Wysocki, Gapless tuning of quantum cascade laser frequency combs with external cavity optical feedback, Opt. Lett. **48**, 363 (2023).

[38] H. Telle, B. Lipphardt, and J. Stenger, Kerr-lens, mode-locked lasers as transfer oscillators for optical frequency measurements, Appl. Phys. B **74**, 1 (2002).

[39] V. Dolgovskiy, N. Bucalovic, P. Thomann, C. Schori, G. Di Domenico, and S. Schilt, Cross-influence between the two servo loops of a fully stabilized Er: Fiber optical frequency comb, J. Opt. Soc. Am. B **29**, 2944 (2012).

[40] A. Hangauer, G. Spinner, M. Nikodem, and G. Wysocki, High frequency modulation capabilities and quasi single-sideband emission from a quantum cascade laser, Opt. Express **22**, 23439 (2014).

[41] S. Borri, S. Bartalini, P. C. Pastor, I. Galli, G. Giusfredi, D. Mazzotti, M. Yamanishi, and P. De Natale, Frequency-Noise Dynamics of Mid-Infrared Quantum Cascade Lasers, IEEE J. Quantum. Electron. **47**, 984 (2011).

[42] N. Corrias, T. Gabbrielli, P. De Natale, L. Consolino, and F. Cappelli, Analog FM free-space optical communication based on a mid-infrared quantum cascade laser frequency comb, Opt. Express **30**, 10217 (2022).

[43] G. Di Domenico, S. Schilt, and P. Thomann, Simple approach to the relation between laser frequency noise and laser line shape, Appl. Opt. **49**, 4801 (2010).

[44] Z. Chen, M. Yan, T. W. Hänsch, and N. Picqué, A phase-stable dual-comb interferometer, Nat. Commun. **9**, 3035 (2018).

[45] A. Foltynowicz, P. Masłowski, A. J. Fleisher, B. J. Bjork, and J. Ye, Cavity-enhanced optical frequency comb spectroscopy in the mid-infrared application to trace detection of hydrogen peroxide, Appl. Phys. B **110**, 163 (2013).

[46] M. Sinhal, Z. Meir, K. Najafian, G. Hegi, and S. Willitsch, Quantum-nondemolition state detection and spectroscopy of single trapped molecules, Science **367**, 1213 (2020).

[47] P. Jansen, H. L. Bethlem, and W. Ubachs, Perspective: Tipping the scales: Search for drifting constants from molecular spectra, J. Chem. Phys. **140**, 010901 (2014).

[48] A. Cournol, M. Manceau, M. Pierens, L. Lecordier, D. B. A. Tran, R. Santagata, B. Argence, A. Goncharov, O. Lopez, M. Abgrall, Y. Le Coq, R. Le Targat, H. Alvarez Martinez, W. K. Lee, D. Xu, P. E. Pottie, R. J.

Hendricks, T. E. Wall, J. M. Bieniewska, B. E. Sauer, M. R. Tarbutt, A. Amy-Klein, S. K. Tokunaga, and B. Darquié, A new experiment to test parity symmetry in cold chiral molecules using vibrational spectroscopy, Quantum Electron. **49**, 288 (2019).

[49] P. B. Changala, M. L. Weichman, K. F. Lee, M. E. Fermann, and J. Ye, Rovibrational quantum state resolution of the C_{60} fullerene, Science **363**, 49 (2019).

[50] M. Germann, A. Hjältén, V. Boudon, C. Richard, K. Krzempek, A. Hudzikowski, A. Głuszek, G. Soboń, and A. Foltynowicz, A methane line list with sub-MHz accuracy in the 1250 to 1380 cm^{-1} range from optical frequency comb Fourier transform spectroscopy, J. Quant. Spectrosc. Radiat. Transf. **288**, 108252 (2022).

[51] M. Bagheri, C. Frez, L. A. Sterczewski, I. Gruidin, M. Fradet, I. Vurgaftman, C. L. Canedy, W. W. Bewley, C. D. Merritt, C. S. Kim, M. Kim, and J. R. Meyer, Passively mode-locked interband cascade optical frequency combs, Sci. Rep. **8**, 3322 (2018).

[52] G. Villares and J. Faist, Quantum cascade laser combs: Effects of modulation and dispersion, Opt. Express **23**, 1651 (2015).

[53] N. Opačak and B. Schwarz, Theory of Frequency-Modulated Combs in Lasers with Spatial Hole Burning, Dispersion, and Kerr Nonlinearity, Phys. Rev. Lett. **123**, 243902 (2019).

Chapter 4

All-Mid-Infrared Comb-Assisted Spectroscopy

After the investigation of locking techniques in the previous chapter, we turn to applications. As proper FCs, QCLs have many potential uses besides DCS. For example, FCs can serve as an optical ruler to measure frequencies which are otherwise too high to be counted directly. This requires the knowledge of both comb degrees of freedom. The repetition rate of QCLs is low enough to be compared to a synthesized RF reference. As for the offset frequency, it is as of now not detectable through self-referencing. Alternatively, an optical reference beating with a comb line provides the necessary knowledge. Then, the frequency of all comb lines can be determined with a given accuracy and exploited, e.g., to calibrate the frequency of another laser for spectroscopy. We implemented such a scheme with a MIR QCL FC in a proof-of-principle experiment reported in Optics Express [1] and reproduced at end of the chapter with permission.

4.1 Summary of the article

A DFB QCL was locked to a molecular transiton of N_2O at about 1292.3 cm^{-1} via wavelength modulation spectroscopy (WMS) [2] and served as an optical reference (see Fig. 1). One of the QCL comb line was phase-locked to the reference by retro-action on the drive current of the comb. The repetition rate of the comb was phase-locked by injection locking of low-noise RF frequency. We characterized the stability of the reference by setting another one at 1309.1 cm^{-1} and comparing the two references with the comb as a transfer oscillator that bridged the half-THz gap (see Fig. 2). Then, we performed comb-calibrated spectroscopy on several lines and obtained their transition frequencies (Fig. 3). The uncertainty budget determined a 100 kHz accuracy for our measurement, where the main limit is not related to the comb but due to the frequency reference. Our results were in excellent agreement with the literature. Note that there is a minor mistake in the uncertainty budget: Δ_f bias uncertainty is actually of type A.

4.2 Further discussion

4.2.1 Application of the referenced comb

The demonstrated 100 kHz accuracy is suitable for the study of ro-vibrational bands with the aim of deriving more accurate Hamiltonian parameters for the molecule [3–6], which in turn, may be relevant for a wide range of applications, e.g., modeling of planetary atmospheres including that of the earth. Alternatively, such a comb could be useful e.g., for comb-calibrated characterization of photonic integrated chips (PICs) [7] and of spectral features of light sources [8] in the MIR. Recent developments in trapping and cooling molecules also suggest the need of MIR combs [9]. Generally, it is a building block of an optical frequency synthesizer [10] for the MIR in combination with an external cavity QCL [11] or Vernier QCLs [12]. A comb with a higher accuracy and a high spectral purity could be useful for spectroscopic measurements related to physics beyond the standard model [13, 14], the coherent control of molecular states [15], or for new applications yet to be discovered.

4.2.2 Improving the frequency reference

The frequency accuracy and precision of the stabilized comb was limited by the reference that we set. Saturation spectroscopy could have increased the frequency precision by one or two orders of magnitude [16, 17], while a different choice (or a pre-calibration) of the transition would have increased the accuracy of the comb. Further improvements can be realized by seeking pure frequency modulation of the DFB QCL, either with an external modulator [18], by using a second actuator [19], or in a specially designed QCL [20, 21]. Enhancement cavities for increasing light-matter interaction could also benefit these performances [22].

4.2.3 A chip-based MIR frequency reference

An optimal solution for referencing should be compatible with photonic integration, as arguably was ours: light generation, sensing, combining, and detection could in principle all be integrated on the same chip [23–25]. Saturation spectroscopy of ro-vibrational transition on chip should also be possible, as was demonstrated for electronic transitions with rubidium [26], using MIR photonics with large evanescent field confinement factor [24]. In particular, the OsO_4 transitions in the 10 µm are secondary frequency standard, measured with about 50-Hz accuracy [27].

Currently, the most accurate and stable optical references are found in the NIR. Moreover, high-quality NIR references traceable to the international system of units (SI) are planned to become available to most European laboratories through a network of optical fibers [28, 29]. It is attractive to exploit those references for MIR applications, but that conventionally requires nonlinear frequency conversion in a bulk crystal and an additional frequency comb [30]. Instead, a simple chip-based NIR-to-MIR link would be preferred. A potential solution could rely on harmonic injection locking [31], e.g., injection of 1.5 µm light into a 3 µm interband cascade lasers (ICLs) with intracavity second-harmonic generation [32], followed by the injection-locking of the latter into a 9 µm QCL enabled by its Kerr nonlinearity. Alternatively, the 1.5 µm laser could lock a 4.5 µm QCL while a 9 µm QCL could be locked by specific design of intracavity nonlinearities [33, 34] to allow second harmonic injection locking. The strength of this solution is that the lasers and waveguides could all be integrated on the same chip for simple but coherent conversion of 1.5 µm radiation to 9 µm. This device could be used wherever fiber-transmitted NIR references are available, i.e. most laboratories in the future.

The perspective of self-referencing QCL combs does not eliminate the need of a chip-based MIR reference. In fact, the frequency noise of the repetition rate is multiplied in the optical domain. Therefore, the best frequency purity is obtained by locking the repetition rate to an optical reference while the offset frequency is locked via f–to–2f interferometry [35]. In that case, QCLs could perhaps even be used for low-noise RF frequency synthesis via optical division [36]. One advantage would be the active generation of the RF signal by the laser instead of photodetection.

4.2.4 Optical feedback

In the article, we wrote that “Minimization of back-reflections to the QCL-OFC was key to achieve a stable phase-lock”. However, the recent findings by Teng *et al.* [37] suggests that optical feedback stabilizes the comb rather than destabilizing it. I would like to make two remarks, which could explain these two apparently-contradictory findings. First, in our implementation, the feedback was not controlled. It was mostly caused by the photodetector which was susceptible to mechanical vibrations and located near the focal point of the beam. The feedback ratio was not characterized but surely less than 1%, and the optical path length unknown. In the other paper, a mirror (which we expect to be steadier than our photodetector) was used at a distance equal to a multiple of the optical length of the QCL chip, and the feedback ratio was optimized. Second, although the feedback phase did not influence their measured linewidth, its variation nevertheless led to mode-hops, which could in our implementation be sufficient to destabilize the PLL despite the injection locking of the repetition rate. However, I believe that more theoretical and experimental investigations are needed to clarify the situation [38].

4.3 Conclusion

In conclusion, we have demonstrated one scheme to obtain a referenced MIR FC with 100-kHz level accuracy and 6-kHz stability at 100-s integration time. These values can be enhanced by improving the frequency reference. MIR FCs are important for spectroscopy, characterization of devices and light-sources, and emerging fields such as the quantum control of molecules. Full integration of the referenced comb should be feasible in the future and will empower MIR technologies.

References

[1] K. N. Komagata, M. Gianella, P. Jouy, F. Kapsalidis, M. Shahmohammadi, M. Beck, R. Matthey, V. J. Wittwer, A. Hugi, J. Faist, L. Emmenegger, T. Südmeyer, and S. Schilt, "Absolute Frequency Referencing in the Long Wave Infrared Using a Quantum Cascade Laser Frequency Comb", Opt. Express **30**, 12891 (2022).

[2] S. Schilt, "Mesure de Traces de Gaz à l'aide de Lasers à Semi-Conducteur" (EPFL, Lausanne, 2002).

[3] P. B. Changala, M. L. Weichman, K. F. Lee, M. E. Fermann, and J. Ye, "Rovibrational Quantum State Resolution of the C_{60} Fullerene", Science **363**, 49 (2019).

[4] A. Hjältén, M. Germann, K. Krzempek, A. Hudzikowski, A. Głuszek, D. Tomaszewska, G. Soboń, and A. Foltynowicz, "Optical Frequency Comb Fourier Transform Spectroscopy of $^{14}N_2{}^{16}O$ at 7.8 µm", J. Quant. Spectrosc. Radiat. Transf. **271**, 107734 (2021).

[5] J. A. Agner, S. Albert, P. Allmendinger, U. Hollenstein, A. Hugi, P. Jouy, K. Keppler, M. Mangold, F. Merkt, and M. Quack, "High-Resolution Spectroscopic Measurements of Cold Samples in Supersonic Beams Using a QCL Dual-Comb Spectrometer*", Mol. Phys. **120**, e2094297 (2022).

[6] M. Germann, A. Hjältén, V. Boudon, C. Richard, K. Krzempek, A. Hudzikowski, A. Głuszek, G. Soboń, and A. Foltynowicz, "A Methane Line List with Sub-MHz Accuracy in the 1250 to 1380 cm^{-1} Range from Optical Frequency Comb Fourier Transform Spectroscopy", J. Quant. Spectrosc. Radiat. Transf. **288**, 108252 (2022).

[7] P. Del'Haye, O. Arcizet, M. L. Gorodetsky, R. Holzwarth, and T. J. Kippenberg, "Frequency Comb Assisted Diode Laser Spectroscopy for Measurement of Microcavity Dispersion", Nat. Photonics **3**, 529 (2009).

[8] T. Herr, K. Hartinger, J. Riemensberger, C. Y. Wang, E. Gavartin, R. Holzwarth, M. L. Gorodetsky, and T. J. Kippenberg, "Universal Formation Dynamics and Noise of Kerr-frequency Combs in Microresonators", Nat. Photonics **6**, 480 (2012).

[9] S. Alighanbari, M. G. Hansen, V. I. Korobov, and S. Schiller, "Rotational Spectroscopy of Cold and Trapped Molecular Ions in the Lamb–Dicke Regime", Nat. Phys. **14**, 555 (2018).

[10] J. D. Jost, J. L. Hall, and J. Ye, "Continuously Tunable, Precise, Single Frequency Optical Signal Generator", Opt. Express **10**, 515 (2002).

[11] A. Hugi, R. Maulini, and J. Faist, "External Cavity Quantum Cascade Laser", Semicond. Sci. Technol. **25**, 083001 (2010).

[12] Y. Bidaux, A. Bismuto, C. Tardy, R. Terazzi, T. Gresch, S. Blaser, A. Muller, and J. Faist, "Extended and Quasi-Continuous Tuning of Quantum Cascade Lasers Using Superstructure Gratings and Integrated Heaters", Appl. Phys. Lett. **107**, 221108 (2015).

[13] S. K. Tokunaga, C. Stoeffler, F. Auguste, A. Shelkovnikov, C. Daussy, A. Amy-Klein, C. Chardonnet, and B. Darquié, "Probing Weak Force-Induced Parity Violation by High-Resolution Mid-Infrared Molecular Spectroscopy", Mol. Phys. **111**, 2363 (2013).

[14] I. V. Kortunov, S. Alighanbari, M. G. Hansen, G. S. Giri, V. I. Korobov, and S. Schiller, "Proton–Electron Mass Ratio by High-Resolution Optical Spectroscopy of Ion Ensembles in the Resolved-Carrier Regime", Nat. Phys. **17**, 569 (2021).

[15] M. Sinhal, Z. Meir, K. Najafian, G. Hegi, and S. Willitsch, "Quantum-Nondemolition State Detection and Spectroscopy of Single Trapped Molecules", Science **367**, 1213 (2020).

[16] F. Cappelli, I. Galli, S. Borri, G. Giusfredi, P. Cancio, D. Mazzotti, A. Montori, N. Akikusa, M. Yamanishi, and S. Bartalini, "Subkilohertz Linewidth Room-Temperature Mid-Infrared Quantum Cascade Laser Using a Molecular Sub-Doppler Reference", Opt. Lett. **37**, 4811 (2012).

[17] A. Gambetta, E. Vicentini, Y. Wang, N. Coluccelli, E. Fasci, L. Gianfrani, A. Castrillo, V. D. Sarno, L. Santamaria, P. Maddaloni, P. D. Natale, P. Laporta, and G. Galzerano, "Absolute Frequency Measurements of CHF_3 Doppler-free Ro-Vibrational Transitions at 8.6 µm", Opt. Lett. **42**, 1911 (2017).

[18] V. Bernard, C. Daussy, G. Nogues, L. Constantin, P. E. Durand, A. Amy-Klein, A. Van Lerberghe, and C. Chardonnet, "CO_2 Laser Stabilization to 0.1-Hz Level Using External Electrooptic Modulation", IEEE J. Quantum Electron. **33**, 1282 (1997).

[19] C. Peng, H. Zhou, L. Zhu, T. Chen, Q. Liu, D. Wang, J. Li, Q. Peng, G. Chen, and Z. Li, "Purified Frequency Modulation of a Quantum Cascade Laser with an All-Optical Approach", Opt. Lett. **42**, 4506 (2017).

[20] Y. Bidaux, A. Bismuto, P. Patimisco, A. Sampaolo, T. Gresch, G. Strubi, S. Blaser, F. K. Tittel, V. Spagnolo, A. Muller, and J. Faist, "Mid Infrared Quantum Cascade Laser Operating in Pure Amplitude Modulation for Background-Free Trace Gas Spectroscopy", Opt. Express **24**, 26464 (2016).

[21] A. Shehzad, P. Brochard, R. Matthey, S. Blaser, T. Gresch, R. Maulini, A. Muller, T. Südmeyer, and S. Schilt, "Electrically-Driven Pure Amplitude and Frequency Modulation in a Quantum Cascade Laser", Opt. Express **26**, 12306 (2018).

[22] O. Acef, "Metrological Properties of CO_2/OsO_4 Optical Frequency Standard", Opt. Commun. **134**, 479 (1997).

[23] B. Schwarz, P. Reininger, D. Ristanić, H. Detz, A. M. Andrews, W. Schrenk, and G. Strasser, "Monolithically Integrated Mid-Infrared Lab-on-a-Chip Using Plasmonics and Quantum Cascade Structures", Nat. Commun. **5**, 4085 (2014).

[24] S. Alberti, A. Datta, and J. Jágerská, "Integrated Nanophotonic Waveguide-Based Devices for IR and Raman Gas Spectroscopy", Sensors **21**, 7224 (2021).

[25] R. Wang, P. Täschler, Z. Wang, E. Gini, M. Beck, and J. Faist, "Monolithic Integration of Mid-Infrared Quantum Cascade Lasers and Frequency Combs with Passive Waveguides", ACS Photonics **9**, 426 (2022).

[26] W. Yang, D. B. Conkey, B. Wu, D. Yin, A. R. Hawkins, and H. Schmidt, "Atomic Spectroscopy on a Chip", Nat. Photonics **1**, 331 (2007).

[27] O. Acef, F. Michaud, and G. Rovera, "Accurate Determination of OsO_4 Absolute Frequency Grid at 28/29 THz", IEEE Trans. Instrum. Meas. **48**, 567 (1999).

[28] A. Bercy, F. Stefani, O. Lopez, C. Chardonnet, P.-E. Pottie, and A. Amy-Klein, "Two-Way Optical Frequency Comparisons at 5×10^{-21} Relative Stability over 100-Km Telecommunication Network Fibers", Phys. Rev. A **90**, 061802 (2014).

[29] D. Husmann, L.-G. Bernier, M. Bertrand, D. Calonico, K. Chaloulos, G. Clausen, C. Clivati, J. Faist, E. Heiri, U. Hollenstein, A. Johnson, F. Mauchle, Z. Meir, F. Merkt, A. Mura, G. Scalari, S. Scheidegger, H. Schmutz, M. Sinhal, S. Willitsch, and J. Morel, "SI-traceable Frequency Dissemination at 1572.06 µm in a Stabilized Fiber Network with Ring Topology", Opt. Express **29**, 24592 (2021).

[30] B. Argence, B. Chanteau, O. Lopez, D. Nicolodi, M. Abgrall, C. Chardonnet, C. Daussy, B. Darquié, Y. Le Coq, and A. Amy-Klein, "Quantum Cascade Laser Frequency Stabilization at the Sub-Hz Level", Nat. Photonics **9**, 456 (2015).

[31] I. I. Zolotoverkh and E. G. Lariontsev, "Dynamics of Injection Locking in a Solid-State Laser with Intracavity Second-Harmonic Generation", Quantum Electron. **30**, 787 (2000).

[32] L. A. Sterczewski, M. Bagheri, C. Frez, C. L. Canedy, I. Vurgaftman, M. Kim, C. S. Kim, C. D. Merritt, W. W. Bewley, and J. R. Meyer, "Near-Infrared Frequency Comb Generation in Mid-Infrared Interband Cascade Lasers", Opt. Lett. **44**, 5828 (2019).

[33] N. Owschimikow, C. Gmachl, A. Belyanin, V. Kocharovsky, D. L. Sivco, R. Colombelli, F. Capasso, and A. Y. Cho, "Resonant Second-Order Nonlinear Optical Processes in Quantum Cascade Lasers", Phys. Rev. Lett. **90**, 043902 (2003).

[34] M. Giovannini, M. Beck, N. Hoyler, and J. Faist, "Second Harmonic Generation in (111)-Oriented InP-based Quantum Cascade Laser", J. Appl. Phys. **101**, 103107 (2007).

[35] T. Fortier and E. Baumann, "20 Years of Developments in Optical Frequency Comb Technology and Applications", Commun. Phys. **2**, 1 (2019).

[36] T. M. Fortier, M. S. Kirchner, F. Quinlan, J. Taylor, J. C. Bergquist, T. Rosenband, N. Lemke, A. Ludlow, Y. Jiang, C. W. Oates, and S. A. Diddams, "Generation of Ultrastable Microwaves via Optical Frequency Division", Nat. Photonics **5**, 425 (2011).

[37] C. C. Teng, J. Westberg, and G. Wysocki, "Gapless Tuning of Quantum Cascade Laser Frequency Combs with External Cavity Optical Feedback", Opt. Lett. **48**, 363 (2023).

[38] C. Silvestri, X. Qi, T. Taimre, and A. D. Rakić, "Frequency Combs and Optical Feedback in Quantum Cascade Lasers: A Unifying Theoretical Framework", ArXiv230504454 Phys., `10.48550/arXiv.2305.04454` (2023).

Research Article | Vol. 30, No. 8 / 11 Apr 2022 / Optics Express 12891

Optics EXPRESS

Absolute frequency referencing in the long wave infrared using a quantum cascade laser frequency comb

K. N. KOMAGATA,[1,*] M. GIANELLA,[2] P. JOUY,[3] F. KAPSALIDIS,[4] M. SHAHMOHAMMADI,[4] M. BECK,[4] R. MATTHEY,[1] V. J. WITTWER,[1] A. HUGI,[3] J. FAIST,[4] L. EMMENEGGER,[2] T. SÜDMEYER,[1] AND S. SCHILT[1]

[1] *Laboratoire Temps-Fréquence, Institut de Physique, Université de Neuchâtel, Avenue de Bellevaux 51, 2000 Neuchâtel, Switzerland*
[2] *Empa, Laboratory for Air Pollution / Environmental Technology, 8600 Dübendorf, Switzerland*
[3] *IRsweep AG, Laubisrütistrasse 44, 8712 Stäfa, Switzerland*
[4] *Institute for Quantum Electronics, ETH Zurich, 8093 Zurich, Switzerland*
[*] *kenichi.komagata@unine.ch*

Abstract: Optical frequency combs (OFCs) based on quantum cascade lasers (QCLs) have transformed mid-infrared spectroscopy. However, QCL-OFCs have not yet been exploited to provide a broadband absolute frequency reference. We demonstrate this possibility by performing comb-calibrated spectroscopy at 7.7 µm (1305 cm^{-1}) using a QCL-OFC referenced to a molecular transition. We obtain 1.5·10^{-10} relative frequency stability (100-s integration time) and 3·10^{-9} relative frequency accuracy, comparable with state-of-the-art solutions relying on nonlinear frequency conversion. We show that QCL-OFCs can be locked with sub-Hz-level stability to a reference for hours, thus promising their use as metrological tools for the mid-infrared.

© 2022 Optica Publishing Group under the terms of the Optica Open Access Publishing Agreement

1. Introduction

The enticing prospect of highly sensitive and selective molecular detection has spurred the development of mid-infrared (MIR) spectrometers [1,2], having strong implications for example in the fields of security [3], health [4], food production [5], and others [6–8]. While Fourier transform infrared spectrometers (FTIRs) based on thermal sources have, for several decades, been the working horse for MIR spectroscopy, optical frequency combs (OFCs) [9] have emerged in the last two decades as the new tool for spectroscopy [1]. In particular, they have allowed the measurement of transition frequencies with unprecedented accuracy [10]. Indeed, they can provide a broadband ruler for measuring optical frequencies through referencing to only two frequencies. Moreover, they are polyvalent in their application to spectroscopy [11], e.g. in dual comb arrangements [12–16], combined with an FTIR [17,18], or in open or closed loop comb-assisted schemes [19–21].

So far, nonlinear frequency conversion has been the main way to perform MIR spectroscopy with referenced OFCs generated in the near-infrared (NIR), at the cost of added complexity, reduced optical output power, and the necessity of sufficient seed power. Integrated photonics based on lithium niobate or silicon nitride promise small-footprint conversion with low pulse energy, but only to wavelengths up to 4.5 µm [8,14,22–24]. In the long-wave infrared (8 µm to 12 µm) and beyond, several experiments successfully determined the absolute frequency of molecular transitions by performing nonlinear frequency conversion [25–35]. The obtained accuracies were typically in the 100-kHz range in the Doppler-limited regime and down to 22 Hz in the Doppler-free regime [10].

#447650 https://doi.org/10.1364/OE.447650
Journal © 2022 Received 23 Nov 2021; revised 27 Jan 2022; accepted 1 Feb 2022; published 4 Apr 2022

Optics EXPRESS

In 2012, quantum cascade lasers (QCL) demonstrated a breakthrough by allowing the direct generation of OFCs in the MIR [36,37]. Since then, the development of a commercial dual comb spectrometer based on QCLs has had a disruptive impact in the fields of chemistry and biology [38,39]. The success of QCLs can be attributed to their small footprint and simple operation. Furthermore, they can be conveniently controlled with their temperature [40], driving current [41–43], and through radio-frequency (RF) injection locking, which locks their GHz-level repetition rate [44–46]. The mode locking of their optical mode is based on four-wave mixing, and while not leading to pulse formation, results in equidistant teeth which were tested to the $7.5{\cdot}10^{-16}$ level [40]. Their phase coherence [42,47], sub-kHz linewidth [41], and sub-Hz locking stabilities [43] promise that QCL-OFCs can be used for metrological purposes. As a matter of fact, QCL-OFCs emitting in the THz range have already been fully referenced and used for spectroscopy [48,49].

However, a fully referenced MIR QCL-OFC has not yet been demonstrated. As has been done for THz QCLs [48], the repetition rate can be locked by RF injection locking and the offset frequency can be controlled via the driving current of the QCL [41,43,50]. Self-referencing via f-to-2f interferometry [51] is not currently achievable for QCLs, although progress in generating picosecond and femtosecond pulses has recently been demonstrated [52,53]. Instead, the QCL-OFC can be locked to a high accuracy MIR frequency reference [54]. These can be obtained by locking MIR lasers to sub-Doppler molecular transitions [55–59] with frequency stabilities and accuracies as good as 0.1 Hz [56] and 90 Hz [58], respectively. Through this approach, we can conceive a QCL-OFC with Hz-level stability and accuracy in a fully MIR implementation.

In this work, we demonstrate for the first time to the best of our knowledge a fully referenced MIR QCL-OFC. We characterize its frequency stability and accuracy and use the broadband reference to perform comb-calibrated Doppler-limited spectroscopy with accuracies on par with state-of-the-art solutions relying on nonlinear frequency conversion [29,35].

2. QCL-OFC referenced to a molecular transition

We have implemented the frequency-referenced QCL-OFC according to the setup detailed in Fig. 1(a). We have locked a distributed-feedback (DFB) QCL (Alpes Lasers) labelled DFB-QCL1 to the R(8) molecular transition in the ν_1 fundamental band of N_2O at about 1292.3 cm^{-1} using wavelength modulation spectroscopy (WMS). A laser driver and temperature controller developed at the University of Neuchâtel was used to drive the QCL at an average current of 436 mA and to stabilize it at a temperature of 23°C. A fast modulation at a frequency f_{wms} of about 50 MHz was applied to the laser current via a dedicated bias-tee, which was custom made as most commercially-available bias-tees have a low-frequency cut-off of around 100 kHz that slightly limits the actuation bandwidth of the QCL. The RF power at the bias-tee input was around −10 dBm. The modulation index is roughly estimated to be between 0.25 and 0.5 from Fig. 1(e). After passing through a gas cell (Wavelength Reference, as all gas cells mentioned in this paper) with a length of 1 cm filled with 10% N_2O at 5 mbar pressure, the beam was detected using a photodetector (PVMI-4TE-8/MIPDCv2-F-250, Vigo System). The low concentration of N_2O was due to contamination by water vapor (see Section 4). The DC and AC components of the detector output signal were split using another bias-tee. All RF components used in this work, unless specified, are off-the-shelf commercial devices from Mini-Circuits. All electronic oscillators used were referenced to a GPS-disciplined hydrogen maser to ensure their long-term stability and accuracy.

The detector DC signal provided the optical transmission through the gas cell [see Fig. 1(b)]. The AC signal was filtered, amplified, and demodulated using an analog mixer at the modulation frequency f_{wms}, providing a WMS derivative signal featuring a slope of about 25 mV/MHz and a zero-crossing point near the center of the transition [see Fig. 1(c)]. The linear range is about 16 MHz. We note that residual amplitude modulation generated a voltage offset, breaking

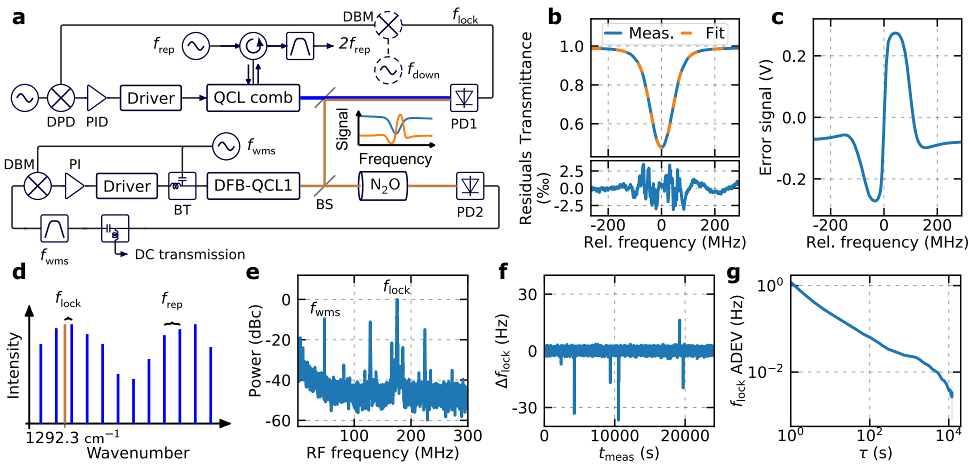

Fig. 1. QCL-OFC stabilization to a molecular reference. (a) Schematized experimental setup. One comb line of the QCL comb is locked to a molecular transition using a DFB-QCL. The intermode beat frequency is locked by RF injection locking. DPD: digital phase detector, PD: photodetector, BS: beam splitter, DBM: double balanced mixer, BT: bias-tee. (b) DC transmission of PD2 when the frequency of DFB-QCL1 is scanned across the N_2O R(8) molecular transition (~38.742 THz) and fit with a Voigt profile. The residuals are shown in the lower panel. (c) Error signal obtained by demodulating the high-pass filtered signal of PD2, giving a zero-crossing point with a slope of 25 mV/MHz near the center of the transition. (d) Schematized equidistant spectrum of the QCL comb (blue) and DFB-QCL1 (brown), illustrating the transfer of the frequency reference given by the latter. (e) Spectrum of the signal from PD1 (20 kHz resolution bandwidth), showing f_{wms}, the beat between DFB-QCL1 and the QCL comb, and its sidebands. (f) Hz-level frequency fluctuations of f_{lock} during a measurement of 6 hours. (g) Corresponding Allan deviation (ADEV) of f_{lock} showing sub-Hz stability beyond integration times (τ) of a few seconds.

the symmetry of the error signal. The error signal was fed to a proportional-integrator (PI) servo-controller (model LB1005-S, New Focus) to generate a feedback signal, which acted on the QCL driving current via the laser driver to stabilize the emission frequency to the zero-crossing point of the error signal. We recorded the error signal from the error monitor channel of the servo controller, which induced saturation to the signal at ±330 mV [see Fig. 1(c)]. This did not affect the locking-point around zero voltage.

The QCL-comb chip was designed and fabricated at ETH Zurich. A wire bond connects the laser active area to a dedicated (RF) port on a printed-circuit board (PCB) designed by IRsweep AG, which allows for efficient RF injection and extraction of the intermode beat signal. The comb was operated at an average current of 1150 mA and a temperature of 16°C using a current and temperature controller developed and fabricated at University of Neuchâtel. The intermode beat frequency at 9.75 GHz was stabilized by RF injection-locking [46] using 20 dBm of RF power injected in the laser chip. A circulator (SFC0712, Fairview Microwave) was used to simultaneously inject the master signal and extract the second harmonic of the intermode beat, which allows monitoring the successful injection locking (monitoring at the intermode beat frequency was not possible due to the weakness of the extracted signal with respect to the strong injected RF signal and the limited isolation of the circulator).

Part of the DFB-QCL1 beam was split by a beam-splitter (BSW510, Thorlabs) before the gas cell to be heterodyned with the QCL-OFC on a fast photodetector (UHSM-10.6 PV-4TE-10.6-0.05-butt, Vigo System). The beams were focused on the photodetector with a lens (2-inch focal length). The heterodyne beat between the comb and DFB-QCL1 was detected beyond the 1.2-GHz bandwidth (specified by the manufacturer) of the photodetector. The heterodyne beat [see Fig. 1(e)] was amplified and compared in phase with a reference signal in a 200-MHz bandwidth digital phase detector (DXD200, MenloSystems) to generate a phase error signal. After amplification in a P-I^2-D servo-controller (D2-125, Vescent Photonics), the resulting correction signal was applied to a modulation port of the laser driver to correct the QCL-OFC current. When necessary, the heterodyne beat was frequency-down-mixed with an RF signal f_{down} to fit the 200-MHz bandwidth of the phase detector. The signal-to-noise ratio (SNR) of the frequency-shifted signal was sufficient to obtain phase locks with beat notes of up to 1.5-GHz offset frequency.

Closing the loop, the heterodyne beat is locked at frequency f_{lock} and features Hz-level fluctuations [Fig. 1(f)], with a stability of 2 Hz and ∼10 mHz at 1-s and 10^4-s integration times, respectively [Fig. 1(g)]. We note moreover that both the phase lock and the RF injection locking can be maintained during more than 6 hours. Minimization of back-reflections to the QCL-OFC was key to achieve a stable phase-lock. This was realized by attenuating the beam by 95% right after its collimation [60].

In this way, one comb line of the QCL-OFC is referenced to a molecular transition while the lock of the mode spacing allows determining the optical frequency of each comb line with the accuracy of the molecular reference. Thus, the comb acts as an optical frequency reference over its entire emission bandwidth [15-dB bandwidth of 40 cm^{-1}, see Fig. 2(e)] with comb lines spaced by f_{rep} = 9.75 GHz as schematized in Fig. 1(d). The center frequency of the N_2O R(8) transition is known within 72 kHz [29], however, the offset Δ_f between the locking point of DFB-QCL1 and the transition center (including the pressure shift) needs to be determined. To this end, DFB-QCL1 was scanned across the transition while recording the error signal and the

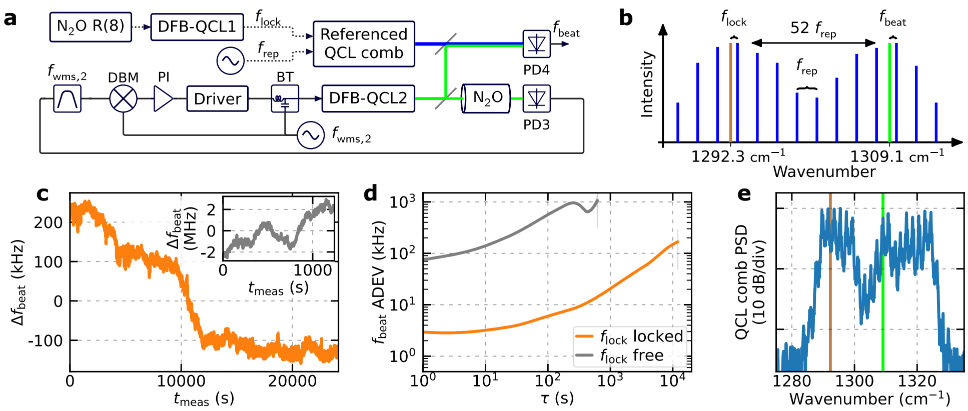

Fig. 2. Assessment of the frequency stability of the stabilized QCL-OFC. (a) Setup comprising the stabilized comb that is controlled by the two frequencies f_{lock} and f_{rep}. f_{lock} determines the offset between the stabilized DFB-QCL1 and one comb line. DFB-QCL2 is locked to a molecular transition in the same way as DFB-QCL1. (b) Schematized spectrum representing the QCL-OFC, DFB-QCL1, and DFB-QCL2 in blue, brown, and green, respectively. The beat note between the comb and DFB-QCL2 is denoted f_{beat}. (c) Frequency fluctuations of f_{beat} when f_{lock} and f_{rep} are stabilized according to section 2. The inset shows a measurement in the absence of f_{lock} stabilization. (d) Corresponding Allan deviation (ADEV) of f_{beat} with open and closed loop of f_{lock}. (e) QCL comb power spectral density (PSD) measured with an FTIR. The emission frequencies of the DFB-QCLs are indicated with vertical lines according to colors from (b).

DC transmission with an oscilloscope (PicoScope 5444D, Pico Technology) prior to locking. A relative frequency scale was obtained from the beat note with one comb line in an open loop [19]. We retrieved Δ_f from the offset between the zero-crossing point of the error signal and the line center, obtained through fitting of the DC transmission with a Voigt profile [see Fig. 1(b,c)]. The absolute frequency of the locking point was then computed from the center frequency of the transition [29], the offset Δ_f, and the pressure shift. The frequency stability and accuracy of the referenced QCL-OFC are assessed in sections 3 and 4, respectively.

3. Frequency stability of the stabilized QCL-OFC

We assessed the frequency stability of the stabilized QCL-OFC by locking a second DFB-QCL, named DFB-QCL2, in the same manner as DFB-QCL1, using WMS [see Fig. 2(a)]. DFB-QCL2 was operated at a current of 199 mA and at a temperature of 7°C, so as to probe the R(30) transition of the ν_1 fundamental band of N_2O in a second gas cell of 1-cm length filled with 50% N_2O at a pressure of 1.5 mbar. The beam transmitted through the cell was detected on a photodetector (LabM-I-10.6, Vigo System), labeled PD3. Part of the beam was combined with the comb and focused on a fast photodiode (UHSM-10.6 PV-4TE-10.6-0.05-butt, Vigo System), labeled PD4, using a lens (1-inch focal length). This beat signal provides an out-of-loop measurement to assess an upper bound of the comb frequency stability.

Indeed, while similar components were used, both DFB-QCLs were locked to different gas cells and at different wavelengths [Fig. 2(b)], such that their frequency fluctuations can be considered as fully uncorrelated. Hence, an upper limit to the frequency instability of the QCL-OFC can be assessed from the beat signal f_{beat} between DFB-QCL2 and one of the comb lines. This measurement is shown in Fig. 2(c,d), where the frequency fluctuations and the Allan deviation of the beat frequency f_{beat} are shown.

The peak-to-peak frequency fluctuations are on the order of 300 kHz over a period of 6 hours. A 3-kHz frequency instability is obtained at 1-s integration time while it increases to 6 kHz at 100 s and 57 kHz at an hour. As expected, fluctuations of f_{beat} increased significantly when f_{lock} was open. The frequency instability at 1-s integration time for the comb with only RF injection locking is 74 kHz and it increases to 570 kHz at 100-s integration time [Fig. 2(c,d)].

Back-reflections to the DFB-QCLs were found to distort the error signal (etalon fringes). Therefore, these were minimized, e.g., the active regions of the fast photodiodes were moved outside of the focal points of the beams. Nevertheless, these are still believed to be the main source of drift of the laser frequencies.

4. Absolute frequency accuracy and spectroscopic measurement

In section 3, we assessed the frequency stability of the stabilized comb. In this section, we assess the absolute frequency accuracy by referencing DFB-QCL2 to the comb, scanning it over different molecular transitions, and comparing the obtained frequencies with experimental values reported in literature with 100 kHz-level accuracies. Then, we also used our setup to measure a less accurately-known transition.

The setup is shown in Fig. 3(a). The frequency comb was stabilized as in Fig. 1(a). DFB-QCL2 (in this section, $f_{\text{wms},2}$ was turned off) was heterodyned with the stabilized comb on PD4. Their beat signal at frequency f_{beat} was mixed with a frequency f_{sweep}, and the mixing product was compared in phase with a reference frequency $f_{\text{lock},2}$ in a digital phase detector (DXD200, Menlo Systems). The resulting phase error signal was used to phase-lock the DFB to the comb, with a tunable frequency offset by sweeping f_{sweep}, which is generated by a digital lock-in amplifier (UHFLI, Zurich Instruments), between 50 MHz and 600 MHz. The error signal was fed to a PI servo controller (LB1005-S, New Focus) which acts on the driving current of DFB-QCL2. Optionally, f_{beat} was down-mixed with a frequency f_{down} prior to being mixed with f_{sweep}.

Synchronously with the sweep, the beam of the DFB is detected using PD3 after passing through a gas cell and the DC transmission is recorded.

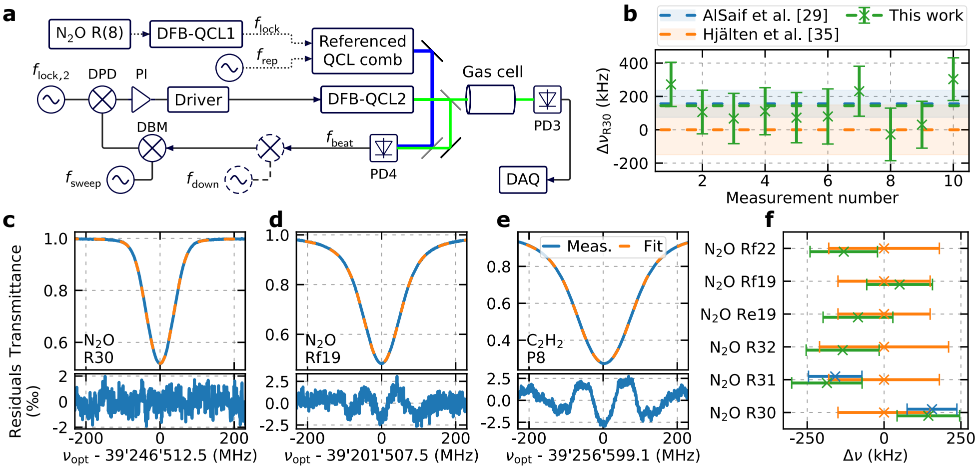

Fig. 3. Assessment of the absolute frequency accuracy and comb-calibrated spectroscopy. (a) Setup. DAQ: data acquisition unit. (b) Comparison of 10 measurements of the frequency of transition R(30) against literature references with 1 σ error bars. The uncertainty of the literature data is represented with the background color. (c-e) Transmittance, fit and residuals of 3 selected transitions. (f) Comparison of the obtained transition frequencies with literature values. The color code follows from (b).

This setup allowed us to perform frequency-calibrated spectroscopic measurements of molecular transitions by sweeping the offset between the stabilized QCL-OFC and DFB-QCL2 in any 550 MHz range between 100 MHz and 1.5 GHz while maintaining their phase lock. The 1.5-GHz bandwidth for the offsets between the DFBs and the comb gives, assuming a fixed transition frequency for DFB-QCL1, a 6-GHz coverage for DFB-QCL2, which represents two thirds of the free spectral range of the comb used in this experiment. Full access could be obtained by changing the locking transition of DFB-QCL1.

Assessment of the frequency accuracy

As a first step, we measured the transition R(30) of N_2O at 1.5 mbar through a 1-cm length gas cell [Fig. 3(c)]. The referencing of the comb to a known transition and the knowledge of all the RF frequencies determines the absolute frequency of DFB-QCL2 within the ambiguity given by the repetition rate of the comb. This ambiguity is lifted by the approximate knowledge of the transition of interest. The sweep over 550 MHz takes 20 s. We fit the frequency-calibrated transmission using a Voigt profile which gives us the center frequency of the transition.

To assess the accuracy of our setup, we performed 10 sets of measurement of the transition R(30). Each set of measurement involved the following steps: (i) scanning DFB-QCL1 10 times over transition R(8) in an open loop to determine Δ_f, as described in section 2, (ii) locking of DFB-QCL1 to transition R(8), (iii) locking of the comb to DFB-QCL1, (iv) sweeping DFB-QCL2 over the resonance 10 times in each direction (20 sweeps in total). Each set of measurement took about 12 minutes (6.6 minutes of actual measurement), and resulted in an absolute frequency value for the transition R(30), which is shown and compared with the measurements of AlSaif *et al.* [29] and Hjälten *et al.* [35] in Fig. 3(b). The 10 sets were performed in the span of a week. Most data points agree with the references and to each other within 1 σ uncertainty, showing that the estimated uncertainties are coherent and unaccounted-for biases are within the uncertainties.

The uncertainty budget for one measurement set is given in Table 1. Through the 10 scans over transition R(8), we obtain 10 measurements of Δ_f with a standard deviation ranging between 236 kHz and 392 kHz, such that the type A uncertainty of the mean is between 78 kHz and 131 kHz (average 103 kHz). We considered a systematic bias of Δ_f of (-83 ± 22) kHz due to the finite scanning speed, measured by scanning in the opposite direction.

Table 1. Uncertainty Budget For 1 Measurement Set

	Type A Uncertainty (kHz)	Type B Uncertainty (kHz)
Offset Δ_f of the locking point from the transition center (10 scans)	78-131	
Δ_f bias uncertainty		22
Fit uncertainty (20 sweeps)	6-10	
Stability of the comb	20	
Pressure shift		60
R8 transition frequency [29]		72
Total uncertainty (1 σ)	128-165	

The 20 sweeps of DFB-QCL2 and their fits show a standard deviation of the center frequency of the R(30) transition between 28 kHz and 44 kHz, such that the standard deviation of the mean is between 6 kHz and 10 kHz (average 8 kHz). The frequency stability of DFB-QCL1 over the measurement time of 15 minutes is 20 kHz.

We also estimated a 60-kHz uncertainty due to pressure shift, corresponding to 2 mbar pressure uncertainty on the gas cells. Indeed, the sealed commercial gas cells contained an undesired high ratio of water vapor, which complicated the task of determining the exact pressure and concentrations of the cells. The R(8) transition is known within 72 kHz [29]. We obtain an uncertainty ranging from 128 kHz to 165 kHz (average 145 kHz) for each set of measurement of the R(30) transition. The uncertainty is reduced to 102 kHz (fractional accuracy of $3{\cdot}10^{-9}$) on the mean of the 10 measurements (using inverse variance weighting). This cannot be significantly improved by repeated measurements since the overall uncertainty is rapidly dominated by the type B uncertainties.

Spectroscopic measurements

As the performance of the frequency-calibrated spectrometer has been assessed, we used it to determine the absolute frequency of other transitions. We studied the additional transitions R(31) and R(32) of the ν_1 fundamental band of N_2O using the same gas cell. Moreover, we studied transitions Re(19), Rf(19), Re(22), and Rf(22) of the $(11^10)\leftarrow(01^10)$ hot band of N_2O using a 10-cm gas cell filled with 15% N_2O at 9 mbar. Unfortunately, the presence of a strong transition near Re(22) did not allow us to make a correct fit of the latter. Finally, we also measured transition P(8) of C_2H_2 through a 8-cm gas cell filled with 12% C_2H_2 at 8 mbar, for which the best available uncertainty is between 3 MHz and 30 MHz [61]. For each transition, we acquired 3 sets of measurements [2 for transition Rf(22)]. For each set, between 10 and 32 scans of DFB-QCL1 and between 10 and 20 sweeps of DFB-QCL2 were acquired. The total uncertainty remains in the same order of magnitude. The final transition frequency and its uncertainty is determined using inverse variance weighting.

We show typical transmission spectra (acquired in one 20-s sweep) and their fit in Fig. 3(c-e) for the transitions R(30) and Rf(19) of N_2O and P(8) of C_2H_2. The obtained transition frequencies are given in Table 2. Moreover, Fig. 3(f) shows the comparison of the obtained N_2O transition frequencies against the available references. All results agree with the literature within the specified uncertainties.

Table 2. Spectroscopic Data

Transition	Measured Line Center (cm^{-1})	Literature (cm^{-1})
N_2O R(30)	1309.122743(3)	1309.1227432(27) [29], 1309.122738(5) [35]
N_2O R(31)	1309.846770(4)	1309.8467707(29) [29], 1309.846776(6) [35]
N_2O R(32)	1310.567203(4)	1310.567207(7) [35]
N_2O Re(19)	1307.540325(4)	1307.540328(5) [35]
N_2O Rf(19)	1307.621542(4)	1307.621540(5) [35]
N_2O Rf(22)	1309.928550(4)	1309.928554(6) [35]
C_2H_2 P(8)	1309.459305(4)	1309.4592(10) [61]

5. Discussion and conclusion

For the first time, to the best of our knowledge, we have fully stabilized a MIR QCL-OFC to a molecular transition and characterized it. All comb lines are known with $3{\cdot}10^{-9}$ relative frequency accuracy, and their relative stability is $1.5{\cdot}10^{-10}$ at 100-s integration time and $5{\cdot}10^{-10}$ at 1000-s integration time. Moreover, we performed comb-referenced laser absorption spectroscopy. This work thus demonstrates the suitability of MIR QCL-OFCs to be used as frequency references.

The limits in frequency stability and accuracy do not originate from the comb itself, but from the laser locked to the molecular transition and from the pressure shift. The actual limit of the QCL-OFC remains to be assessed, but stabilities as good as 1 Hz at 1-s integration time can be expected from the in-loop stability of the locked beat signals. Locking of the QCL-OFC to state-of-the-art MIR sub-Doppler references [55–59] with stabilities down to the sub-Hz level could open paths for MIR metrological studies. However, the accuracies demonstrated in this work are already comparable to other works requiring nonlinear frequency conversion [29,35] and are largely sufficient for room-temperature Doppler-limited spectroscopy.

The large free spectral range of 10 GHz of the QCL-OFC is practical for closed-loop comb-assisted spectroscopy over hundreds of MHz, as the problem of the heterodyne beat reaching near zero frequency and folding is avoided [21,34]. However, the available detectors can provide sufficient SNR for phase-locking only up to 1.5-GHz offsets, such that accessing the full optical spectrum requires changing the transition frequency of the locked laser. A smaller free spectral range on the order of 2-5 GHz is preferred in this regard. This issue also needs to be solved for referencing a swept dual comb spectrometer [62], where the beat between the comb and the locked laser will span half of the free spectral range.

Lastly, the bandwidth of the spectroscopy was limited by DFB-QCL2 to a few wavenumbers. The use of an external cavity QCL and state-of-the-art QCL-OFCs [60] would allow to reach bandwidths of 70 cm^{-1}, competing with the existing techniques based on nonlinear frequency conversion [29,35]. In the near-future, broadening of the comb bandwidth, frequency referencing in a swept dual comb spectrometer, and self-referencing are three advances that will make QCL-OFCs more performant and attractive for MIR spectroscopy.

Funding. Swiss Space Office (MdP COSMICS); Schweizerischer Nationalfonds zur Förderung der Wissenschaftlichen Forschung (200020_178864, 40B2-1_176584); Horizon 2020 Framework Programme (871529).

Acknowledgement. We thank Alpes Lasers for providing the two DFB-QCLs used in this experiment. We acknowledge insightful discussions with Alexandre Parriaux.

Disclosures. The authors declare no conflicts of interest.

Data availability. Data underlying the results presented in this paper are available EUDAT B2SHARE repository: b2share (2021), Ref. [63].

References

1. A. Schliesser, N. Picqué, and T. W. Hänsch, "Mid-infrared frequency combs," Nat. Photonics **6**(7), 440–449 (2012).

2. J. Haas and B. Mizaikoff, “Advances in Mid-Infrared Spectroscopy for Chemical Analysis,” Annu. Rev. Anal. Chem. **9**(1), 45–68 (2016).
3. C. J. Breshike, C. A. Kendziora, R. Furstenberg, T. J. Huffman, V. Nguyen, N. Budack, Y. Yoon, and R. A. McGill, “Hyperspectral imaging using active infrared backscatter spectroscopy for detection of trace explosives,” Opt. Eng. **59**(09), 1 (2020).
4. N. M. Ralbovsky and I. K. Lednev, “Vibrational Spectroscopy for Detection of Diabetes: A Review,” Appl. Spectrosc. **75**(8), 929–946 (2021).
5. M. De Marchi, V. Toffanin, M. Cassandro, and M. Penasa, “Invited review: Mid-infrared spectroscopy as phenotyping tool for milk traits,” J. Dairy Sci. **97**(3), 1171–1186 (2014).
6. ÁI López-Lorente and B. Mizaikoff, “Mid-infrared spectroscopy for protein analysis: potential and challenges,” Anal. Bioanal. Chem. **408**(11), 2875–2889 (2016).
7. V. Villanueva-López, L. C. Pacheco-Londoño, R. Villarreal-González, J. R. Castro-Suarez, A. Román-Ospino, W. Ortiz-Rivera, N. J. Galán-Freyle, and S. P. Hernandez-Rivera, “API Content and Blend Uniformity Using Quantum Cascade Laser Spectroscopy Coupled with Multivariate Analysis,” Pharmaceutics **13**(7), 985 (2021).
8. G. Ycas, F. R. Giorgetta, J. T. Friedlein, D. Herman, K. C. Cossel, E. Baumann, N. R. Newbury, and I. Coddington, “Compact mid-infrared dual-comb spectrometer for outdoor spectroscopy,” Opt. Express **28**(10), 14740 (2020).
9. T. Udem, R. Holzwarth, and T. W. Hänsch, “Optical frequency metrology,” Nature **416**(6877), 233–237 (2002).
10. B. Argence, B. Chanteau, O. Lopez, D. Nicolodi, M. Abgrall, C. Chardonnet, C. Daussy, B. Darquié, Y. Le Coq, and A. Amy-Klein, “Quantum cascade laser frequency stabilization at the sub-Hz level,” Nat. Photonics **9**(7), 456–460 (2015).
11. N. Picqué and T. W. Hänsch, “Frequency comb spectroscopy,” Nat. Photonics **13**(3), 146–157 (2019).
12. Z. Zhang, T. Gardiner, and D. T. Reid, “Mid-infrared dual-comb spectroscopy with an optical parametric oscillator,” Opt. Lett. **38**(16), 3148–3150 (2013).
13. I. Coddington, N. Newbury, and W. Swann, “Dual-comb spectroscopy,” Optica **3**(4), 414–426 (2016).
14. G. Ycas, F. R. Giorgetta, E. Baumann, I. Coddington, D. Herman, S. A. Diddams, and N. R. Newbury, “High-coherence mid-infrared dual-comb spectroscopy spanning 2.6 to 5.2 µm,” Nat. Photonics **12**(4), 202–208 (2018).
15. A. V. Muraviev, V. O. Smolski, Z. E. Loparo, and K. L. Vodopyanov, “Massively parallel sensing of trace molecules and their isotopologues with broadband subharmonic mid-infrared frequency combs,” Nat. Photonics **12**(4), 209–214 (2018).
16. H. Timmers, A. Kowligy, A. Lind, F. C. Cruz, N. Nader, M. Silfies, G. Ycas, T. K. Allison, P. G. Schunemann, S. B. Papp, and S. A. Diddams, “Molecular fingerprinting with bright, broadband infrared frequency combs,” Optica **5**(6), 727–732 (2018).
17. J. Mandon, G. Guelachvili, and N. Picqué, “Fourier transform spectroscopy with a laser frequency comb,” Nat. Photonics **3**(2), 99–102 (2009).
18. F. Adler, P. Masłowski, A. Foltynowicz, K. C. Cossel, T. C. Briles, I. Hartl, and J. Ye, “Mid-infrared Fourier transform spectroscopy with a broadband frequency comb,” Opt. Express **18**(21), 21861–21872 (2010).
19. P. Del'Haye, O. Arcizet, M. L. Gorodetsky, R. Holzwarth, and T. J. Kippenberg, “Frequency comb assisted diode laser spectroscopy for measurement of microcavity dispersion,” Nat. Photonics **3**(9), 529–533 (2009).
20. M. Lamperti, B. AlSaif, D. Gatti, M. Fermann, P. Laporta, A. Farooq, and M. Marangoni, “Absolute spectroscopy near 7.8 µm with a comb-locked extended-cavity quantum-cascade-laser,” Sci. Rep. **8**(1), 1292 (2018).
21. R. Gotti, T. Puppe, Y. Mayzlin, J. Robinson-Tait, S. Wójtewicz, D. Gatti, B. Alsaif, M. Lamperti, P. Laporta, F. Rohde, R. Wilk, P. Leisching, W. G. Kaenders, and M. Marangoni, “Comb-locked frequency-swept synthesizer for high precision broadband spectroscopy,” Sci. Rep. **10**(1), 2523 (2020).
22. H. Guo, W. Weng, J. Liu, F. Yang, W. Hänsel, C. S. Brès, L. Thévenaz, R. Holzwarth, T. J. Kippenberg, and T. J. Kippenberg, “Nanophotonic supercontinuum-based mid-infrared dual-comb spectroscopy,” Optica **7**(9), 1181–1188 (2020).
23. E. Baumann, F. R. Giorgetta, W. C. Swann, A. M. Zolot, I. Coddington, and N. R. Newbury, “Spectroscopy of the methane ν_3 band with an accurate midinfrared coherent dual-comb spectrometer,” Phys. Rev. A **84**(6), 062513 (2011).
24. E. Baumann, E. V. Hoenig, E. F. Perez, G. M. Colacion, F. R. Giorgetta, K. C. Cossel, G. Ycas, D. R. Carlson, D. D. Hickstein, K. Srinivasan, S. B. Papp, N. R. Newbury, and I. Coddington, “Dual-comb spectroscopy with tailored spectral broadening in Si_3N_4 nanophotonics,” Opt. Express **27**(8), 11869 (2019).
25. A. Amy-Klein, A. Goncharov, C. Daussy, C. Grain, O. Lopez, G. Santarelli, and C. Chardonnet, “Absolute frequency measurement in the 28-THz spectral region with a femtosecond laser comb and a long-distance optical link to a primary standard,” Appl. Phys. B **78**(1), 25–30 (2004).
26. A. Gambetta, N. Coluccelli, M. Cassinerio, T. T. Fernandez, D. Gatti, A. Castrillo, A. Ceausu-Velcescu, E. Fasci, L. Gianfrani, L. Santamaria, V. Di Sarno, P. Maddaloni, P. De Natale, P. Laporta, and G. Galzerano, “Frequency-comb-assisted precision laser spectroscopy of CHF_3 around 8.6 µm,” J. Chem. Phys. **143**(23), 234202 (2015).
27. A. Gambetta, M. Cassinerio, N. Coluccelli, E. Fasci, A. Castrillo, L. Gianfrani, D. Gatti, M. Marangoni, P. Laporta, and G. Galzerano, “Direct phase-locking of a 8.6-µm quantum cascade laser to a mid-IR optical frequency comb: application to precision spectroscopy of N_2O,” Opt. Lett. **40**(3), 304–307 (2015).

Optics EXPRESS

28. A. Gambetta, E. Vicentini, Y. Wang, N. Coluccelli, E. Fasci, L. Gianfrani, A. Castrillo, V. D. Sarno, L. Santamaria, P. Maddaloni, P. D. Natale, P. Laporta, and G. Galzerano, "Absolute frequency measurements of CHF_3 Doppler-free ro-vibrational transitions at 8.6 μm," Opt. Lett. **42**(10), 1911–1914 (2017).
29. B. AlSaif, M. Lamperti, D. Gatti, P. Laporta, M. Fermann, A. Farooq, O. Lyulin, A. Campargue, and M. Marangoni, "High accuracy line positions of the ν1 fundamental band of $^{14}N_2{}^{16}O$," J. Quant. Spectrosc. Radiat. Transfer **211**, 172–178 (2018).
30. A. Gambetta, E. Vicentini, N. Coluccelli, Y. Wang, T. T. Fernandez, P. Maddaloni, P. De Natale, A. Castrillo, L. Gianfrani, P. Laporta, and G. Galzerano, "Versatile mid-infrared frequency-comb referenced sub-Doppler spectrometer," APL Photonics **3**(4), 046103 (2018).
31. B. AlSaif, D. Gatti, M. Lamperti, P. Laporta, A. Farooq, and M. Marangoni, "Comb-calibrated sub-Doppler spectroscopy with an external-cavity quantum cascade laser at 7.7 μm," Opt. Express **27**(17), 23785–23790 (2019).
32. R. Santagata, D. B. A. Tran, B. Argence, O. Lopez, S. K. Tokunaga, F. Wiotte, H. Mouhamad, A. Goncharov, M. Abgrall, Y. L. Coq, H. Alvarez-Martinez, R. L. Targat, W. K. Lee, D. Xu, P.-E. Pottie, B. Darquié, and A. Amy-Klein, "High-precision methanol spectroscopy with a widely tunable SI-traceable frequency-comb-based mid-infrared QCL," Optica **6**(4), 411–423 (2019).
33. P. B. Changala, M. L. Weichman, K. F. Lee, M. E. Fermann, and J. Ye, "Rovibrational quantum state resolution of the C 60 fullerene," Science **363**(6422), 49–54 (2019).
34. M. Lamperti, R. Gotti, D. Gatti, M. K. Shakfa, E. Cané, F. Tamassia, P. Schunemann, P. Laporta, A. Farooq, and M. Marangoni, "Optical frequency metrology in the bending modes region," Commun. Phys. **3**(1), 175 (2020).
35. A. Hjältén, M. Germann, K. Krzempek, A. Hudzikowski, A. Głuszek, D. Tomaszewska, G. Soboń, and A. Foltynowicz, "Optical frequency comb Fourier transform spectroscopy of $^{14}N_2{}^{16}O$ at 7.8 μm," J. Quant. Spectrosc. Radiat. Transfer **271**, 107734 (2021).
36. A. Hugi, G. Villares, S. Blaser, H. C. Liu, and J. Faist, "Mid-infrared frequency comb based on a quantum cascade laser," Nature **492**(7428), 229–233 (2012).
37. J. Faist, G. Villares, G. Scalari, M. Rösch, C. Bonzon, A. Hugi, and M. Beck, "Quantum Cascade Laser Frequency Combs," Nanophotonics **5**(2), 272–291 (2016).
38. E. Lins, S. Read, B. Unni, S. M. Rosendahl, and I. J. Burgess, "Microsecond Resolved Infrared Spectroelectrochemistry Using Dual Frequency Comb IR Lasers," Anal. Chem. **92**(9), 6241–6244 (2020).
39. J. L. Klocke, M. Mangold, P. Allmendinger, A. Hugi, M. Geiser, P. Jouy, J. Faist, and T. Kottke, "Single-Shot Sub-microsecond Mid-infrared Spectroscopy on Protein Reactions with Quantum Cascade Laser Frequency Combs," Anal. Chem. **90**(17), 10494–10500 (2018).
40. G. Villares, A. Hugi, S. Blaser, and J. Faist, "Dual-comb spectroscopy based on quantum-cascade-laser frequency combs," Nat. Commun. **5**(1), 5192 (2014).
41. F. Cappelli, G. Campo, I. Galli, G. Giusfredi, S. Bartalini, D. Mazzotti, P. Cancio, S. Borri, B. Hinkov, J. Faist, and P. De Natale, "Frequency stability characterization of a quantum cascade laser frequency comb," Laser Photonics Rev. **10**(4), 623–630 (2016).
42. F. Cappelli, L. Consolino, G. Campo, I. Galli, D. Mazzotti, A. Campa, M. Siciliani de Cumis, P. Cancio Pastor, R. Eramo, M. Rösch, M. Beck, G. Scalari, J. Faist, P. De Natale, and S. Bartalini, "Retrieval of phase relation and emission profile of quantum cascade laser frequency combs," Nat. Photonics **13**(8), 562–568 (2019).
43. K. Komagata, A. Shehzad, G. Terrasanta, P. Brochard, R. Matthey, M. Gianella, P. Jouy, F. Kapsalidis, M. Shahmohammadi, M. Beck, V. J. Wittwer, J. Faist, L. Emmenegger, T. Südmeyer, A. Hugi, and S. Schilt, "Coherently-averaged dual comb spectrometer at 7.7 μm with master and follower quantum cascade lasers," Opt. Express **29**(12), 19126–19139 (2021).
44. J. Hillbrand, A. M. Andrews, H. Detz, G. Strasser, and B. Schwarz, "Coherent injection locking of quantum cascade laser frequency combs," Nat. Photonics **13**(2), 101–104 (2019).
45. M. R. St-Jean, M. I. Amanti, A. Bernard, A. Calvar, A. Bismuto, E. Gini, M. Beck, J. Faist, H. C. Liu, and C. Sirtori, "Injection locking of mid-infrared quantum cascade laser at 14 GHz, by direct microwave modulation," Laser Photonics Rev. **8**(3), 443–449 (2014).
46. F. Kapsalidis, B. Schneider, M. Singleton, M. Bertrand, E. Gini, M. Beck, and J. Faist, "Mid-infrared quantum cascade laser frequency combs with a microstrip-like line waveguide geometry," Appl. Phys. Lett. **118**(7), 071101 (2021).
47. M. Singleton, P. Jouy, M. Beck, and J. Faist, "Evidence of linear chirp in mid-infrared quantum cascade lasers," Optica **5**(8), 948–953 (2018).
48. L. Consolino, M. Nafa, F. Cappelli, K. Garrasi, F. P. Mezzapesa, L. Li, A. G. Davies, E. H. Linfield, M. S. Vitiello, P. De Natale, and S. Bartalini, "Fully phase-stabilized quantum cascade laser frequency comb," Nat. Commun. **10**(1), 2938 (2019).
49. L. Consolino, M. Nafa, M. De Regis, F. Cappelli, K. Garrasi, F. P. Mezzapesa, L. Li, A. G. Davies, E. H. Linfield, M. S. Vitiello, S. Bartalini, and P. De Natale, "Quantum cascade laser based hybrid dual comb spectrometer," Commun. Phys. **3**(1), 69 (2020).
50. J. Westberg, L. A. Sterczewski, and G. Wysocki, "Mid-infrared multiheterodyne spectroscopy with phase-locked quantum cascade lasers," Appl. Phys. Lett. **110**(14), 141108 (2017).

51. H. R. Telle, G. Steinmeyer, A. E. Dunlop, J. Stenger, D. H. Sutter, and U. Keller, "Carrier-envelope offset phase control: A novel concept for absolute optical frequency measurement and ultrashort pulse generation," Appl. Phys. B **69**(4), 327–332 (1999).
52. J. Hillbrand, N. Opačak, M. Piccardo, H. Schneider, G. Strasser, F. Capasso, and B. Schwarz, "Mode-locked short pulses from an 8 μm wavelength semiconductor laser," Nat. Commun. **11**(1), 5788 (2020).
53. P. Täschler, M. Bertrand, B. Schneider, M. Singleton, P. Jouy, F. Kapsalidis, M. Beck, and J. Faist, "Femtosecond pulses from a mid-infrared quantum cascade laser," Nat. Photonics **15**(12), 919–924 (2021).
54. C. C. Teng, J. Westberg, and G. Wysocki, "Frequency Stabilization of a Quantum Cascade Dual-Comb Spectrometer to a Molecular Transition," in *Conference on Lasers and Electro-Optics (CLEO)* (2020), paper SF2G.3.
55. O. Acef, "Metrological properties of CO2OsO4 optical frequency standard," Opt. Commun. **134**(1-6), 479–486 (1997).
56. V. Bernard, C. Daussy, G. Nogues, L. Constantin, P. E. Durand, A. Amy-Klein, A. V. Lerberghe, and C. Chardonnet, "CO_2 laser stabilization to 0.1-Hz level using external electrooptic modulation," IEEE J. Quantum Electron. **33**(8), 1282–1287 (1997).
57. F. Cappelli, I. Galli, S. Borri, G. Giusfredi, P. Cancio, D. Mazzotti, A. Montori, N. Akikusa, M. Yamanishi, S. Bartalini, and P. D. Natale, "Subkilohertz linewidth room-temperature mid-infrared quantum cascade laser using a molecular sub-Doppler reference," Opt. Lett. **37**(23), 4811–4813 (2012).
58. P. L. T. Sow, S. Mejri, S. K. Tokunaga, O. Lopez, A. Goncharov, B. Argence, C. Chardonnet, A. Amy-Klein, C. Daussy, and B. Darquié, "A widely tunable 10-μm quantum cascade laser phase-locked to a state-of-the-art mid-infrared reference for precision molecular spectroscopy," Appl. Phys. Lett. **104**(26), 264101 (2014).
59. E. Vicentini, A. Gambetta, N. Coluccelli, V. Di Sarno, P. Maddaloni, P. De Natale, A. Castrillo, L. Gianfrani, P. Laporta, and G. Galzerano, "Absolute frequency stabilization of a QCL at 8.6 μm by modulation transfer spectroscopy," Opt. Lett. **45**(17), 4948 (2020).
60. P. Jouy, J. M. Wolf, Y. Bidaux, P. Allmendinger, M. Mangold, M. Beck, and J. Faist, "Dual comb operation of λ ~ 8.2 μm quantum cascade laser frequency comb with 1 W optical power," Appl. Phys. Lett. **111**(14), 141102 (2017).
61. I. E. Gordon, L. S. Rothman, C. Hill, R. V. Kochanov, Y. Tan, P. F. Bernath, M. Birk, V. Boudon, A. Campargue, K. V. Chance, B. J. Drouin, J.-M. Flaud, R. R. Gamache, J. T. Hodges, D. Jacquemart, V. I. Perevalov, A. Perrin, K. P. Shine, M.-A. H. Smith, J. Tennyson, G. C. Toon, H. Tran, V. G. Tyuterev, A. Barbe, A. G. Császár, V. M. Devi, T. Furtenbacher, J. J. Harrison, J.-M. Hartmann, A. Jolly, T. J. Johnson, T. Karman, I. Kleiner, A. A. Kyuberis, J. Loos, O. M. Lyulin, S. T. Massie, S. N. Mikhailenko, N. Moazzen-Ahmadi, H. S. P. Müller, O. V. Naumenko, A. V. Nikitin, O. L. Polyansky, M. Rey, M. Rotger, S. W. Sharpe, K. Sung, E. Starikova, S. A. Tashkun, J. V. Auwera, G. Wagner, J. Wilzewski, P. Wcisło, S. Yu, and E. J. Zak, "The HITRAN2016 molecular spectroscopic database," J. Quant. Spectrosc. Radiat. Transfer **203**, 3–69 (2017).
62. M. Gianella, A. Nataraj, B. Tuzson, P. Jouy, F. Kapsalidis, M. Beck, M. Mangold, A. Hugi, J. Faist, and L. Emmenegger, "High-resolution and gapless dual comb spectroscopy with current-tuned quantum cascade lasers," Opt. Express **28**(5), 6197–6208 (2020).
63. K. Komagata, M. Gianella, P. Jouy, F. Kapsalidis, M. Shahmohammadi, M. Beck, R. Matthey, V. J. Wittwer, A. Hugi, J. Faist, L. Emmenegger, T. Südmeyer, and S, Schilt EUDAT B2SHARE Repository", b2share, (2021). http://doi.org/10.23728/b2share.b84f40e2619846298a125f831a737f4e

Chapter 5

Calibrating Frequency-Swept Dual Comb Spectroscopy

The comb mode spacing is an important parameter of FCs which is determinant for the application. In the context of frequency comb spectroscopy, the spacing naturally defines the frequency interval between each sampled spectral point. For example, a 10-GHz spacing is suitable for liquid samples with broad spectral features but in the gas phase, the features are much smaller : important information can be lost, unsampled, between the comb lines. To adapt the FC spacing for the sample under study would be ideal but this agility is limited. Indeed, with the exception of electro-optic combs [1], the spacing of FCs is primarily set by the length of the generating cavity, and this length is seldom or scarcely tunable. Moreover, while QCLs of different lengths could be fabricated, each for their application, short QCLs are more advantageous in terms of optical bandwidth as the dispersion over a round-trip is smaller. They are also more compact and robust.

Instead of reducing the spacing, spectral interleaving can be used for the sampling of narrow features by step-tuning or continuous sweeping of the repetition rate and/or offset frequency [2, 3]. This offers additional agility to set the spectral point spacing independently of the comb spacing. However, an accurate frequency calibration of the acquired spectra requires a dedicated scheme due to two conditions met with QCLs: the offset frequency is not detected and the repetition frequency is large. The undetected offset requires an optical reference as seen in chapter 4, but the beat of the reference with the nearest comb line will span at least half the repetition rate, which is a large RF bandwidth to process. Moreover, the calibration scheme should ideally be compatible with fast refresh rates enabled by the QCL comb [3].

I developed such a calibration scheme, which we then employed and characterized with the dual comb spectrometer built by Dr. Michele Gianella. The work was published in Physical Review Research and is reproduced here in accordance with the CC-BY 4.0 license under which it was published [4].

5.1 Summary of the article

We developed a scheme to calibrate the frequency axis of spectra acquired by fast continuous spectral interleaving of FCs with a 10-GHz mode spacing. The idea is to get equidistant markers during the sweep by generating synthetic sidebands in the RF domain on an optical frequency reference (see Fig. 1). The markers are then used to reconstruct the frequency-vs-time trajectory of a comb line, and with parallel knowledge of the repetition rate, that of all comb lines (Fig. 2). We measured respectively the ν_1 and the ν_4 ro-vibrational bands of N_2O and CH_4 in the range between 1265 cm^{-1} and 1310 cm^{-1}. The former measurement was used to characterize the calibration scheme while the latter provided a line list for the literature. We determined that the center frequency of the transitions with the best SNR could be retrieved with 600 kHz accuracy in 54-ms measurements (Fig. 3). Moreover, we characterized the agility of the spectrometer by measuring spectra with various sweep times and spectral point spacing from 27 ms (1.3 MHz) to 216 ms (160 kHz), see Fig. 4.

5.2 Further discussion

5.2.1 Detailed comparison with another MIR spectrometer

Compared to the work by Hjältén *et al.* [5], the obtained frequency accuracy is lower by a factor 6 for an acquisition time $2.8 \cdot 10^5$ shorter. While the first explanation to this positive result may be the high brightness of QCLs compared to DFG sources, another phenomena needs to be taken into account: "the additional multiplexed penalty $1/\sqrt{M_\mathrm{F}}$" [6], where M_F is the number of spectral elements involved in the Fourier transform. Indeed, as highlighted in Ref. [7], the SNR (in terms of absorbance) in DCS and Fourier transform spectrometers in the detector noise limit is generally

$$\mathrm{SNR_F} = \frac{\sqrt{\tau}}{M_\mathrm{F}} \frac{P}{\sigma_\mathrm{NEP}}, \tag{5.1}$$

whereas in time-multiplexed schemes, i.e., frequency-swept spectroscopy, it is

$$\mathrm{SNR_T} = \frac{\sqrt{2\tau}}{\sqrt{M_\mathrm{T}}} \frac{P}{\sigma_\mathrm{NEP}}, \tag{5.2}$$

where τ is the measurement time, M_T the number of time-multiplexed elements, P the average detected power, and σ_NEP the noise-equivalent power. Explicitly, for the same number of elements M, time-multiplexing has a $\sqrt{2M}$ SNR advantage over parallel detection with Fourier transform. This is valid when the dominant noise source is the noise-equivalent power of the photodetector.

For both our work and the work by Hjältén *et al.* [5], there is a combination of Fourier transforms and time-multiplexing. We can estimate that the SNR in such case of interleaved-comb spectroscopy is given as

$$\mathrm{SNR_I} = \frac{\sqrt{\tau}}{M_\mathrm{F}\sqrt{M_\mathrm{T}}} \frac{P}{\sigma_\mathrm{NEP}}. \tag{5.3}$$

Then, our short measurement time is explained by the fact that $M_\mathrm{T} \gg M_\mathrm{F}$ whereas it is the opposite for them. Table 5.1 summarizes the parameters used in the two works, also including the spectral point spacing Δ_sps, and the measured and computed noise-equivalent absorbance (NEA) evaluated for the measurement time τ, $\mathrm{NEA_{meas}}$ and $\mathrm{NEA_{comp}}$. I used the formula $\mathrm{NEA_{comp}} = 1/\mathrm{SNR_I}$, with an additional factor 2 for the asymmetric DCS configuration.

I compare now the two works quantitatively. Considering that their $\mathrm{NEA_{meas}}$ is better by a factor 50, their power 18 times weaker, and that they have a factor 2 advantage over us, a longer averaging time of $2 \cdot 10^5$ is estimated if all other parameters were then same. This is close to the actual ratio. However, while the measured and computed NEA match for Hjältén *et al.* [5], signifying that they were limited by detector noise, these do not match for us, meaning that other noise sources dominated the detector noise. A similar observation was reported in [8]. The additional source of noise is unknown. Further investigations, e.g., on the amplitude noise in QCL FCs [9], begs to be carried out. Thus, our too large NEA by a factor 7 was compensated by the parameters M_T and M_F which granted a factor 5 advantage over Hjältén *et al.* [5].

Concerning the frequency accuracy $\Delta\nu_\mathrm{un}$ on the transition center frequencies, our worse NEA was compensated by the smaller spectral point spacing and more intense absorption (peak absorption α_pk of 3.3 compared to 0.9). With the rule of thumb that $\Delta\nu_\mathrm{un} \propto \sqrt{\Delta_\mathrm{sps}\mathrm{NEA}/\alpha_\mathrm{pk}}$, I compute that we should obtain $\Delta\nu_\mathrm{un} = 370$ kHz given their best uncertainty of 100 kHz, which is close to the standard deviation of 300 kHz of the fits of our best lines.

Table 5.1: Comparison of the parameters in Ref. [5] with our work.

	τ (s)	P (µW)	σ_{NEP} (pW/$\sqrt{\text{Hz}}$)	M_{T}	M_{F}	Δ_{sps} (MHz)	NEA_{mes}	NEA_{comp}
Ref. [5]	15 120	14	50	14	19 200	9	0.002	0.002
Our work	0.054	250	30	16 000	120	0.66	0.1	0.015
Ratio	$2.8 \cdot 10^5$	1/18	1.7	$8.8 \cdot 10^{-4}$	160	14	1/50	0.13

5.3 Conclusion

We have demonstrated that QCL-based DCS can be performed with sub-MHz frequency in free-running mode. Moreover, we developed a scheme for the frequency calibration of FC with multi-GHz mode spacing. Although the large comb mode spacing of QCLs seem to be a disadvantage for high-resolution spectroscopy, it is actually the opposite, as it directly lowers the SNR penalty $1/\sqrt{M_{\text{F}}}$ [6]. Combined with their high-brightness and the now proven ability for fast *and* calibrated tuning, QCL-based dual comb and other Fourier transform spectrometers [8] are a serious competition to other technologies, in particular Fourier transform spectrometers based on DFG sources with low mode-spacing and low the average power. However, more thorough investigation of the limiting noise sources will be necessary to unfold their full potential. Moreover, the prospect of exploiting the natural frequency chirp of QCLs [10] in a similar fashion to upconversion time-stretch spectroscopy is exciting in the context of nanosecond-scale refresh rates and high SNR [7].

References

[1] A. Parriaux, K. Hammani, and G. Millot, “Electro-Optic Frequency Combs”, Adv. Opt. Photonics **12**, 223 (2020).

[2] E. Baumann, F. R. Giorgetta, W. C. Swann, A. M. Zolot, I. Coddington, and N. R. Newbury, “Spectroscopy of the Methane N_3 Band with an Accurate Midinfrared Coherent Dual-Comb Spectrometer”, Phys. Rev. A **84**, 062513 (2011).

[3] M. Gianella, A. Nataraj, B. Tuzson, P. Jouy, F. Kapsalidis, M. Beck, M. Mangold, A. Hugi, J. Faist, and L. Emmenegger, “High-Resolution and Gapless Dual Comb Spectroscopy with Current-Tuned Quantum Cascade Lasers”, Opt. Express **28**, 6197 (2020).

[4] K. N. Komagata, V. J. Wittwer, T. Südmeyer, L. Emmenegger, and M. Gianella, "Absolute Frequency Referencing for Swept Dual-Comb Spectroscopy with Midinfrared Quantum Cascade Lasers", Phys. Rev. Res. **5**, 013047 (2023).

[5] A. Hjältén, M. Germann, K. Krzempek, A. Hudzikowski, A. Głuszek, D. Tomaszewska, G. Soboń, and A. Foltynowicz, "Optical Frequency Comb Fourier Transform Spectroscopy of $^{14}N_2{}^{16}O$ at 7.8 µm", J. Quant. Spectrosc. Radiat. Transf. **271**, 107734 (2021).

[6] I. Coddington, N. Newbury, and W. Swann, "Dual-Comb Spectroscopy", Optica **3**, 414 (2016).

[7] K. Hashimoto, T. Nakamura, T. Kageyama, V. R. Badarla, H. Shimada, R. Horisaki, and T. Ideguchi, "Upconversion Time-Stretch Infrared Spectroscopy", Light Sci. Appl. **12**, 48 (2023).

[8] S. Markmann, M. Franckié, M. Bertrand, M. Shahmohammadi, A. Forrer, P. Jouy, M. Beck, J. Faist, and G. Scalari, "Frequency Chirped Fourier-Transform Spectroscopy", Commun. Phys. **6**, 53 (2023).

[9] T. Gabbrielli, N. Bruno, N. Corrias, S. Borri, L. Consolino, M. Bertrand, M. Shahmohammadi, M. Franckié, M. Beck, J. Faist, A. Zavatta, F. Cappelli, and P. De Natale, "Intensity Correlations in Quantum Cascade Laser Harmonic Frequency Combs", Adv. Photonics Res. **3**, 2200162 (2022).

[10] M. Singleton, P. Jouy, M. Beck, and J. Faist, "Evidence of Linear Chirp in Mid-Infrared Quantum Cascade Lasers", Optica **5**, 948 (2018).

Editors' Suggestion

Absolute frequency referencing for swept dual-comb spectroscopy with midinfrared quantum cascade lasers

K. N. Komagata,[1,*] V. J. Wittwer,[1] T. Südmeyer,[1] L. Emmenegger,[2] and M. Gianella[2,†]

[1]*Laboratoire Temps-Fréquence, Institut de Physique, Université de Neuchâtel, Avenue de Bellevaux 51, 2000 Neuchâtel, Switzerland*

[2]*Laboratory for Air Pollution / Environmental Technology, Empa, Überlandstrasse 129, 8600 Dübendorf, Switzerland*

(Received 4 August 2022; accepted 9 December 2022; published 26 January 2023)

Quantum cascade laser (QCL) frequency combs have revolutionized midinfrared (MIR) spectroscopy by their high brightness and fast temporal resolution, and are a promising technology for fully integrated and cost-effective sensors. As for other integrated comb sources such as microcombs and interband cascade lasers, QCLs have a comb spacing of several GHz, which is adequate for measurements of wide absorbing structures, typically found in liquid or solid samples. However, high-resolution gas-phase spectra require spectral interleaving and frequency calibration. We developed a frequency calibration scheme for fast interleaved measurements with combs featuring multi-GHz spacing. We then demonstrate dual-comb spectroscopy with a best accuracy of 600 kHz in single-shot 54 ms measurements spanning 40 cm^{-1} (1.2 THz) using QCLs at 7.8 µm (38.4 THz). This work paves the way for unambiguous and fast fingerprinting of complex molecular mixtures in the MIR with integrated comb sources.

DOI: 10.1103/PhysRevResearch.5.013047

I. INTRODUCTION

Over the last two decades, dual-comb spectroscopy [1,2] has developed into a powerful tool for applications requiring fast temporal resolution, high spectral accuracy, and broad spectral coverage. It has enabled difficult or previously impossible measurements, such as multispecies trace gas detection in open path [3], monitoring of irreversible processes with microsecond resolution [4], hyperspectral 3D imaging [5], and fast determination of isotope ratios of multiple species [6]. Moreover, photonic chip integrated comb sources such as microcombs [7], quantum cascade lasers (QCLs) [8], and interband cascade lasers [9] are potential game changers, by enabling mass-producible integrated gas sensors for demanding fields, such as health, security, environment, and industrial process monitoring.

However, these integrated comb sources, due to their small size, have large (compared to fiber mode-locked lasers) repetition rates, f_{rep}, on the order of 10 GHz or higher. The large f_{rep}, while allowing a high temporal resolution, leads to a sparse spectrum, where narrow molecular absorption is potentially lost between the comb teeth.

This limitation is not unique to dual-comb spectroscopy or to integrated comb sources, and has been addressed by interleaving many (up to many thousands) offset spectra, where f_{rep} and/or the offset frequency, f_o, are tuned in steps [10–16] or continuously [17,18].

Step-tuning of referenced combs typically consists of stepping the repetition rate by tens of Hz with dwell times on the order of seconds or more. Thus, the full interleaved spectrum is acquired in tens or hundreds of seconds and the frequency accuracy is that of the static comb [12,15]. We note that step-tuning was also used with free running midinfrared (MIR) QCLs, where a full spectrum was obtained in 1200 s with an accuracy better than 12 MHz [16]. Continuous sweeps yield faster measurements with higher spectral point density. However, they require an adapted frequency calibration scheme. The endless frequency comb was proposed by Benkler *et al.* [19], but it is not convenient in the MIR as it requires electro-optic components and pulsed emission. Alternatively, the use of an unbalanced Mach-Zehnder interferometer provided frequency scales with 10 MHz level precision for NIR microcombs [18] and MIR QCLs [20], with sweep times of 50 µs and 30 ms, respectively.

In this work, we present a method to calibrate fast continuous sweeps of multi-GHz frequency combs with sub-MHz accuracy, which can be applied independently of the wavelength range. We thus demonstrate a QCL-based MIR dual-comb spectrometer with a unique combination of fast acquisition, high-frequency accuracy, and high spectral point density.

As a proof of concept, we measure 43 transitions of the ν_1 rovibrational band of N_2O and 56 transitions belonging to the ν_4 band of CH_4. With the former measurement, we characterize the accuracy of the computed frequency scale and assess the precision of the measurement at varying scanning speeds. The latter provides an independent measurement of the transition frequencies of CH_4 which were recently published [21].

Rapid scanning and high accuracy are critical features for fingerprinting of complex molecular mixtures and parallel

*Corresponding author: kenichi.komagata@unine.ch

†Present address: IRsweep AG, Laubisrütistrasse 44, 8712 Stäfa, Switzerland.

Published by the American Physical Society under the terms of the Creative Commons Attribution 4.0 International license. Further distribution of this work must maintain attribution to the author(s) and the published article's title, journal citation, and DOI.

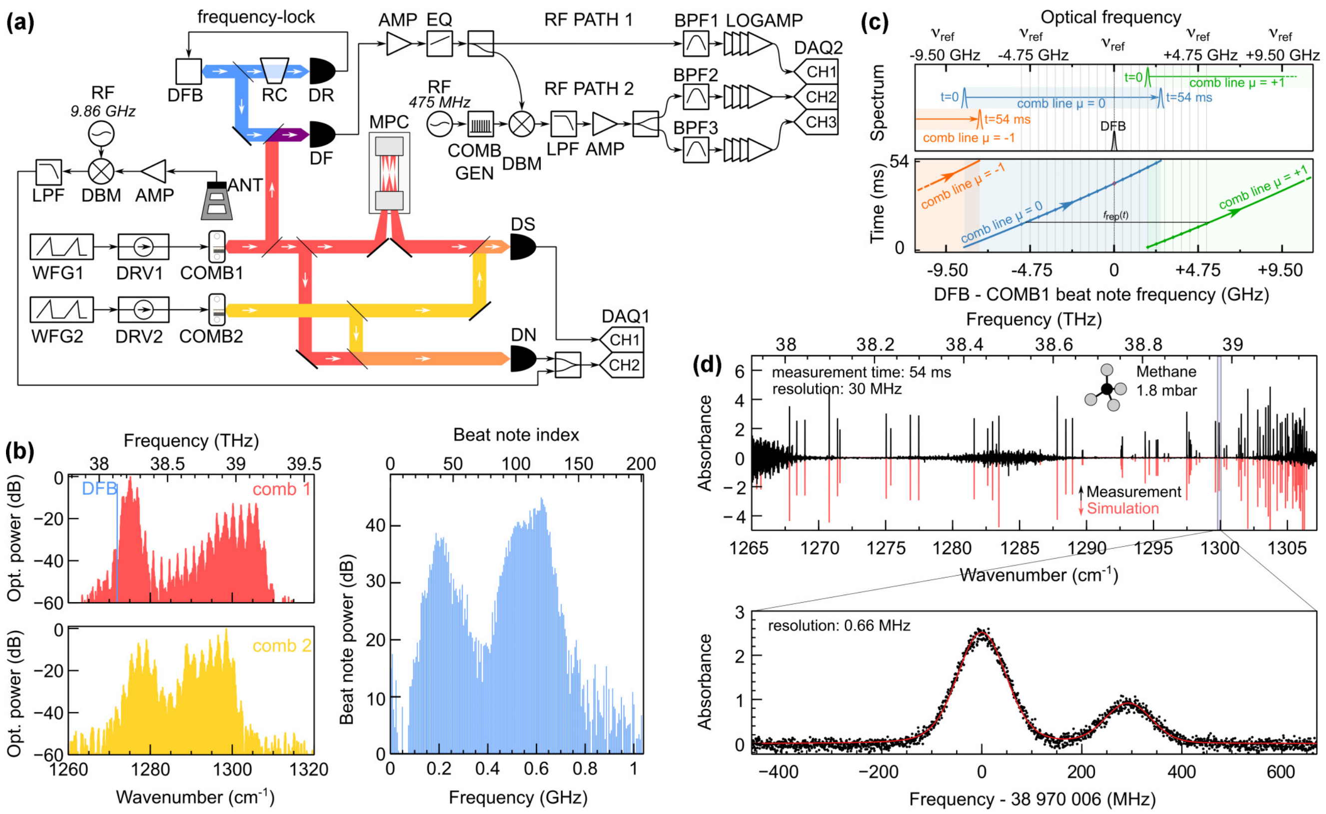

FIG. 1. Experimental setup and schematic for accurate frequency scale. (a) Experimental setup featuring the distributed feedback (DFB) laser serving as frequency reference, the gapless dual comb spectrometer, and the setups to measure the repetition rate and the optical frequency during an acquisition. MPC: multipass cell, AMP: amplifier, BPF, LPF: bandpass (low-pass) filter, DBM: double-balanced mixer, LOGAMP: logarithmic amplifier, EQ: equalizer, COMB GEN: comb generator, WFG: wave form generator, DAQ: data acquisition unit, DS, DN, DR, DF: photodetector (see main text). (b) Optical spectra of COMB1, COMB2, the position of the reference DFB laser, and the multi-heterodyne beat spectrum. (c) Schematic of the referencing scheme of the optical frequencies of COMB1 while they are tuned across more than one free-spectral range ($f_{\rm rep}$), relying on the use of a synthetic comb. (d) Absorption spectrum of low-pressure methane acquired in 54 ms by our spectrometer. The top panel is digitally filtered for visibility while the lower panel features two absorption lines at the original resolution of 660 kHz.

frequency modulated lidar [22]. Accordingly, we trust that our enhanced method for frequency axis calibration is a highly valuable asset for ranging and MIR sensing.

II. SPECTROMETER DESCRIPTION

Our dual-comb spectrometer is composed of two QCL frequency combs (COMB1 and COMB2), similarly to a previous work [17], and is schematized in Fig. 1(a). COMB1 is the interrogating comb which probes the sample contained in a multipass cell, and COMB2 is the local oscillator. The repetition frequency of the combs, $f_{\rm rep} \approx 9.88$ GHz, is too large to sample Doppler-broadened gas-phase spectra of small molecules. Therefore, we tune the driving current to scan the comb lines across $f_{\rm rep}$ and interleave spectra to reduce the spectral point spacing by 4 orders of magnitude. The local oscillator comb is tuned synchronously to keep the multi-heterodyne spectrum within the detection bandwidth of the system [see Fig. 1(b)]. The interferograms measured on the photodetectors DS and DN are divided into slices of length $\tau = 13.1$ μs, which are sufficiently long to resolve the beat notes (beat note spacing, $\Delta f_{\rm rep} \approx 4.5$ MHz). A lower limit for the spectral resolution, $\delta\nu$, can be estimated from the effective slice length, $\tau/3.77$, and the tuning rate, $\dot{\nu}$,

$$\delta\nu = \dot{\nu}(\tau/3.77). \quad (1)$$

The employed flat-top apodization reduces the effective length of the slice by a factor of 3.77. For example, the spectrometer can acquire spectra spanning 40 cm^{-1} (1.2 THz) in 54 ms at a point spacing and resolution of 0.66 MHz, allowing measurement of low-pressure methane [see Fig. 1(d)]. The noise-equivalent absorbance and noise-equivalent absorption coefficient depend on the signal-to-noise ratio (SNR) of the corresponding beat note [see Fig. 1(b)]. For strong beat notes, they are of the order of 3×10^{-4} Hz$^{-1/2}$ and 8×10^{-8} cm^{-1} Hz$^{-1/2}$, respectively, given the absorption path length of 36 m in the multipass cell.

The distributed feedback QCL (DFB) is locked to a molecular transition [N_2O, fundamental ν_1 band, P(14)] via wavelength modulation spectroscopy and acts as an optical frequency reference with frequency $\nu_{\rm ref}$ [23]. The beat frequency, f_b, between the reference laser and COMB1 is detected on a 1.2 GHz bandwidth detector (DF). The frequency, $\nu_\mu(t)$, of all lines, $\mu = 0, \pm1, \pm2, \ldots$, of the interrogating

75

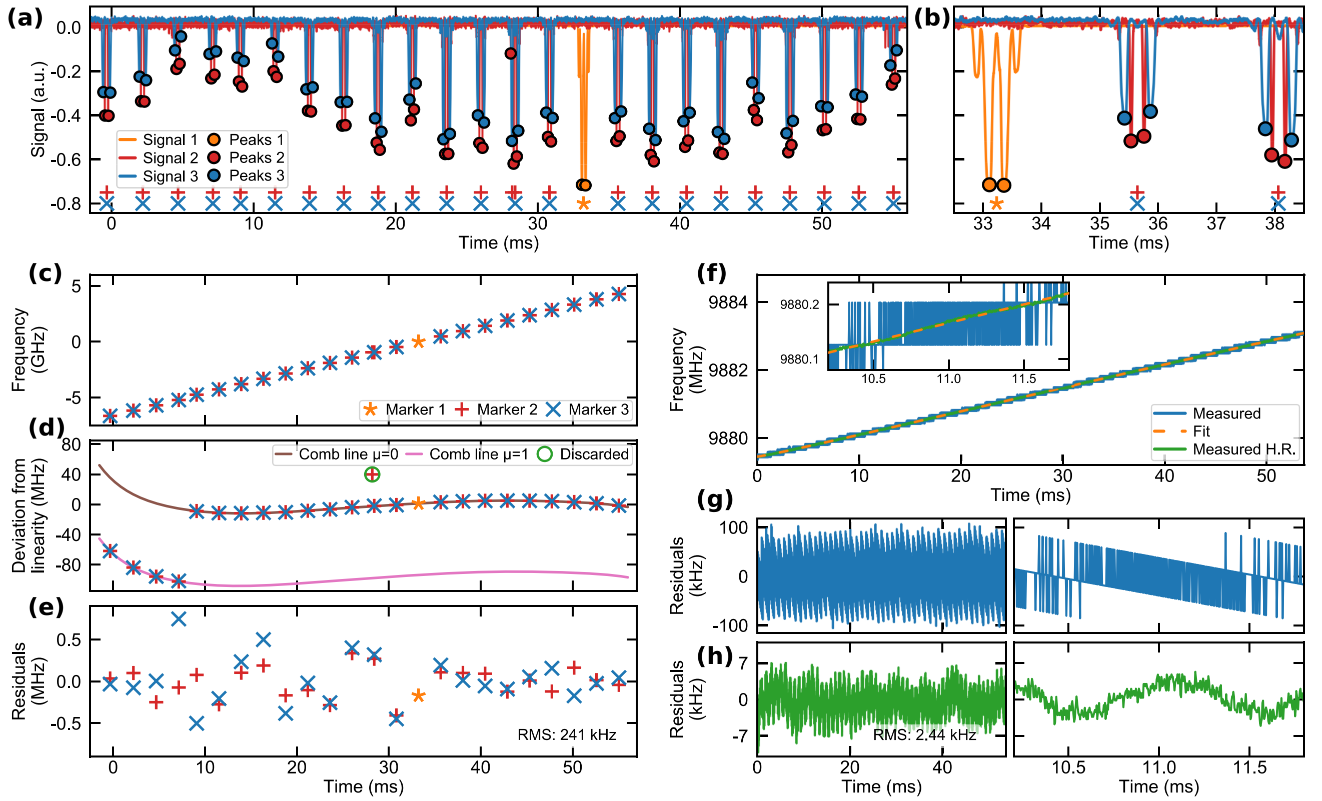

FIG. 2. Assessment of f_b and f_{rep} over a gapless measurement (sweep range $\geqslant f_{\mathrm{rep}}$). (a) Filtered marker signal digitized by DAQ2 [see Fig. 1(a)] as a function of time (solid lines) and pulses localized by the algorithm (filled circles). The mean position of two pulses gives the marker position shown by a star, plus, or x. (b) Zoom over 3 pairs of pulses. (c) Frequency of the markers as a function of time. (d) Frequency of the markers minus the linear trend and polynomial fitting of the comb line frequency. The first 4 pairs of marker originate from the beat with another comb line ($\mu = 1$ instead of $\mu = 0$). (e) Residuals from the fit from (d). (f) Measured f_{rep} using two methods as a function of time and fit. The inset shows the a zoom over a smaller time interval. (g), (h) Residuals of f_{rep} measured through the fast processor (g), which is limited by the integration time, or measured with high resolution (H.R.) (h). The right plot shows a zoom over a smaller interval. The fit using the processor data is accurate for the H.R. data within 2.4 kHz.

comb over the time of the scan is computed from the measured repetition rate, $f_{\mathrm{rep}}(t)$, and beat frequency, $f_b(t)$, at each slice of the sweep, and is given by

$$\nu_\mu(t) = \nu_{\mathrm{ref}} + f_b(t) + \mu f_{\mathrm{rep}}(t). \tag{2}$$

III. EVALUATION OF THE FREQUENCY AXIS

Thus, the reconstruction of the frequency axis of the interleaved spectra requires accurate knowledge of $f_b(t)$ and $f_{\mathrm{rep}}(t)$ at each slice of the sweep. An approach to determine $f_b(t)$ and $f_{\mathrm{rep}}(t)$ would be to measure and digitize them before applying a Fourier transform with a moving window. However, this is not a satisfying solution for $f_b(t)$ as it requires a costly high-speed digitizer and a custom or nitrogen-cooled detector that accommodates the sweeps of $f_b(t)$ over the large RF bandwidth of 5 GHz (corresponding to $f_{\mathrm{rep}}/2$). Besides the costs, that approach necessitates the storage and processing (Fourier transform) of large data sets, which are already demanded supplies for the processing of the dual-comb interferogram and especially needed for QCL-based dual combs [24].

We therefore apply another approach for the measurement of $f_b(t)$, based on the open-loop solution proposed in 2009 by Del'Haye *et al.* [25] with a few notable changes. Here, the reference laser is fixed while the comb is swept by approximately f_{rep}. Therefore, a single pair of peaks is detected through RF path 1 [see Fig. 1(a)], which is not sufficient to calibrate the entire sweep. These are observed at the instants when the bandpass filter BPF1 transmits the beat to the rectifying logarithmic amplifier (LOGAMP). The recorded signal on channel 1 of DAQ2 is shown in Figs. 2(a) and 2(b) as signal 1.

To increment the number of frequency markers, we implement a second RF path [RF path 2; see Fig. 1(a)], where we mix the beat with an $f_{\mathrm{RF}} = 475$ MHz spaced harmonic RF comb. The RF comb provides a synthetic grid of frequencies centered on the reference laser frequency, ν_{ref}, and having a spacing of f_{RF} [see Fig. 1(c)], whereby the time of passage of ν_0 across each grid line is measured. Hence, the determination of $f_b(t)$ [or $\nu_0(t)$] is based on the measurement of the times at which f_b equals multiples of f_{RF}. These markers allow us to map the frequency of $f_b(t)$ [or $\nu_0(t)$] versus time, as shown in Fig. 2(c). The marker on channel 1 allows identification of $\nu_0(t_0)$ modulo f_{rep}.

However, the large RF bandwidth required to measure f_b throughout the sweep still poses a challenge, as the specified

76

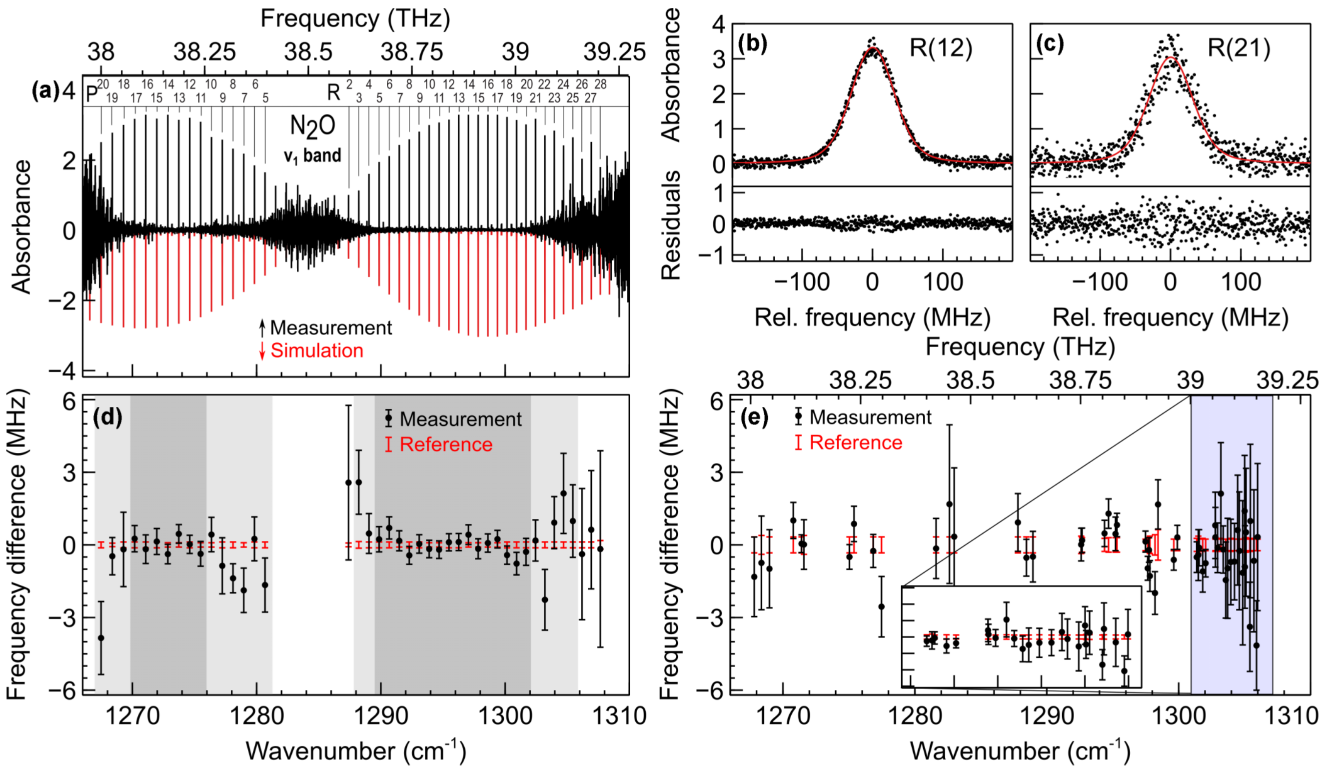

FIG. 3. Single-shot spectra of N_2O and retrieved line centers of N_2O and CH_4 (a) Single-shot spectra of the ν_1 fundamental band of nitrous oxide with 660 kHz spectral point spacing, acquired in 54 ms and comparison with simulation. (b), (c) Zoom of (a) on two different lines illustrating high/low SNR, and residuals of the Voigt fit (shown in red). (d) Retrieved line centers from (a) compared with literature reference [15,27] with the total 1 σ uncertainty shown as the error bars. The dark (light) gray regions depict the frequency ranges where the accuracy is better than 0.6 MHz (2 MHz). (e) Same as (d) for CH_4 averaged over 15 acquisitions, where the reference is taken from Ref. [21]. A zoom over the congested region (blue shading) is shown in the inset.

bandwidth of the photodetector is only 1.2 GHz. We thus used logarithmic amplifiers to increase the marker detection dynamic range and gain equalizers (EQ) to reduce signal strength imbalances. Moreover, in order to further balance the signal strength and optimize the RF mixers, the signals were split below and above 3.8 GHz [not shown in Fig. 1(c)]. Further information can be found in the Appendix and in Note 1 of the Supplemental Material [26].

These adaptations enabled the retrieval of frequency-equidistant markers over the entire sweep [see Fig. 2(c)], determined by the pairs of peaks in signals 2 and 3. We plot the markers after removal of the linear trend in Fig. 2(d). The first 4 sets of markers originate from the beating with a higher comb line $\mu = 1$ [see Fig. 1(c)], which was unavoidable to accommodate a sweep about 10% larger than f_{rep}. We fit the markers with a 10th-order polynomial using a two comb line model separated by $f_{\text{rep}}(t)$. The algorithm is robust against spurious peaks, which produce markers that can be discarded if they do not fit within a certain tolerance region. The residuals of the fit are shown in Fig. 2(e). The standard deviation of the fit residuals is found to be 241 kHz, which is useful for assessing the quality of the fit and for estimating the uncertainties of the adapted marker scheme in this implementation. The polynomial order was chosen to reduce the fit residuals while avoiding the overfitting of the sets of markers numbering to approximately 20.

The repetition rate, detected by the horn antenna, is down-mixed to ∼20 MHz, digitized on DAQ1, channel 2, and processed together with the interferogram [see Fig. 1(a)]. The resolution is limited to 76 kHz due to the finite length ($\tau = 13.1$ μs) of the slices [see Fig. 2(f)]. We fit these data using a 10th-order polynomial. The residuals are limited by the resolution as shown in Figs. 2(g) and 2(h). On a control measurement, we recorded the raw digitized data from DAQ1, channel 2, and computed $f_{\text{rep}}(t)$ with higher resolution by taking longer slices for the Fourier transform. The residuals between the fit from the low-resolution data and the high-resolution data are shown in Fig. 2(h), showing correspondence within 2.4 kHz. The high-resolution data feature oscillations of f_{rep} due to back-reflection from the photodetectors back to COMB1. The period is close to those originating from the limited resolution. The fringes hinder the in-depth study of the optimal polynomial order for the fitting.

IV. RETRIEVED LINE CENTER ACCURACY

Figure 3(a) shows a spectrum of the fundamental ν_1 band of nitrous oxide acquired in a single sweep of 54 ms. The bimodal comb amplitude distribution gives rise to a variable SNR across the spectrum, as can be seen in Figs. 3(b) and 3(c). We used a Voigt fit with fixed Gaussian width (for each transition) to retrieve the line centers of the molecular transitions.

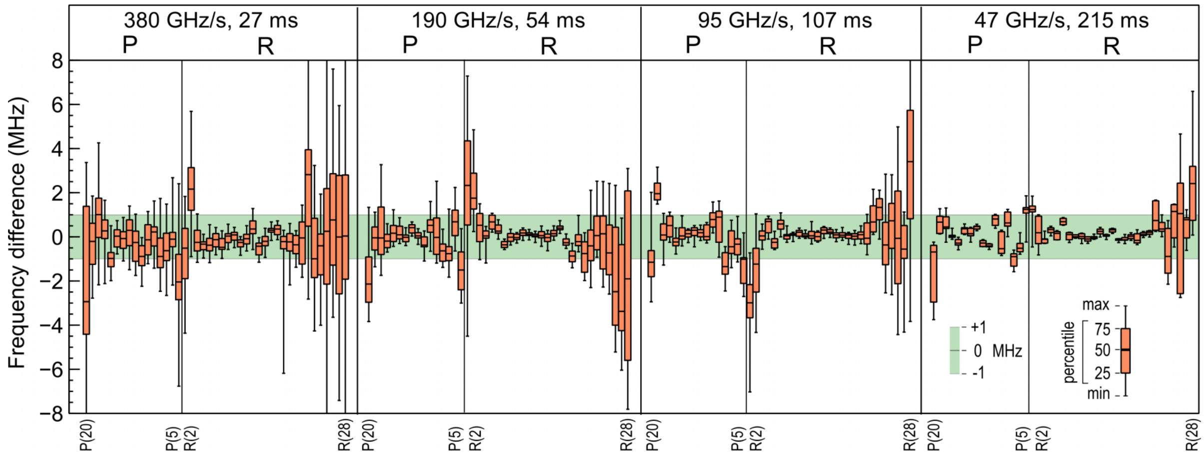

FIG. 4. Frequency precision for varying scanning speed. Statistical spread of the retrieved line centers compared with literature values at 4 different scan speeds, decreasing from left to right by factors of 2. The precision increases with the scan time.

The line centers were then corrected for zero pressure by subtracting the estimated pressure-induced shift.

We benchmark the frequency accuracy of our spectrometer by comparing the computed line center frequencies to those obtained by two other groups with a 100 kHz level accuracy [15,27]. Based on multiple sets of measurements over the course of a few weeks, we estimate that we retrieve, in a single-shot acquisition, 40 line centers [spanning 30.4 cm^{-1} (911 GHz)] with a 1 σ accuracy better than 2 MHz, among which 23 lines [spanning 17.1 cm^{-1} (513 GHz)] are retrieved with an accuracy better than 0.6 MHz, as can be seen in Fig. 3(d).

This estimation includes the uncertainties of the reference laser frequency ν_{ref} [180 kHz after correction of a systematic bias of (180 ± 100) kHz], f_{rep} [2.6 kHz after the correction of a systematic bias of (2.9 ± 0.7) kHz], the fit of the markers as in Fig. 2(e) (240 kHz), and the standard deviation of the retrieved line center frequencies over 12 consecutive 54 ms measurements (below 300 kHz for the lines with the best SNR; see Fig. 4). The retrieved line centers and the uncertainties are consistent with the literature values. The uncertainty on ν_{ref} includes type B uncertainties stemming from the literature value of the reference transition (72 kHz [27]) and from the frequency offset between the lock point and the center of the transitions (130 kHz [23]). All other uncertainties are of type A, including those on the biases. The biases and their uncertainties were computed by comparing our measured N_2O transition frequencies to the literature values.

The frequency accuracy of the spectrometer allows us to retrieve the line centers of CH_4 with a higher accuracy than in the HITRAN database [28]. Our results are given in Table 1 of the Supplemental Material [26]. For this measurement, we averaged the retrieved line centers over 15 measurements. In Fig. 3(e), we compare our results with the recent data published in Ref. [21]. We observe consistency between the results, considering the 1 σ uncertainty. Their spectrometer granted a higher-frequency accuracy while requiring acquisition times of hundreds of seconds for a full interleaved spectrum. We note that we applied the biases determined from the N_2O measurement.

V. SCANNING SPEED

The scanning speed of the spectrometer can be varied to measure spectra in between 27 ms to 216 ms. Thus, the spectral point spacing and tuning rates span from $\delta\nu = 1.3$ MHz to 160 kHz, and $\dot{\nu} = 380$ GHz/s to 47 GHz/s, respectively, according to Eq. (1). We estimate an accumulated chirp [22] rate of 44 THz/s to 5.6 THz/s, considering 120 lines which sweep in parallel.

At faster rates, the optical comb lines no longer tune continuously. We have previously observed that optical feedback can cause one or both combs to change state, whereby the frequencies and the envelope of the combs suddenly change. This manifests itself in a sudden change in the envelope and/or spacing of the beat note pattern. Slower tuning is possible but requires a larger buffer in the acquisition unit.

Figure 4 displays the statistics in the form of box plots of the retrieved N_2O line centers with respect to literature reference for varying scanning speeds. Scan speeds up to 380 GHz/s do not induce noticeable offsets in the retrieved line centers, within the uncertainties. This shows that delays due to the RF scheme are negligible. Potential delays at faster scanning speeds could be assessed and corrected from a reference measurement.

VI. DISCUSSION

We have demonstrated a fast and accurate midinfrared dual-comb spectrometer. The combs were emitted by quantum cascade lasers, which can be tuned over their free spectral range (f_{rep}) in tens of milliseconds to provide high-resolution spectra of broad molecular bands. We calibrated the frequency axis by measuring the beat between the interrogating comb and a reference laser and by acquiring the comb's repetition rate. Moreover, we have enhanced the marker method [25] using a synthetic comb, to process the fast chirp of the beat between the comb and the reference laser. This method is compatible with other integrated comb technologies featuring multi-GHz repetition frequencies such as microresonator combs [7], and could also be applied to comb-calibrated spectroscopy [25].

Our agile spectrometer provides unique performances in terms of acquisition speed and frequency accuracy compared to other broadband spectrometers with small (<10 MHz) spectral point spacing [15,25,27,29,30]. Indeed, it is faster at acquiring a full spectra than a stepped comb [15,27], and the accumulated chirp, thanks to the parallel scanning of the comb lines, is larger than the chirp commonly used in tunable laser spectroscopy [25,29,30]. Moreover, the adapted marker scheme yields an absolute frequency axis, which allows unambiguous identification of the molecular transitions even with the large chirp. Thus, our spectrometer is a promising candidate toward an on-chip gas sensor that is highly sensitive and selective to many relevant molecules, allowing real-time monitoring of complex gas mixtures at Hz-level refresh rates in industrial processes for example.

Finally, we believe that the spectrometer sensitivity, bandwidth, and power-efficiency will improve thanks to ongoing development in quantum cascade laser frequency combs, such as mutual stabilization [24,31], dispersion management [32], and full spectrometer integration [33].

Data underlying the results presented in this paper are available at the EUDAT B2SHARE repository b2share [34].

ACKNOWLEDGMENTS

We thank Prof. Jérôme Faist and Dr. Mathieu Bertrand at ETH for providing the QCL combs and lending the horn antenna used in this work. We also thank Dr. Stéphane Schilt for fruitful discussions concerning the marker scheme. We acknowledge funding from the Schweizerischer Nationalfonds zur Förderung der Wissenschaftlichen Forschung (Grant No. 40B2-1_176584).

APPENDIX: ADDITIONAL EXPERIMENTAL DETAILS

1. Lasers

The two laser sources were InGaAs/AlInAs on InP-based dual-stack QCLs [17,35]. They were 4.5 mm long ($f_{rep} \approx$ 9.88 GHz, $\Delta f_{rep} \approx 4.5$ MHz) and had both end facets uncoated. The combs emitted several hundred mW of optical power over $\sim$50 cm^{-1} (1.5 THz) in the 1300 cm^{-1} (39 THz) range [see Fig. 1(b)]. A pair of neutral density filters immediately attenuated the optical power in each beam to approximately 20 mW. Two polarizers in front of the detectors [not shown in Fig. 1(a)] finally attenuated the power to about 0.5 mW. The lasers were operated at constant temperature of 1.9 °C and 2.2 °C, respectively. The combs were electrically driven by a pair of QubeCL drivers (ppqSense). The bias currents for the two combs were 1532 mA and 1226 mA, respectively. The currents were modulated by asymmetric triangular wave forms (WFG1 and WFG2 are the two outputs of an ArbStudio 1102, LeCroy wave form generator) with the currents initially decreasing at constant rate during a time $T = 30$ ms, 60 ms, 120 ms, or 240 ms and returning to the initial value over a shorter time $0.25T$. The peak-to-peak current modulation amplitude was approximately 90 mA for both lasers. This required a modification of the QubeCL drivers which, by default, do not allow such large current modulations.

2. Beam splitters

The beam splitters were custom made to obtain the appropriate power ratios at each photodetector. They were designed for reflecting 1%, 10%, or 50% at an angle of incidence of 45 ° for *s*-polarized light from 1220 to 1370 cm^{-1} (36.6 to 41.1 THz). They were produced by ion beam sputtering (IBS) on 5 mm thick wedged (0.5 °) CaF_2 substrates with an antireflection coating on the back side to minimize undesired interference effects.

3. Data acquisition and processing

Two 1 GHz bandwidth MIR photodetectors were employed to measure the sample (DS) and to normalize laser intensity and phase noise (DN). Each beat note arising from heterodyning of two comb lines appears on both detectors and their amplitudes are measured simultaneously. The division (DS/DN) of the amplitudes yields a ratio in which common-mode fluctuations in magnitude and phase are canceled. The detector outputs were sampled at 2.5 GSa/s with 12 bit resolution by the data acquisition unit DAQ1 (ADQ32, Teledyne), generating 10 Gbyte/s of raw data for the duration of the sweep. The data acquisition was triggered at $t = 0.07T$ after the start of the (decreasing) current ramp and continued for a duration of 27 ms, 54 ms, 107 ms, or 215 ms, which corresponds to 2^{26}, 2^{27}, 2^{28}, or 2^{29} samples at 2.5 GSa/s. The clocks of DAQ1 [Fig. 1(a)] and of the synthesizer generating the 475 MHz fundamental for the synthetic comb generator were referenced to a GPS-disciplined clock (GPSDO, Leo Bodnar).

A custom software (C++ and CUDA) was used to process the two interferograms. The program is capable of fully processing (from raw data to absorbance values) 25 27-ms-long sweeps per second, corresponding to a raw data throughput of 6.75 Gbyte/s, or 67.5% of the maximum raw data input rate. The interferograms were first divided into slices of length $2^{15} = 32\,768$ samples, corresponding to 13.1 µs. The beat note amplitudes were computed for each slice by fast Fourier transform, from which the sample's absorbance was determined.

4. Measurement of the markers and retrieval of the frequency axis

The optical frequency reference, ν_{ref}, was provided by a distributed feedback QCL (DFB, Alpes Lasers) packaged in a TO3 can and emitting a continuous wave (cw) beam. The laser was locked to a molecular transition [N_2O, fundamental ν_1 band, P(14)] by means of a wavelength modulation scheme, in a similar implementation to that in [23]. The wavelength modulation signal at 14 MHz was sent to the laser via a custom-made bias tee. The proportional-integral controller (LB1005-S, Newport) and the laser driver (QCL500 LAB, Wavelength Electronics) assured a locking bandwidth $\geqslant$100 kHz. Diluted N_2O gas flowed through a 15-cm-long custom-made gas cell at a constant pressure of 2 mbar (pressure regulator: PC Series, Alicat).

The lock point frequency was determined relative to the center frequency of the P(14) transition by recording both the error and the transmission signals while slowly tuning the

79

laser over the transition with the feedback loop open. By comparing the dual-comb spectra with the literature, we observed that the reference laser drifted with a standard deviation on the order of 250 kHz over a few days. We thus made sure to reassess the lock point before each measurement (within 6 hours), leading to the 180 kHz uncertainty of the laser lock point.

The heterodyne beat between the DFB reference laser and COMB1 is detected on the fast photodetector (UHSM-10.6 PV-4TE-10.6-0.05-butt, Vigo System). Through RF path 1, two pulses are transmitted in rapid succession when $f_b(t)$ passes near zero and are amplified by a logarithmic amplifier (ZX47-60LN-S+, Minicircuits). The timings of the two peaks, $t_0^{\pm}$, fulfill $f_b(t_0^{\pm}) = \pm f_{\text{bp},1}$, where $f_{\text{bp},1} = 25$ MHz is the center frequency of BPF1. We assume linear chirping of the beat between t_0^- and t_0^+, so that $f_b(t_0) = 0$, where t_0 is the mean of t_0^+ and t_0^-. With Eq. (2) we find $\nu_0(t_0) = \nu_{\text{ref}}$.

As for RF path 2, $f_b(t)$ is mixed with an RF comb with spacing f_{RF}. Therefore, each time the DFB-comb beat, $f_b(t)$, nears a multiple of f_{RF}, two double pulses are recorded on channels 2 and 3 of DAQ2 [signal 2 and signal 3 in Figs. 2(a) and 2(b)]. The timings, $t_n^{\pm}$, of the two pulses of the nth $(n = \pm 1, \pm 2, \ldots)$ double pulse fulfill $f_b(t_n^{\pm}) = n f_{\text{RF}} \pm f_{\text{bp,i}}$, where $f_{\text{bp},2} = 21$ MHz, $f_{\text{bp},3} = 45$ MHz are the center frequencies of BPF2 and BPF3, respectively. For the mean times, $t_n = (t_n^- + t_n^+)/2$, we find, as before, $f_b(t_n) = n f_{\text{RF}}$ and with Eq. (2), $\nu_0(t_n) = \nu_{\text{ref}} + n f_{\text{RF}}$. More details concerning the processing of the markers can be found in Fig. 1 and Note 1 of the Supplemental Material [26].

As postprocessing, we first smooth the marker signals with a low-pass filter. Then we detect the peaks which match specific criteria in terms of prominence, width, and proximity to other lines using a peak-finding algorithm (find_peaks, scipy). If two peaks have the appropriate time delay, we establish that f_b was at a multiple integer n of f_{RF} at the mean time of the two peaks. The integer n is guessed from linear interpolation using marker 1 and an estimated chirp. The discontinuity from the change of comb line can be easily recognized and the markers originating from comb line $\mu = 1$ can be used to determine the frequency of comb line $\mu = 0$ by knowledge of $f_{\text{rep}}(t)$.

We fit the markers with polynomials of increasing orders up to 10, keeping the coefficients of the previous order as initial guess and providing the initial guess for the new coefficient from the residuals of the previous fit. A larger weight is given to marker 2 as BPF2 is narrower than the other bandpass filters. After the fits with the 4th and 8th order polynomial, markers outside a tolerance of 50 MHz and 10 MHz are discarded, respectively. This allows the removal of most spurious peaks, which do not align in the plot Fig. 2(d).

5. Measurement of the repetition rate

In QCL frequency combs, the beating of all co-existing modes in the laser produces a measurable voltage modulation on the laser electrodes with frequency equal to f_{rep} [36]. The laser module features a 50 Ω transmission line on a printed circuit board that connects an SMA connector at the back of the housing to a point very close (within 1 mm) to the back facet of the laser. From there, a short bond wire establishes an electrical connection to the laser's top electrode. This pathway can be used for RF injection or to measure f_{rep}. However, connecting cables and other circuitry to the SMA port tends to increase laser phase noise. It is observable as a broadening of the beat notes. Therefore, a horn antenna (ANT, PowerLOG 40040, Aaronia) was pointed at the open SMA connector. The detected f_{rep} was then amplified and down-mixed to ∼20 MHz to enable its measurement on one channel of DAQ1.

6. Gas sample preparation and measurement

We dynamically diluted N_2O gas with nitrogen to a concentration of about of 450 ppmv and flowed the diluted mixture through the multipass cell (MPC). We then closed off the cell and pumped down to 1.5 mbar, which provided sufficiently strong absorption lines and sufficiently low pressure to be reasonably close to the Doppler-broadened limit and, more importantly, to minimize the pressure-induced shift on the measured transitions. Multiple sweeps were taken but not averaged together. The time delay between sweeps was several seconds, to ensure proper synchronization of the two data sets acquired by the two DAQs, which were read out by independent software. By integrating both DAQs in the same processing routine, the acquisition rate (sweeps per unit time) could be increased significantly (about 12 54-ms-long sweeps per second).

[1] F. Keilmann, C. Gohle, and R. Holzwarth, Time-domain mid-infrared frequency-comb spectrometer, Opt. Lett. **29**, 1542 (2004).

[2] I. Coddington, N. Newbury, and W. Swann, Dual-comb spectroscopy, Optica **3**, 414 (2016).

[3] F. R. Giorgetta, J. Peischl, D. I. Herman, G. Ycas, I. Coddington, N. R. Newbury, and K. C. Cossel, Open-path dual-comb spectroscopy for multispecies trace gas detection in the 4.5–5 μm spectral region, Laser Photonics Rev. **15**, 2000583 (2021).

[4] J. L. Klocke, M. Mangold, P. Allmendinger, A. Hugi, M. Geiser, P. Jouy, J. Faist, and T. Kottke, Single-shot sub-microsecond mid-infrared spectroscopy on protein reactions with quantum cascade laser frequency combs, Anal. Chem. **90**, 10494 (2018).

[5] E. Vicentini, Z. Wang, K. Van Gasse, T. W. Hänsch, and N. Picqué, Dual-comb hyperspectral digital holography, Nat. Photonics **15**, 890 (2021).

[6] A. Parriaux, K. Hammani, C. Thomazo, O. Musset, and G. Millot, Isotope ratio dual-comb spectrometer, Phys. Rev. Res. **4**, 023098 (2022).

[7] T. J. Kippenberg, A. L. Gaeta, M. Lipson, and M. L. Gorodetsky, Dissipative Kerr solitons in optical microresonators, Science **361**, eaan8083 (2018).

[8] A. Hugi, G. Villares, S. Blaser, H. C. Liu, and J. Faist, Mid-infrared frequency comb based on a quantum cascade laser, Nature (London) **492**, 229 (2012).

[9] M. Bagheri, C. Frez, L. A. Sterczewski, I. Gruidin, M. Fradet, I. Vurgaftman, C. L. Canedy, W. W. Bewley, C. D. Merritt,

C. S. Kim, M. Kim, and J. R. Meyer, Passively mode-locked interband cascade optical frequency combs, Sci. Rep. **8**, 3322 (2018).

[10] Y.-D. Hsieh, Y. Iyonaga, Y. Sakaguchi, S. Yokoyama, H. Inaba, K. Minoshima, F. Hindle, T. Araki, and T. Yasui, Spectrally interleaved, comb-mode-resolved spectroscopy using swept dual terahertz combs, Sci. Rep. **4**, 3816 (2014).

[11] G. Villares, A. Hugi, S. Blaser, and J. Faist, Dual-comb spectroscopy based on quantum-cascade-laser frequency combs, Nat. Commun. **5**, 5192 (2014).

[12] A. V. Muraviev, D. Konnov, and K. L. Vodopyanov, Broadband high-resolution molecular spectroscopy with interleaved mid-infrared frequency combs, Sci. Rep. **10**, 18700 (2020).

[13] P.-L. Luo, Long-wave mid-infrared time-resolved dual-comb spectroscopy of short-lived intermediates, Opt. Lett. **45**, 6791 (2020).

[14] T. Lin, A. Dutt, C. Joshi, X. Ji, C. T. Phare, Y. Okawachi, A. L. Gaeta, and M. Lipson, Broadband ultrahigh-resolution chip-scale scanning soliton dual-comb spectroscopy, arXiv:2001.00869.

[15] A. Hjältén, M. Germann, K. Krzempek, A. Hudzikowski, A. Głuszek, D. Tomaszewska, G. Soboń, and A. Foltynowicz, Optical frequency comb Fourier transform spectroscopy of $^{14}N_2{}^{16}O$ at 7.8 μm, J. Quant. Spectrosc. Radiat. Transfer **271**, 107734 (2021).

[16] M. Lepère, O. Browet, J. Clément, B. Vispoel, P. Allmendinger, J. Hayden, F. Eigenmann, A. Hugi, and M. Mangold, A mid-infrared dual-comb spectrometer in step-sweep mode for high-resolution molecular spectroscopy, J. Quant. Spectrosc. Radiat. Transfer **287**, 108239 (2022).

[17] M. Gianella, A. Nataraj, B. Tuzson, P. Jouy, F. Kapsalidis, M. Beck, M. Mangold, A. Hugi, J. Faist, and L. Emmenegger, High-resolution and gapless dual comb spectroscopy with current-tuned quantum cascade lasers, Opt. Express **28**, 6197 (2020).

[18] N. Kuse, G. Navickaite, M. Geiselmann, T. Yasui, and K. Minoshima, Frequency-scanned microresonator soliton comb with tracking of the frequency of all comb modes, Opt. Lett. **46**, 3400 (2021).

[19] E. Benkler, F. Rohde, and H. R. Telle, Endless frequency shifting of optical frequency comb lines, Opt. Express **21**, 5793 (2013).

[20] M. Gianella, S. Vogel, V. J. Wittwer, T. Südmeyer, J. Faist, and L. Emmenegger, Frequency axis for swept dual-comb spectroscopy with quantum cascade lasers, Opt. Lett. **47**, 625 (2022).

[21] M. Germann, A. Hjältén, V. Boudon, C. Richard, K. Krzempek, A. Hudzikowski, A. Głuszek, G. Soboń, and A. Foltynowicz, A methane line list with sub-MHz accuracy in the 1250 to 1380 cm^{-1} range from optical frequency comb Fourier transform spectroscopy, J. Quant. Spectrosc. Radiat. Transfer **288**, 108252 (2022).

[22] J. Riemensberger, A. Lukashchuk, M. Karpov, W. Weng, E. Lucas, J. Liu, and T. J. Kippenberg, Massively parallel coherent laser ranging using a soliton microcomb, Nature (London) **581**, 164 (2020).

[23] K. N. Komagata, M. Gianella, P. Jouy, F. Kapsalidis, M. Shahmohammadi, M. Beck, R. Matthey, V. J. Wittwer, A. Hugi, J. Faist, L. Emmenegger, T. Südmeyer, and S. Schilt, Absolute frequency referencing in the long wave infrared using a quantum cascade laser frequency comb, Opt. Express **30**, 12891 (2022).

[24] K. Komagata, A. Shehzad, G. Terrasanta, P. Brochard, R. Matthey, M. Gianella, P. Jouy, F. Kapsalidis, M. Shahmohammadi, M. Beck, V. J. Wittwer, J. Faist, L. Emmenegger, T. Südmeyer, A. Hugi, and S. Schilt, Coherently-averaged dual comb spectrometer at 7.7 μm with master and follower quantum cascade lasers, Opt. Express **29**, 19126 (2021).

[25] P. Del'Haye, O. Arcizet, M. L. Gorodetsky, R. Holzwarth, and T. J. Kippenberg, Frequency comb assisted diode laser spectroscopy for measurement of microcavity dispersion, Nat. Photonics **3**, 529 (2009).

[26] See Supplemental Material at http://link.aps.org/supplemental/10.1103/PhysRevResearch.5.013047 for more information on the processing of the markers and the measured methane line list.

[27] B. AlSaif, M. Lamperti, D. Gatti, P. Laporta, M. Fermann, A. Farooq, O. Lyulin, A. Campargue, and M. Marangoni, High accuracy line positions of the ν_1 fundamental band of $^{14}N_2{}^{16}O$, J. Quant. Spectrosc. Radiat. Transfer **211**, 172 (2018).

[28] I. Gordon, L. Rothman, R. Hargreaves, R. Hashemi, E. Karlovets, F. Skinner, E. Conway, C. Hill, R. Kochanov, Y. Tan, P. Wcisło, A. Finenko, K. Nelson, P. Bernath, M. Birk, V. Boudon, A. Campargue, K. Chance, A. Coustenis, B. Drouin *et al.*, The HITRAN2020 molecular spectroscopic database, J. Quant. Spectrosc. Radiat. Transfer **277**, 107949 (2022).

[29] A. Nishiyama, D. Ishikawa, and M. Misono, High resolution molecular spectroscopic system assisted by an optical frequency comb, J. Opt. Soc. Am. B **30**, 2107 (2013).

[30] R. Gotti, T. Puppe, Y. Mayzlin, J. Robinson-Tait, S. Wójtewicz, D. Gatti, B. Alsaif, M. Lamperti, P. Laporta, F. Rohde, R. Wilk, P. Leisching, W. G. Kaenders, and M. Marangoni, Comb-locked frequency-swept synthesizer for high precision broadband spectroscopy, Sci. Rep. **10**, 2523 (2020).

[31] J. Hillbrand, M. Bertrand, V. Wittwer, N. Opacak, F. Kapsalidis, M. Gianella, L. Emmenegger, B. Schwarz, T. Südmeyer, M. Beck, and J. Faist, Synchronization of frequency combs by optical injection, Opt. Express **30**, 36087 (2022).

[32] G. Villares, S. Riedi, J. Wolf, D. Kazakov, M. J. Süess, P. Jouy, M. Beck, and J. Faist, Dispersion engineering of quantum cascade laser frequency combs, Optica **3**, 252 (2016).

[33] B. Schwarz, P. Reininger, D. Ristanić, H. Detz, A. M. Andrews, W. Schrenk, and G. Strasser, Monolithically integrated mid-infrared lab-on-a-chip using plasmonics and quantum cascade structures, Nat. Commun. **5**, 4085 (2014).

[34] K. N. Komagata, V. J. Wittwer, T. Südmeyer, L. Emmenegger, and M. Gianella, Data set for "Absolute frequency referencing for swept dual-comb spectroscopy with midinfrared quantum cascade lasers", https://doi.org/10.23728/b2share.2a4682099b614b38b90952e42b8a425f (2022).

[35] P. Jouy, J. M. Wolf, Y. Bidaux, P. Allmendinger, M. Mangold, M. Beck, and J. Faist, Dual comb operation of $\lambda \sim 8.2$ μm quantum cascade laser frequency comb with 1 W optical power, Appl. Phys. Lett. **111**, 141102 (2017).

[36] M. Piccardo, D. Kazakov, N. A. Rubin, P. Chevalier, Y. Wang, F. Xie, K. Lascola, A. Belyanin, and F. Capasso, Time-dependent population inversion gratings in laser frequency combs, Optica **5**, 475 (2018).

Supplementary Information for Absolute Frequency Referencing for Swept Dual-Comb Spectroscopy with Midinfrared Quantum Cascade Lasers

K. N. Komagata[1,*], V. J. Wittwer[1], T. Südmeyer[1], L. Emmenegger[2], and M. Gianella[2,3]
[1]*Laboratoire Temps-Fréquence, Institut de Physique, Université de Neuchâtel, Avenue de Bellevaux 51, 2000 Neuchâtel, Switzerland*
[2]*Laboratory for Air Pollution / Environmental Technology, Empa, Überlandstrasse 129, 8600 Dübendorf, Switzerland*
[3]*Present address: IRsweep AG, Laubisrütistrasse 44, 8712 Stäfa, Switzerland*
[*]*Corresponding author: kenichi.komagata@unine.ch*
(Dated: January 9, 2023)

Supplementary Note 1. PROCESSING OF THE MARKERS

Supplementary Figure 1 schematizes the RF scheme used to calibrate the frequency of the beatnote between a comb line and the reference laser detected on the photodetector DF [see Fig. 1(a) of the main text]. The signal is equalized (VEQY-8-63+, Minicircuits) and amplified (ZX60-6013E-S+, Minicircuits), and equalized again, before being split in two branches for processing the high and low frequencies separately. The equalization is such that near-DC frequencies are attenuated by 44 dB, while the attenuation is only 7 dB at 5 GHz. The low frequency branch is amplified, then split once more. One sub-branch is sent to `BPF1` and is amplified by a logarithmic amplifier (ZX47-60LN-S+, Minicircuits).

The other sub-branch is high-pass filtered at 225 MHz, equalized, and then mixed with the low-frequency branch of the RF comb (see Supplementary Figure 1). The high-frequency branch of the photodetector signal is high-pass filtered at 3.8 GHz, equalized, and amplified before being mixed with the high-frequency branch of the RF comb. The RF comb is generated by sending a 8 dBm 475 MHz sine signal into a comb generator (TBCG2, Tekbox) and amplifying the output signal (LNA-4050, RFbay Inc.). The RF comb is then equalized and split into a high- and low-frequency branch, which are likewise equalized, filtered and amplified before being sent to the mixers mentioned above. The two mixing products are combined, low-pass filtered at 120 MHz, and amplified, before being split once more and filtered with `BPF2` and `BPF3` at 21 MHz and 45 MHz, respectively. Their bandwidths are 3.5 MHz and 8 MHz, respectively.

REFERENCES

[1] I. Gordon, L. Rothman, R. Hargreaves, R. Hashemi, E. Karlovets, F. Skinner, E. Conway, C. Hill, R. Kochanov, Y. Tan, P. Wcisło, A. Finenko, K. Nelson, P. Bernath, M. Birk, V. Boudon, A. Campargue, K. Chance, A. Coustenis, B. Drouin, J. Flaud, R. Gamache, J. Hodges, D. Jacquemart, E. Mlawer, A. Nikitin, V. Perevalov, M. Rotger, J. Tennyson, G. Toon, H. Tran, V. Tyuterev, E. Adkins, A. Baker, A. Barbe, E. Canè, A. Császár, A. Dudaryonok, O. Egorov, A. Fleisher, H. Fleurbaey, A. Foltynowicz, T. Furtenbacher, J. Harrison, J. Hartmann, V. Horneman, X. Huang, T. Karman, J. Karns, S. Kassi, I. Kleiner, V. Kofman, F. Kwabia–Tchana, N. Lavrentieva, T. Lee, D. Long, A. Lukashevskaya, O. Lyulin, V. Makhnev, W. Matt, S. Massie, M. Melosso, S. Mikhailenko, D. Mondelain, H. Müller, O. Naumenko, A. Perrin, O. Polyansky, E. Raddaoui, P. Raston, Z. Reed, M. Rey, C. Richard, R. Tóbiás, I. Sadiek, D. Schwenke, E. Starikova, K. Sung, F. Tamassia, S. Tashkun, J. Vander Auwera, I. Vasilenko, A. Vigasin, G. Villanueva, B. Vispoel, G. Wagner, A. Yachmenev, and S. Yurchenko, The hitran2020 molecular spectroscopic database, J. Quant. Spectrosc. Radiat. Transf. **277**, 107949 (2022).

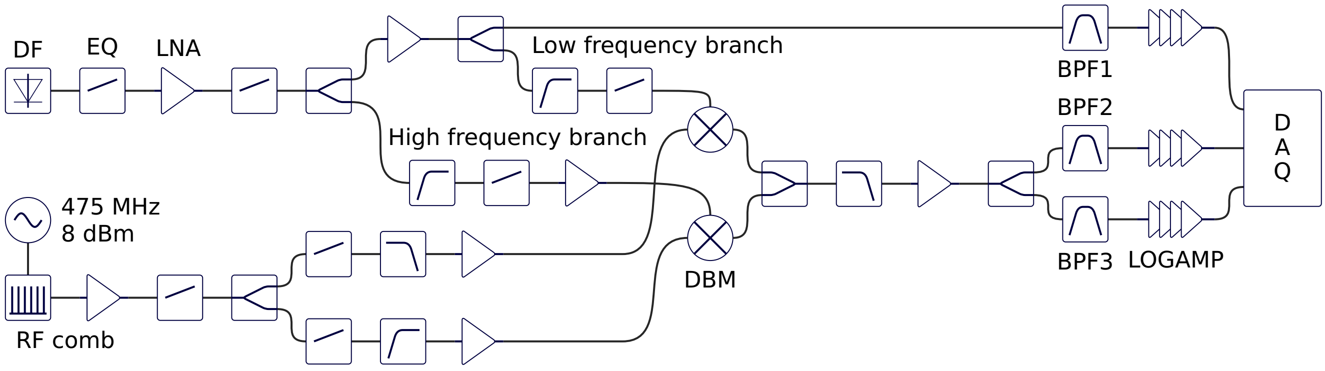

Supplementary Figure 1. Schematized Marker scheme with including separation into two branches for the processing of the high and low frequency components. DF: photodetector [see Fig. 1(a) of the main text], EQ: equalizer, LNA: low noise amplifier, BPF: bandpass filter, DBM: double balanced mixer, LOGAMP: logarithmic amplifier.

Transition (J',C',α') - (J",C",α")	Line center (cm^{-1})
(5, A2, 2) - (6, A1, 1)	1267.822296(55)
(5, F2, 4) - (6, F1, 1)	1268.367774(65)
(5, F1, 3) - (6, F2, 2)	1268.976244(54)
(5, A1, 1) - (6, A2, 1)	1270.785068(25)
(5, F1, 4) - (6, F2, 1)	1271.406911(12)
(5, E, 3) - (6, E, 1)	1271.589462(34)
(4, F2, 3) - (5, F1, 2)	1275.041674(17)
(4, E, 2) - (5, E, 1)	1275.386810(24)
(4, F1, 3) - (5, F2, 1)	1276.844312(23)
(4, F2, 4) - (5, F1, 1)	1277.473279(42)
(3, F1, 3) - (4, F2, 1)	1281.610531(41)
(3, E, 2) - (4, E, 1)	1282.62456(11)
(3, F2, 2) - (4, F1, 1)	1282.984142(95)
(2, A1, 1) - (3, A2, 1)	1287.813273(40)
(2, F1, 2) - (3, F2, 1)	1288.457016(25)
(2, F2, 2) - (3, F1, 1)	1288.950985(35)
(10, F1, 3) - (10, F2, 1)	1292.610277(23)
(10, A1, 2) - (10, A2, 1)	1292.677897(17)
(1, F1, 1) - (2, F2, 1)	1294.379266(18)
(1, E, 1) - (2, E, 1)	1294.684342(20)
(9, F2, 3) - (9, F1, 1)	1295.212700(23)
(9, F1, 3) - (9, F2, 1)	1295.326105(16)
(8, A2, 1) - (8, A1, 1)	1297.486522(14)
(8, F2, 3) - (8, F1, 1)	1297.656959(16)
(8, E, 2) - (8, E, 1)	1297.750892(17)
(11, A1, 2) - (11, A2, 1)	1297.819233(21)
(11, F1, 5) - (11, F2, 2)	1298.205596(29)
(11, E, 3) - (11, E, 1)	1298.437452(34)
(7, F2, 2) - (7, F1, 1)	1299.629814(14)
(7, F1, 3) - (7, F2, 1)	1299.899492(17)
(6, E, 2) - (6, E, 1)	1301.371150(21)
(9, E, 3) - (9, E, 1)	1301.491649(35)
(6, F1, 2) - (6, F2, 1)	1301.553893(25)
(9, F2, 4) - (9, F1, 2)	1301.824890(29)
(6, A1, 1) - (6, A2, 1)	1302.044327(19)
(8, F1, 3) - (8, F2, 1)	1302.777043(46)
(5, F2, 2) - (5, F1, 1)	1302.787450(41)
(9, A2, 2) - (9, A1, 1)	1302.950378(34)
(10, A2, 2) - (10, A1, 1)	1303.200731(70)
(5, F1, 2) - (5, F2, 1)	1303.378292(32)
(7, A1, 2) - (7, A2, 1)	1303.571715(52)
(4, A2, 1) - (4, A1, 1)	1303.712214(69)
(8, F2, 4) - (8, F1, 2)	1303.955066(59)
(4, F2, 2) - (4, F1, 1)	1304.232185(53)
(7, F1, 4) - (7, F2, 2)	1304.472072(76)
(4, E, 1) - (4, E, 1)	1304.599775(81)
(3, F2, 1) - (3, F1, 1)	1304.857914(99)
(6, F1, 3) - (6, F2, 2)	1305.002823(77)
(7, E, 2) - (7, E, 1)	1305.024853(57)
(9, F2, 5) - (9, F1, 3)	1305.106730(88)
(3, F1, 2) - (3, F2, 1)	1305.400123(61)
(2, E, 1) - (2, E, 1)	1305.43730(11)
(2, F1, 1) - (2, F2, 1)	1305.707066(98)
(5, F2, 3) - (5, F1, 2)	1305.903988(62)
(4, F1, 2) - (4, F2, 1)	1305.98730(10)
(6, A2, 1) - (6, A1, 1)	1306.269344(86)

Supplementary Table I. Measured line list of the methane ν_4 band. The upper (lower) levels are labeled with a single (double) prime and are denoted according to the Hitran [1] notation.

Chapter 6

Conclusion and Outlook

6.1 Discussion

In this thesis, I have explored frequency stabilization and calibration methods for QCLs and their application as OFCs for the MIR. In this concluding chapter, I would like to review the results and discuss their relevance in the strategic fields of applications of the MIR. Then, I will end with an outlook on the next interesting research investigations.

6.1.1 Review of the results

In chapter 2, I developed a scheme for coherent averaging in DCS with QCLs to obtain high sensitivity at reduced computational costs. The issue of limited stabilization bandwidth led me to chapter 3, where I presented a method to enslave them with higher fidelity than before. In this undertaking, I characterized the comb coherence in terms of phase noise and demonstrated high spectral purity for all comb lines. Next, I extended the range of applications of MIR QCL FCs by demonstrating frequency referencing both in DCS (chapter 5) and in a comb-calibrated scheme (chapter 4). The schemes allowed the determination of molecular transition frequencies with sub-MHz accuracy. More importantly, I discussed the mode-spacing of QCLs, and hinted at the SNR advantage of QCL FC for frequency comb spectroscopy due to the large spacing and high power. That combination is challenging to match using DFG or OPO sources and makes the results of this thesis all the more relevant.

6.1.2 Relevance for applications

In spectroscopy and sensing, the high locking bandwidth will be beneficial for coupling into enhancement cavities [1]. These could enable extreme sensitivity to trace gases such as $^{14}CO_2$ [2, 3] for isotope ratio measurements. Although the current MIR mirrors have poor reflectivity compared to the NIR counterparts, active developments are being pursued [4]. The methods for coherent averaging will also contribute to higher sensitivity. Combined with the SNR advantage of QCLs due to the large mode spacing and high power, this will lead to unprecedented sensitivity and measurement times for sensing applications.

Moreover, the accurate frequency calibration for direct or comb-assisted spectroscopy will be useful for the study of molecular physics by accurate retrieval of the transition frequencies, lineshape parameters, and intensities [5, 6]. The tight phase-locking ability implies that QCL FCs with sub-Hz linewidths could be achieved using DFB QCLs locked to state-of-the-art NIR references [7]. Then, a fixed DFB QCL and a longer crystal can be used for a better conversion efficiency and the QCL FC could serve as a broadband reference for spectroscopy applications requiring Hz-level accuracy [8]. QCL FCs could in overall simplify the complexity of such measurements.

Free-space MIR telecommunications could also benefit from the results presented in this thesis. The fast response to NIR radiation suggests direct conversion of NIR communication channels to the MIR by shining of the QCL. Besides communications by modulation of the intermode beat [9], referenced MIR combs could also define and provide communication bands for dense spectral multiplexing using auxiliary lasers. Eventually, with maturation of MIR technology, individual comb lines could be independently modulated for massively-parallel communications [10].

6.2 Outlook

The development of other MIR technologies such as coatings [4], detectors [11], modulators [12], and PIC [13–15] will surely open a plethora of rejoicing possibilities and improve our quality of life. These cannot be accurately predicted due to the singular nature of progress [16]. For example, PIC are key for self-referencing QCL OFCs but they could equally enable simple nonlinear conversion between the NIR and the MIR and make QCLs to a large extent irrelevant. Therefore, I am not persuaded that QCLs will be the photonic tool of choice in the future. However, I do believe that they have sufficient potential to motivate further investigations. In particular, I showed in chapter 3 that they they have a sufficient control bandwidth for most applications, and that the comb equation holds also for fast phase fluctuations. I conclude this thesis by describing three research directions, with their motivation, and potential impact.

First, the generation of shorter and more powerful pulses [17–20] combined with the development of MIR nonlinear waveguide [14] could enable octave spanning spectra and offset frequency detection. Then, the offset frequency could be locked-tightly using NIR light as an actuator. The repetition rate could be phase-locked in different manners: by electrical or optical injection locking [21, 22], or in a PLL, by comparing it to an RF [23] or an optical reference. The last option would grant the best optical purity by avoiding the multiplication of the repetition rate by large numbers [24]. Doppler-free molecular transitions [25, 26] could be used and eventually integrated on chip [27]. Moreover, chip-based cascaded harmonic links could be explored for converting fiber-transmitted NIR references [28]. This would result in an on-chip octave spanning low-noise referenced MIR FC, which could be used for most OFC applications.

Second, although QCL are chip-based devices, their operation requires bulky components due to the high drive voltage and current they need and the corresponding dissipated power to be evacuated by water cooling. Decreasing the threshold current for DFB QCLs is possible by shortening the active region and increasing the facet reflectivity [29]. The short active region could be continued with a passive section to set the right repetition frequency [30]. However, with high facet reflectivity, another way of inducing large power discontinuities will be required to ensure comb operation [31]. Improving their efficiency [32] and additionally reducing the voltage to complementary metal-oxide semiconductor–compatible values will allow their straightforward integration into a large scope of systems, from handheld devices to satellites. They could then become ubiquitous tools for medicine, industry, and security among others, thanks to wafer scale fabrication at low unit-cost.

Third, theoretical developments have reduced the complex Maxwell-Bloch equations [33] to a Master equation [34], where the main contribution to the Kerr nonlinearity was identified as Bloch gain [35]. This was followed by the derivation of a mean field equation, which highlighted an non-localized chirped state in QCLs and other semiconductor based FCs [31]. Thanks to these breakthroughs, a more thorough understanding of the mode-locking dynamics in QCLs has been accessed. It can be expected that these and further insights will help in designing and exploiting new generations of QCL FCs with optimal performances. In DCS for example, improving the spectral shape and the free-running intensity [36] and frequency noise will enhance the sensitivity. As a comparison, OFC generation based on dissipative Kerr solitons has been strongly backed-up by the Lugiato-Lefever equation since their inception [37]. The equation or variants thereof has helped the development of this technology in various directions, such as the understanding of the breathing dynamics [38], dynamic spectral tuning using multiple cavities [39], or dynamics of soliton self-injection locking [40]. Moreover, I believe that theoretical and experimental investigations of QCLs will continue to reveal more of interesting physics [19, 41, 42] such as the interplay between emergence, non-hermitian physics, and topology as I have explored previously within my Master's thesis [39, 43–45]. The understanding of those phenomena in controlled systems will surely catalyze further development in photonics, and could even allude to the dynamics of more complex systems, such as life, the universe, and consciousness.

References

[1] A. Foltynowicz, P. Masłowski, A. J. Fleisher, B. J. Bjork, and J. Ye, "Cavity-Enhanced Optical Frequency Comb Spectroscopy in the Mid-Infrared Application to Trace Detection of Hydrogen Peroxide", Appl. Phys. B **110**, 163 (2013).

[2] G. Genoud, J. Lehmuskoski, S. Bell, V. Palonen, M. Oinonen, M.-L. Koskinen-Soivi, and M. Reinikainen, "Laser Spectroscopy for Monitoring of Radiocarbon in Atmospheric Samples", Anal. Chem. **91**, 12315 (2019).

[3] L. Emmenegger, A. Nataraj, M. Gianella, J. Faist, and B. Tuzson, "Low-Temperature Mid-IR Absorption Spectroscopy for Isotopomer-Specific Measurements", in EGU General Assembly, EGU23-16250 (Apr. 24, 2023).

[4] G.-W. Truong, L. W. Perner, G. Winkler, S. B. Cataño-Lopez, C. Nguyen, D. Follman, O. H. Heckl, and G. D. Cole, "Transmission-Dominated Mid-Infrared Supermirrors with Finesse Exceeding 200 000", arXiv.2209.09902 Phys., `10.48550/arXiv.2209.09902` (2022).

[5] M. Germann, A. Hjältén, V. Boudon, C. Richard, K. Krzempek, A. Hudzikowski, A. Głuszek, G. Soboń, and A. Foltynowicz, "A Methane Line List with Sub-MHz Accuracy in the 1250 to 1380 cm^{-1} Range from Optical Frequency Comb Fourier Transform Spectroscopy", J. Quant. Spectrosc. Radiat. Transf. **288**, 108252 (2022).

[6] J. A. Agner, S. Albert, P. Allmendinger, U. Hollenstein, A. Hugi, P. Jouy, K. Keppler, M. Mangold, F. Merkt, and M. Quack, "High-Resolution Spectroscopic Measurements of Cold Samples in Supersonic Beams Using a QCL Dual-Comb Spectrometer*", Mol. Phys. **120**, e2094297 (2022).

[7] B. Argence, B. Chanteau, O. Lopez, D. Nicolodi, M. Abgrall, C. Chardonnet, C. Daussy, B. Darquié, Y. Le Coq, and A. Amy-Klein, “Quantum Cascade Laser Frequency Stabilization at the Sub-Hz Level”, Nat. Photonics **9**, 456 (2015).

[8] R. Santagata, D. B. A. Tran, B. Argence, O. Lopez, S. K. Tokunaga, F. Wiotte, H. Mouhamad, A. Goncharov, M. Abgrall, Y. L. Coq, H. Alvarez-Martinez, R. L. Targat, W. K. Lee, D. Xu, P.-E. Pottie, B. Darquié, and A. Amy-Klein, “High-Precision Methanol Spectroscopy with a Widely Tunable SI-traceable Frequency-Comb-Based Mid-Infrared QCL”, Optica **6**, 411 (2019).

[9] N. Corrias, T. Gabbrielli, P. De Natale, L. Consolino, and F. Cappelli, “Analog FM Free-Space Optical Communication Based on a Mid-Infrared Quantum Cascade Laser Frequency Comb”, Opt. Express **30**, 10217 (2022).

[10] P. Marin-Palomo, J. N. Kemal, M. Karpov, A. Kordts, J. Pfeifle, M. H. P. Pfeiffer, P. Trocha, S. Wolf, V. Brasch, M. H. Anderson, R. Rosenberger, K. Vijayan, W. Freude, T. J. Kippenberg, and C. Koos, “Microresonator-Based Solitons for Massively Parallel Coherent Optical Communications”, Nature **546**, 274 (2017).

[11] T. Dougakiuchi and N. Akikusa, “Application of High-Speed Quantum Cascade Detectors for Mid-Infrared, Broadband, High-Resolution Spectroscopy”, Sensors **21**, 5706 (2021).

[12] H. Dely, M. Joharifar, X. Pang, D. Gacemi, T. Salgals, R. Schatz, Y.-T. Sun, T. Bonazzi, E. Rodriguez, Y. Todorov, A. Vasanelli, A. Udalcovs, S. Spolitis, V. Bobrovs, O. Ozolins, S. Popov, and C. Sirtori, “High Bitrate Data Transmission in the 8-14 µm Atmospheric Window Using an External Stark-effect Modulator with Digital Equalization”, Opt. Express **31**, 7259 (2023).

[13] B. Schwarz, P. Reininger, D. Ristanić, H. Detz, A. M. Andrews, W. Schrenk, and G. Strasser, “Monolithically Integrated Mid-Infrared Lab-on-a-Chip Using Plasmonics and Quantum Cascade Structures”, Nat. Commun. **5**, 4085 (2014).

[14] M. Montesinos-Ballester, C. Lafforgue, J. Frigerio, A. Ballabio, V. Vakarin, Q. Liu, J. M. Ramirez, X. Le Roux, D. Bouville, A. Barzaghi, C. Alonso-Ramos, L. Vivien, G. Isella, and D. Marris-Morini, “On-Chip Mid-Infrared Supercontinuum Generation from 3 to 13 µm Wavelength”, ACS Photonics **7**, 3423 (2020).

[15] S. Alberti, A. Datta, and J. Jágerská, "Integrated Nanophotonic Waveguide-Based Devices for IR and Raman Gas Spectroscopy", Sensors **21**, 7224 (2021).

[16] D. Deutsch, *The Beginning of Infinity: Explanations That Transform the World*, Reprint edition (Penguin Books, New York, Jan. 2012).

[17] J. Hillbrand, N. Opačak, M. Piccardo, H. Schneider, G. Strasser, F. Capasso, and B. Schwarz, "Mode-Locked Short Pulses from an 8 µm Wavelength Semiconductor Laser", Nat. Commun. **11**, 5788 (2020).

[18] P. Täschler, M. Bertrand, B. Schneider, M. Singleton, P. Jouy, F. Kapsalidis, M. Beck, and J. Faist, "Femtosecond Pulses from a Mid-Infrared Quantum Cascade Laser", Nat. Photonics **15**, 919 (2021).

[19] B. Meng, M. Singleton, J. Hillbrand, M. Franckié, M. Beck, and J. Faist, "Dissipative Kerr Solitons in Semiconductor Ring Lasers", Nature Photonics **16**, 142 (2022).

[20] P. Täschler, L. Miller, F. Kapsalidis, M. Beck, and J. Faist, "Short Pulses from a Gain-Switched Quantum Cascade Laser", Optica **10**, 507 (2023).

[21] J. Hillbrand, A. M. Andrews, H. Detz, G. Strasser, and B. Schwarz, "Coherent Injection Locking of Quantum Cascade Laser Frequency Combs", Nat. Photonics **13**, 101 (2019).

[22] K. N. Komagata, A. Parriaux, M. Bertrand, J. Hillbrand, M. Beck, V. J. Wittwer, J. Faist, and T. Südmeyer, "Coherent Control of Mid-Infrared Frequency Comb by Optical Injection of Near-Infrared Light", ArXiv230501508 Phys., `10.48550/arXiv.2305.01508` (2023).

[23] A. Shehzad, P. Brochard, R. Matthey, F. Kapsalidis, M. Shahmohammadi, M. Beck, A. Hugi, P. Jouy, J. Faist, T. Südmeyer, and S. Schilt, "Frequency Noise Correlation between the Offset Frequency and the Mode Spacing in a Mid-Infrared Quantum Cascade Laser Frequency Comb", Opt. Express **28**, 8200 (2020).

[24] T. Fortier and E. Baumann, "20 Years of Developments in Optical Frequency Comb Technology and Applications", Commun. Phys. **2**, 1 (2019).

[25] V. Bernard, C. Daussy, G. Nogues, L. Constantin, P. E. Durand, A. Amy-Klein, A. Van Lerberghe, and C. Chardonnet, "CO_2 Laser Stabilization to 0.1-Hz Level Using External Electrooptic Modulation", IEEE J. Quantum Electron. **33**, 1282 (1997).

[26] F. Cappelli, I. Galli, S. Borri, G. Giusfredi, P. Cancio, D. Mazzotti, A. Montori, N. Akikusa, M. Yamanishi, and S. Bartalini, "Subkilohertz Linewidth Room-Temperature Mid-Infrared Quantum Cascade Laser Using a Molecular Sub-Doppler Reference", Opt. Lett. **37**, 4811 (2012).

[27] W. Yang, D. B. Conkey, B. Wu, D. Yin, A. R. Hawkins, and H. Schmidt, "Atomic Spectroscopy on a Chip", Nat. Photonics **1**, 331 (2007).

[28] A. Bercy, F. Stefani, O. Lopez, C. Chardonnet, P.-E. Pottie, and A. Amy-Klein, "Two-Way Optical Frequency Comparisons at 5×10^{-21} Relative Stability over 100-Km Telecommunication Network Fibers", Phys. Rev. A **90**, 061802 (2014).

[29] Z. Wang, F. Kapsalidis, R. Wang, M. Beck, and J. Faist, "Ultra-Low Threshold Lasing through Phase Front Engineering via a Metallic Circular Aperture", Nat. Commun. **13**, 230 (2022).

[30] R. Wang, P. Täschler, Z. Wang, E. Gini, M. Beck, and J. Faist, "Monolithic Integration of Mid-Infrared Quantum Cascade Lasers and Frequency Combs with Passive Waveguides", ACS Photonics **9**, 426 (2022).

[31] D. Burghoff, "Unraveling the Origin of Frequency Modulated Combs Using Active Cavity Mean-Field Theory", Optica **7**, 1781 (2020).

[32] Q. Lu, D. Wu, S. Slivken, and M. Razeghi, "High Efficiency Quantum Cascade Laser Frequency Comb", Sci. Rep. **7**, 43806 (2017).

[33] G. Villares and J. Faist, "Quantum Cascade Laser Combs: Effects of Modulation and Dispersion", Opt. Express **23**, 1651 (2015).

[34] N. Opačak and B. Schwarz, "Theory of Frequency-Modulated Combs in Lasers with Spatial Hole Burning, Dispersion, and Kerr Nonlinearity", Phys. Rev. Lett. **123**, 243902 (2019).

[35] N. Opačak, S. D. Cin, J. Hillbrand, and B. Schwarz, "Frequency Comb Generation by Bloch Gain Induced Giant Kerr Nonlinearity", Phys. Rev. Lett. **127**, 093902 (2021).

[36] T. Gabbrielli, N. Bruno, N. Corrias, S. Borri, L. Consolino, M. Bertrand, M. Shahmohammadi, M. Franckié, M. Beck, J. Faist, A. Zavatta, F. Cappelli, and P. De Natale, "Intensity Correlations in Quantum Cascade Laser Harmonic Frequency Combs", Adv. Photonics Res. **3**, 2200162 (2022).

[37] T. Herr, V. Brasch, J. D. Jost, C. Y. Wang, N. M. Kondratiev, M. L. Gorodetsky, and T. J. Kippenberg, "Temporal Solitons in Optical Microresonators", Nat. Photonics **8**, 145 (2013).

[38] H. Guo, E. Lucas, M. H. P. Pfeiffer, M. Karpov, M. Anderson, J. Liu, M. Geiselmann, J. D. Jost, and T. J. Kippenberg, "Intermode Breather Solitons in Optical Microresonators", Phys. Rev. X **7**, 041055 (2017).

[39] A. Tikan, J. Riemensberger, K. Komagata, S. Hönl, M. Churaev, C. Skehan, H. Guo, R. N. Wang, J. Liu, P. Seidler, and T. J. Kippenberg, "Emergent Nonlinear Phenomena in a Driven Dissipative Photonic Dimer", Nat. Phys. **17**, 604 (2021).

[40] A. S. Voloshin, N. M. Kondratiev, G. V. Lihachev, J. Liu, V. E. Lobanov, N. Y. Dmitriev, W. Weng, T. J. Kippenberg, and I. A. Bilenko, "Dynamics of Soliton Self-Injection Locking in Optical Microresonators", Nat. Commun. **12**, 235 (2021).

[41] M. Shahmohammadi, M. J. Süess, R. Peretti, F. Kapsalidis, A. Forrer, M. Beck, and J. Faist, "Exceptional Point Singularities in Multi-Section DFB Lasers", New Journal of Physics **24**, 053047 (2022).

[42] S. Kacmoli, D. L. Sivco, and C. F. Gmachl, "Photonic Molecule Based on Coupled Ring Quantum Cascade Lasers", ArXiv230411484 Phys., `10.48550/arXiv.2304.11484` (2023).

[43] K. Komagata, A. Tusnin, J. Riemensberger, M. Churaev, H. Guo, A. Tikan, and T. J. Kippenberg, "Dissipative Kerr Solitons in a Photonic Dimer on Both Sides of Exceptional Point", Commun. Phys. **4**, 1 (2021).

[44] A. Tikan, A. Tusnin, J. Riemensberger, M. Churaev, X. Ji, K. N. Komagata, R. N. Wang, J. Liu, and T. J. Kippenberg, "Protected Generation of Dissipative Kerr Solitons in Supermodes of Coupled Optical Microresonators", Sci. Adv. **8**, eabm6982 (2022).

[45] A. K. Tusnin, A. M. Tikan, K. Komagata, and T. J. Kippenberg, "Spatio-Temporal Dissipative Kerr Solitons and Regularized Wave-Collapses in Chains of Nonlinear Microresonators", ArXiv210411731 Phys., `10.48550/arXiv.2104.11731` (2022).

Kenichi N. Komagata
Rue des hirondelles 36
2502 Bienne
Tel.: +4177 488 9220
E-mail: kenickoma@gmail.com

CURRICULUM VITAE

Experiences

PhD in physics, with Prof. T. Südmeyer — Aug. 2019 – June 2023

University of Neuchâtel, laboratoire temps-fréquence

Spectroscopy with quantum cascade lasers frequency combs in the mid-infrared. Frequency stabilization, stability assessment, frequency calibration. Comb-calibrated and dual comb spectroscopy. Development of different locking schemes. In collaboration with EMPA, ETHZ, and IRsweep through the SNF bridge "CombTrace" project.

Master's project, with Prof. T. J. Kippenberg — Sept. 2018 – Aug. 2019

EPFL, laboratory of photonics and quantum measurement

Research on soliton generation and dynamics in an array of coupled microresonators. I first studied the new physical system using numerical tools on the EPFL computational cluster. I found and chose interesting parameters and designed samples to be fabricated. I performed experiments on these samples. Novel phenomena like tunable enhancement of comb lines were found. The phenomena were understood based on the analytical formalism I developed.

Internship, with Prof. V. Savona — Sept. 2017 – Aug. 2018

EPFL, laboratory of theoretical physics of nanosystems

Modelling and simulation of an array of driven-dissipative nonlinear quantum oscillators.

Internship, with Prof. M. Grioni — Aug. – Sept. 2017

EPFL, laboratoire de spectroscopie électronique

Set up of an automatized measurement for angle-resolved photoelectron spectroscopy using LabView.

Bachelor internship, with Prof. S. Tarucha — Sept. 2016 – July 2017

Tokyo University, Tarucha laboratory

Introduction to quantum information, graphene, quantum dots, flying qubits with electrons.

Education

Master and **Bachelor** in Physics, EPFL — Sept. 2014 – Aug. 2019

Thesis with Prof. T. J. Kippenberg: "Dissipative Kerr solitons in strongly coupled microresonator networks"
2nd place in IBM Q best paper award in extracurricular project with Prof. M. A. Dupertuis
5.78/6 average grade in Master's cycle
Exchange year in Tokyo university in 3rd year Bachelor.

Maturité gymnasiale bilingue — Aug. 2010 – July 2013

French german bilingual high school, specification: physics and applied math

Languages

French: native proficiency
English: professional working proficiency
Japanese: limited working proficiency
German: limited working proficiency

Distinctions and grants

High average grade of 5.78 out of 6 on the Master cycle at EPFL.
IBM Q Best Paper Award 2018: 2nd place with the extracurricular project led by Prof. M. A. Dupertuis.
EPFL mobility grant for an academic exchange at the university of Tokyo for the 3rd year of Bachelor.
Championnat des jeux mathématiques et logiques 2010: 1st place at the national qualifications.

Aptitudes and skills

Personal: Learning agility, adaptivity, creativity, flexibility, sense of initiative
Social: Team work, empathy, communication, multiculturalism, public speaking.

Analytical: Data analysis, development and use of models, critical and mathematical analysis.
Project management: Development of an idea, planning, prioritization, purchasing of components.
Programming: Object oriented programming, C++, Matlab, python, LabView, LaTeX, numerical simulations.
Experimental: Fiber and free space optics, spectroscopy, frequency stabilization, RF electronics, use of complex instruments.

Personal data

Born the 19th of June 1994 in Minamiuonuma-shi, Niigata, Japan.
Swiss and Japanese nationality.
Married on the 6th of January 2016 in Biel, 3 children.

References

Prof. Thomas Südmeyer, Head of Laboratoire temps-fréquence, University of Neuchâtel, Switzerland
Prof. Tobias J. Kippenberg, Head of Laboratory of Photonics and Quantum Measurements, EPFL, Switzerland
Prof. Seigo Tarucha, Head of Quantum Functional System Research Group, Riken, Japan

Selected publications

K. N. Komagata, V. J. Wittwer, T. Südmeyer, L. Emmenegger, and M. Gianella, "Absolute frequency referencing for swept dual-comb spectroscopy with midinfrared quantum cascade lasers," Phys. Rev. Res. 5(1), 013047 (2023).

K. N. Komagata, M. Gianella, P. Jouy, F. Kapsalidis, M. Shahmohammadi, M. Beck, R. Matthey, V. J. Wittwer, A. Hugi, J. Faist, L. Emmenegger, T. Südmeyer, and S. Schilt, "Absolute frequency referencing in the long wave infrared using a quantum cascade laser frequency comb," Opt. Express 30(8), 12891 (2022).

A. Tikan, A. Tusnin, J. Riemensberger, M. Churaev, X. Ji, K. N. Komagata, R. N. Wang, J. Liu, and T. J. Kippenberg, "Protected generation of dissipative Kerr solitons in supermodes of coupled optical microresonators," Sci. Adv. 8(13), eabm6982 (2022).

K. Komagata, A. Shehzad, G. Terrasanta, P. Brochard, R. Matthey, M. Gianella, P. Jouy, F. Kapsalidis, M. Shahmohammadi, M. Beck, V. J. Wittwer, J. Faist, L. Emmenegger, T. Südmeyer, A. Hugi, and S. Schilt, "Coherently-averaged dual comb spectrometer at 7.7 µm with master and follower quantum cascade lasers," Opt. Express 29(12), 19126–19139 (2021).

K. Komagata, A. Tusnin, J. Riemensberger, M. Churaev, H. Guo, A. Tikan, and T. J. Kippenberg, "Dissipative Kerr solitons in a photonic dimer on both sides of exceptional point," Commun. Phys. 4(1), 1–13 (2021).

A. Tikan, J. Riemensberger, K. Komagata, S. Hönl, M. Churaev, C. Skehan, H. Guo, R. N. Wang, J. Liu, P. Seidler, and T. J. Kippenberg, "Emergent nonlinear phenomena in a driven dissipative photonic dimer," Nat. Phys. 17(5), 604–610 (2021).

D. Cruz, R. Fournier, F. Gremion, A. Jeannerot, K. Komagata, T. Tosic, J. Thiesbrummel, C. L. Chan, N. Macris, M.-A. Dupertuis, and C. Javerzac-Galy, "Efficient Quantum Algorithms for GHZ and W States, and Implementation on the IBM Quantum Computer," Adv. Quantum Techol. 2(5–6), 1900015 (2019).

UNIVERSITÉ DE NEUCHÂTEL

Rectorat
Fbg de l'Hôpital 41
2000 Neuchâtel
Tél. +41 32 718 10 20
messagerie.rectorat@unine.ch

Pledge of Honour*

I hereby declare that I have read and understood the material explaining plagiarism and the prevention thereof provided by the University of Neuchâtel and that I understand the procedures of accurate citation and bibliographical practice.

I confirm that my paper is the result of my personal research and is solely my own work.

I affirm that any formulation, idea, research, reasoning or analysis borrowed from a third party is correctly and accurately indicated as such, clearly and transparently, and in such a way that the original source is immediately recognisable, in respect of citation techniques and the author's rights.

I am aware that not documenting source material or not citing clearly, correctly and completely constitutes plagiarism.

I am aware that plagiarism is considered a serious offence within the University and that any case of plagiarism can entail administrative sanctions and disciplinary consequences (including expulsion).

I have understood that in the case of plagiarism, the file will automatically be transferred to the Rector's office.

In light of the above, **I declare that I have not plagiarised, nor committed any other kind of fraud.**

Last name: Komagata

First name: Kenichi N.

Course of study: Physics

Faculty: Faculty of science

Place and date: Neuchâtel, May 2023

Signature: Komagata KN

****

This form is to be filled in by each student writing a significant paper (especially a Bachelor's or Master's thesis) or a Doctoral thesis. It must be included with each paper submitted.

*The text of this form has largely been inspired by the Rector's office's directive 0.3 bis *Directive de la direction 0.3 bis*, entitled *Formulaire Code de déontologie en matière d'emprunts, de citations et d'exploitation de sources diverses*, of the University of Lausanne, April 23rd 2007, and adapted for the requirements of the University of Neuchâtel.